

Water Responsive Mechano-adaptive Elastomer Composites based on Active Filler Morphology

Von der Fakultät Maschinenwesen

der

Technische Universität Dresden

zur

Erlangung des akademischen Grades

Doktoringenieur (Dr.-Ing.)

angenommene Dissertation

M.Tech. Tamil Selvan Natarajan

Geb. am 26.11.1989 in Erode, Indien

Tag der Einreichung	:23.08.2019
Tag der Verteidigung	:14.01.2019
Gutachter	:Prof. Dr. rer. nat. habil. Gert Heinrich :PD Dr.-Ing. habil. Katrin Reincke
Vorsitzender der Promotionskommission	:Prof. Dr.-Ing. habil. Chokri Cherif

I dedicate this thesis to my father, mother and brother

Acknowledgements

I would like to express my heartfelt gratitude to Prof. Gert Heinrich for providing me with an opportunity to carry out my dissertation under him. I consider myself extremely blessed to work with such a humble and kind human being like him. I am thankful for the valuable discussions and suggestions he made towards my work.

I would like to greatly appreciate the tireless guidance and encouragement of Dr. Amit Das throughout the course of my Ph.D life. I would like to acknowledge him for his invaluable professional/personal suggestions and also for showing me by example, how to be motivated even in tough times. I would like to extend my sincere thanks to Jun. Prof. Sven Wießner for accommodating and providing with nice atmosphere in the Elastomer department. I would also express my sincere thanks to Dr. Klaus W. Stöckelhuber for his insightful suggestions and perspectives. I should also mention about his ever smiling nature, which has become one of the aspirations for my life. Finally, I should not forget to thank Mr. René Jurk for his constant guidance in effectively using all the instruments in Elastomer laboratory.

I am thankful to my collaborators Dr. Petr Formanek for TEM characterization, Mrs. Sabine Krause for thermal analysis, Dr. Regine Boldt for SEM analysis, Dr. Mikhail Malanin for FTIR analysis, Mr. Holger Scheibner for stress-strain analysis and Dr. Dieter Jehnichen for XRD analysis. I am very grateful to Mrs. Anne Hofmann for the non-technical assistance, whenever needed. I thankfully acknowledge the support of Mr. Joseph Fields (Zeon Chemicals) for supplying the raw materials and for his valuable suggestions.

I am extremely indebted to Eshwaran and Parthiban for assisting me in all aspects of my life during my Ph.D days. I would also like to extend my sincere thanks to my fellow colleagues and friends Sankar, Minoj, Anik, Sakrit, Shib and others. I express my deep gratitude to all of my friends and their families in Dresden, who has made my time in Dresden a memorable one.

Last but not the least, I would like to acknowledge my father, mother, brother and other family members, who has been a constant source of support and encouragement in my life.

Eidesstattliche Erklärung

Ich versichere weiterhin, dass

(a) ich die vorliegende Arbeit mit dem Titel “Water Responsive Mechano-adaptive Elastomer Composites based on Active Filler Morphology” ohne unzulässige Hilfe Dritter und ohne Benutzung anderer als der angegebenen Hilfsmittel angefertigt habe. Die aus fremden Quellen direkt oder indirekt übernommenen Gedanken sind als solche kenntlich gemacht.

(b) ich die vorliegende Arbeit bisher weder im Inland noch im Ausland in gleicher oder ähnlicher Form einer anderen Prüfungsbehörde zum Zwecke einer Promotion oder eines anderen Prüfungsverfahrens vorgelegt habe und diese auch zu keinem Zeitpunkt veröffentlicht worden ist.

(c) ich bei der Auswahl und Auswertung des Materials sowie bei der Herstellung des Manuskripts die Unterstützungsleistungen der im Antrag genannten Betreuer/innen in Anspruch genommen habe.

(d) keine weiteren Personen bei der geistigen Herstellung der vorliegenden Arbeit beteiligt waren.

(e) ich keine Hilfe eines/r Promotionsberaters/in Anspruch genommen habe.

(f) keine, weder unmittelbar noch mittelbar, geldwerten Leistungen im Zusammenhang mit dem Inhalt der vorliegenden Dissertation an Dritte erfolgt sind.

(g) die Bedingungen gemäß § 10 Abs. 2 der Promotionsordnung eingehalten worden, sofern es sich bei der eingereichten Dissertation um eine kumulative Dissertation handelt.

Dresden, den 14.01.19

Tamil Selvan Natarajan

Abstract

Mechanically adaptable elastomer composites are a class of stimuli responsive polymer composites which can reversibly change its mechanical properties when it comes in contact with stimuli like electric field, light, water, solvents, ions and others. Mechanically adaptable composites are mainly inspired from the sea cucumber dermis which has the ability to change the stiffness of its dermis rapidly and reversibly (connecting tissue) when it is immersed in water.

In this work, efforts have been made to develop mechano-adaptive elastomer composites using water as stimuli. In such a case, elastomer composite should absorb water significantly, in order to respond quickly to the stimuli. Therefore, as a first step, stable and repeatable water swellable elastomer composites have been developed by blending epichlorohydrin terpolymer (GECO) with an ethylene oxide based hydrophilic polymer resin (GEPO).

Two different approaches have been thereafter explored to develop mechano-adaptive composites based on the developed water swellable elastomer composite. In the first approach, the solid–liquid phase transition of the absorbed water is used to tune mechanical properties around 0 °C. The solidified absorbed water (ice crystals) below 0 °C, acts as reinforcing filler, enhancing the mechanical properties (*hard state*). The ice crystals liquefy above 0 °C and plasticize the polymer chain, thereby reducing the mechanical properties (*soft state*). In the second approach, the polymorphic transition of calcium sulphate (CaSO_4) in presence of water/heat have been exploited by dispersing it as filler in the developed water swellable elastomer composite. Mechanical adaptability is realized by the reinforcement caused when the composite is exposed to water treatment process. Further, this mechanical strength (reinforcement) can be brought back to its initial *soft state* (unreinforced state) by the heat treatment process. This reversible reinforcing and non-reinforcing ability of the calcium sulphate filler is attributed to the differences in polymer–filler interaction, due to the *in situ* morphology transformation (micro to nano) of the filler particles.

This study reveals the possibility of utilizing conventional rubber technology in developing mechanically adaptable composites with an easily accessible stimulus like water. The two strategies explored here present huge opportunities in developing future smart materials.

Kurzzusammenfassung

Mechanisch-adaptive Elastomer-Verbundwerkstoffe sind eine Klasse von stimuli-responsiven Polymer-Verbundwerkstoffen, welche ihre mechanischen Eigenschaften reversibel verändern können, wenn sie mit Stimuli, wie z.B. einem elektrischem Feld, Licht, Wasser, Lösungsmitteln oder Ionen angeregt werden. Mechanisch anpassbare Verbundwerkstoffe sind hauptsächlich von der Haut der Seegurke inspiriert, welche in der Lage ist, die Steifigkeit ihrer Dermis (Bindegewebe) beim Eintauchen in Wasser schnell und reversibel zu verändern.

Ziel dieser Arbeit war, mechanisch-adaptive Elastomer-Verbundwerkstoffe zu entwickeln, welche Wasser als Stimulus nutzen. Für diese Anwendung sollte das Elastomermaterial Wasser in einer signifikanten Menge aufnehmen können, um schnell auf den externen Reiz zu reagieren. Daher wurden in einem ersten Schritt stabile und reversibel wasserquellbare Elastomerblends hergestellt, indem ein Epichlorhydrin-Terpolymer (GECO) mit einem hydrophilen Polymerharz auf Ethylenoxidbasis (GEPO) verschnitten wurde.

In der Folge wurden zwei verschiedene Ansätze zur Entwicklung mechanisch-adaptiver Verbundwerkstoffe auf Basis des so entwickelten wasserquellbaren Elastomerkomposites verfolgt. Beim ersten Ansatz wird der Fest-Flüssig-Phasenübergang des aufgenommenen Wassers genutzt, um die mechanischen Eigenschaften im, Bereich von 0 °C einzustellen. Das erstarrte absorbierte Wasser (Eiskristalle) wirkt unter 0 °C als verstärkender Füllstoff und verbessert die mechanischen Eigenschaften (harter Zustand). Die Eiskristalle verflüssigen sich oberhalb von 0 °C und plastifizieren das Polymer, wodurch die mechanische Verstärkung wieder herabgesetzt wird (weicher Zustand). Im zweiten Ansatz wurde der polymorphe Übergang von Calciumsulfat (CaSO_4) in Gegenwart von Wasser bzw. Wärme genutzt, indem es als Füllstoff in einem wasserquellbaren Elastomerkomposit dispergiert wurde. Die mechanische Adaptierbarkeit wird durch die mechanische Verstärkung erreicht, welche bei der Wasseraufnahme des Verbundwerkstoffes entsteht. Anschließend kann diese mechanische Festigkeit (Verstärkung) durch eine Wärmebehandlung wieder in ihren ursprünglichen weichen Zustand (unverstärkter Zustand) zurückgeführt werden. Diese reversible Schaltbarkeit der Verstärkungswirkung des Calciumsulfat-Füllstoffes wird auf die Unterschiede in der Polymer-Füllstoff-Wechselwirkung aufgrund der Transformation der *in situ*-Morphologie (Mikro zu Nano) der Füllstoffpartikel zurückgeführt.

Die vorliegende Arbeit verdeutlicht die Möglichkeiten des Einsatzes konventioneller Kautschuktechnologie bei der Entwicklung mechanisch anpassbarer Komposite mit einem

leicht zugänglichen Stimulus wie Wasser. Die beiden hier untersuchten Strategien eröffnen enorme Perspektiven bei der Konzeption zukünftiger intelligenter Materialien.

Contents

1	Introduction.....	1
1.1	General introduction	1
1.2	Aim and motivation of the work.....	3
1.3	Scope of the work	5
2	Literature review.....	7
2.1	Mechanically adaptive polymer composites.....	7
2.1.1	Mechanical adaptability triggered by different stimuli	7
2.1.2	Water induced mechano-adaptive composites	10
2.1.3	Possible future applications of mechanically adaptive systems.....	14
2.2	Water absorption in elastomer composites	16
2.2.1	Strategies used for developing water swellable elastomer composites.....	17
2.2.2	States of water present in the polymers.....	20
2.2.3	Effect of water absorption on the thermal and mechanical properties	22
2.2.4	Kinetics of diffusion of water in the hydrophilic polymers	24
2.2.5	Application of water swellable elastomer composites	25
2.3	Calcium sulphate and its polymorphic transition	26
3	Experimental.....	30
3.1	Materials	30
3.1.1	Polymers.....	30
3.1.2	Fillers.....	31
3.2	Preparation of rubber composites	32
3.2.1	Compounding and mixing	32
3.2.2	Curing study and molding	34
3.3	Characterization.....	35
3.3.1	Water swelling studies	35
3.3.2	Thermal analysis (DSC and TGA).....	36

3.3.3	Dynamic mechanical analysis (DMA)	36
3.3.4	Stress–strain studies	37
3.3.5	Fourier transform infrared spectroscopy (FTIR).....	38
3.3.6	Morphological analysis	39
3.3.7	X-ray diffraction (XRD).....	40
3.3.8	Raman spectroscopy.....	40
4	Results and discussions.....	42
4.1	Development of novel water swellable elastomer composites based on GECCO/GEPO	42
4.1.1	Miscibility of the polymer blend (GECCO/GEPO) systems	42
4.1.2	Water absorption behavior of GECCO/GEPO blends	49
4.1.3	Effect of water swelling on thermal and mechanical properties	54
4.1.4	Cyclic water swellable characteristics.....	58
4.2	Thermo-responsive mechano-adaptable composites based on solid–liquid phase transition of absorbed water.	60
4.2.1	Quantitative analysis of <i>in situ</i> formed ice crystals.....	61
4.2.2	Characterization of the filler (ice crystals) morphology	64
4.2.3	Polymer–filler interaction	68
4.2.4	Mechanical adaptability analysis	71
4.3	Utilization of <i>in situ</i> polymorphic alteration of the filler structure in designing mechanically adaptive elastomer composites.....	77
4.3.1	Process and conditions for mechanical adaptability	79
4.3.2	Investigation of phase transition characteristics of CaSO ₄ filler.....	83
4.3.3	<i>In situ</i> morphology transformation analysis.....	86
4.3.4	Mechanical adaptability investigations	89
5	Conclusions and outlook.....	96
5.1	Conclusions	96
5.2	Outlooks.....	99

6	References.....	100
7	Appendix.....	109
8	Abbreviations.....	111
9	Symbols	114
10	Figures	117
11	Tables.....	123
12	Publications.....	124

1 Introduction

1.1 General introduction

Stimuli responsive polymers are a wide class of materials which can alter their physical/chemical properties upon exposure to external stimuli like electricity, temperature, humidity, pH, etc. The past decade has seen commercialization of some of the stimuli responsive polymers in the field of aerospace and biomedical engineering¹. One such class of stimuli responsive polymers are the mechanically adaptable polymers, which can change its mechanical properties with respect to external stimuli. These types of materials are synonymously called as mechanically switchable, rigidity tunable, variable stiffness, or mechanically adaptable composites².

The idea behind mechanical switchability/adaptability is largely inspired from marine animals, especially sea cucumber dermis, which can reversibly alter their stiffness in response to a threat/environment³. The hierarchical composite structure of rigid collagen fibrils embedded in a softer viscoelastic hydrogel matrix helps sea cucumber dermis in controlling the stiffness. The differential interaction between the collagen fibrils are known to be the mechanism behind the adaptability, where the aggregated state leads to the high modulus and the disconnected/dispersed state leads to the lower modulus⁴. Similar to sea cucumber dermis, natural materials like wood, hemicellulose, and spider silk also exhibit this special property, when it comes in contact with humidity. These types of biologically inspired systems have attracted huge interest among scientists. In the biological domain, research is being carried out to understand the survival mechanism of the organisms, however engineers and chemist are striving to transfer this knowledge to develop high performance materials for robotics and other applications⁵.

In terms of exposure conditions, it is possible to use large variety of stimuli, ranging from common stimuli like moisture, electricity to the sophisticated Ultraviolet (UV) light and ozone. Due to the large availability and economical concerns, moisture and electricity has garnered huge attention in the development of adaptable composites. In most of the cases, the functional groups on the polymer chain or the functional fillers present in the composite respond to the stimuli and thus stimulating the variable stiffness (adaptability). These stiffness variations might be fully or partially reversible or completely irreversible and their respective response time (fast or slow) depends on the material and the stimuli adopted to alter the mechanical properties. In addition to stiffness variation with time, stiffness variations in space

and shape adaptations are also classified under mechanically adaptable materials, but in this thesis focus is given only on the stiffness variation with time.

Many of the reported mechano-adaptable polymers exploit the transitions in the conformation and configuration of the polymer structure in presence of an external stimulus. Glass transition in polymers is one such case, where 100–1000 times alteration in mechanical properties can be achieved reversibly. One of the simplest mechanisms could be plasticization of the polymer chains with the help of plasticizers (water or suitable solvents) and is supposed to be the key mechanism behind natural materials like hemicellulose⁶. Another widely used mechanism in obtaining variable stiffness is by varying the cross-link density of the polymer system. Cross-links can be classified as covalent (permanent) and non-covalent (temporary) bonds between the polymer chains. For designing mechanically switchable structures, the density of non-covalent interaction between the polymer chains are altered (broken and reformed) to yield such effects. These types of cross-links are also called as sacrificial bonds and is one of the major mechanism behind several natural materials (nacre, human bone) exhibiting adaptable properties⁷. Cross-link density is found to be tuned by several stimuli like UV light, redox chemicals, pH, etc⁸.

There are huge prospects in exploiting the activity of the dispersed filler for obtaining stimuli induced adaptability in the polymer composites. For example, low melting alloy/phase change materials embedded in the polymers can be triggered by Joule's heating mechanism, where the applied electrical current causes increase in the temperature of the composite leading to the melting/softening of the dispersed filler and thus attaining the rigidity tuning or switchability^{2b, 9}. Interaction between the fillers dispersed in the polymer matrix has been altered, between aggregated and dispersed state, in order to obtain a polymer composites which can mimic the reversible stiffness capabilities of the sea cucumber dermis^{4b}. Similarly, the alignment of the dispersed filler particles can be tuned by magnetic field/electric field, leading to the alteration of the mechanical properties, which is also called as magneto-rheological/electro-rheological polymers¹⁰. Strain stiffening, irreversible stiffening occurs during repetitive application of a mechanical force/strain to the polymer composite containing reinforcing fillers, can also be applied for one-way mechanically adaptive systems¹¹. The *in situ* microstructure transformation of the dispersed filler in polymer composites upon exposure to external stimuli (like water) has also been utilized to alter the reinforcing efficiencies of the fillers and thus exhibiting variable stiffness¹².

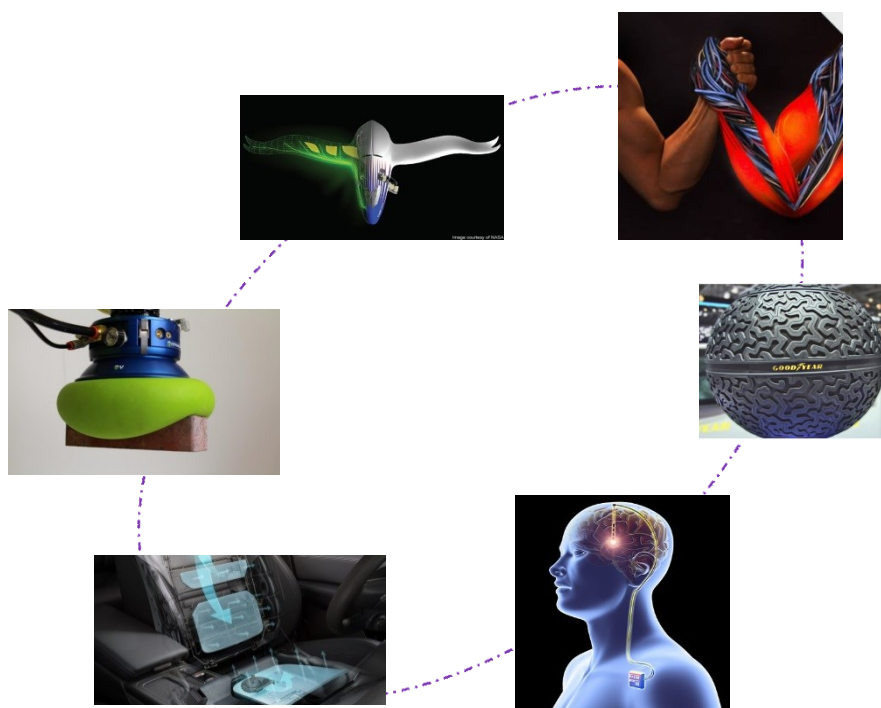


Figure 1.1 Future applications of mechanically switchable materials (images adapted from¹³).

Stimuli responsive elastomer composites have received huge interest in soft robotics and soft matter technologies which composes mostly of elastomers, gels and colloidal suspensions. Due to the similar elastic and rheological properties of the soft elastomer materials with the biological counter parts, these types of soft materials/machines become an automatic choice for the robotic materials¹⁴. More specifically, mechanically adaptive elastomer composites could play a key role in designing sensors, actuators, artificial muscles and skin materials used in humanoid robots^{2a, 9a, 15}. Additionally, mechanically adaptive composites could also be used in several areas like dynamic implants, active orthoses, protective clothing, switchable membranes, smart seating, smart tires, deployable structures and smart sealing applications (Figure 1.1)¹⁶.

1.2 Aim and motivation of the work

The main idea behind this work is to develop elastomer composites which can vary between *hard* and *soft states* when exposed to external stimuli. Based on the literature survey, it is found that several materials and stimuli were reported for achieving mechanically adaptable polymer composites, but very little work focuses on elastomer science and technology for

preparing such smart materials. The few reported literatures utilizing the elastomer matrices are very stiff, due to the presence of large amount of fillers and hence cannot be considered to exhibit flexible and rubbery characteristics¹². Thus, the major objectives behind this work are listed as follows:

- a) **Elastic characteristics:** The developed adaptable composites should retain its flexibility/rubbery characteristics in both the *hard* and *soft states*, for example, high elongation at break or high stretchability.
- b) **Easily accessible stimuli:** To develop adaptable composites using water, an abundantly available stimulus, rather than other common stimuli like electricity, UV light, ionic strength or mechanical forces. This approach aims in avoiding the need of extra chemicals/equipment/energy.
- c) **Rapid response:** To design and develop elastomer composites which can respond rapidly to the external stimuli and thus enhancing the applicability of the developed materials.
- d) **Simple, scalable and inexpensive:** Exploiting the highly successful elastomer technology in preparing stimuli responsive materials and in doing so, the developed materials could be fast tracked for commercialization.

Based on the above objectives, two different approaches involving different phase transition mechanisms of the materials are explored by dispersing it as filler in elastomer composites.

- i. Solid–liquid phase transition of the absorbed water is utilized in altering the mechanical property of the composites between *hard* and *soft states* at different temperatures.
- ii. Polymorphic transition of the dispersed calcium sulphate filler and the corresponding *in situ* morphology transformation with the absorption of water, is expected to yield reversible adaptable characteristics.

In order to design water induced adaptive composites that can respond quickly, the elastomer composites need to absorb water as much as possible. Due to the unavailability of the stable water swellable elastomer composites commercially, a novel polymer blend system containing elastomer and hydrophilic polymer resin is developed with repeatable water absorption characteristics.

1.3 Scope of the work

Chapter 1 provides a general introduction about the mechanically adaptable composites and its possible future applications. The aim and motivation behind this work are also highlighted in this chapter.

Chapter 2 presents a current state-of-the-art of work involving the detailed description of the different methods, concepts and materials utilized for developing mechanically adaptable polymer materials. This overview also distinguished the different stimuli (like electricity, water, strain and other chemical stimuli) involved in obtaining mechanical adaptability. Additionally, the existing knowledge about the development of water swellable elastomer composites are critically analyzed and discussed. Furthermore, the fundamental understanding of water swelling process and its effect on the physical properties has also been reviewed.

Chapter 3 is concerned with the specifications of the utilized materials along with the compounding recipes used in the preparation of the elastomer composites. The methods and processes involved in the preparation of elastomer composites are also described in this section. Additionally, the experimental methods and the analytical techniques used for characterizing the composites are also presented in this chapter.

Chapter 4 presents the results and discussions related to this work. This chapter is mainly divided in to 3 sub-chapters. **Chapter 4.1** deals with the development of novel water swellable elastomer blend system, which is used for obtaining water responsive mechanically adaptive elastomer composites. Differential scanning calorimetry (DSC) and dynamic mechanical analysis (DMA) studies are utilized to understand the miscibility/compatibility between the polymers in the blend, which is one of the essential property of a blend system. Further, water swelling abilities of the developed elastomer blends, mechanism and kinetics of water swelling process are presented in this chapter. More specifically, in the application point of view, the retention of mechanical and thermal properties of the developed water-swollen elastomer blends are also critically discussed here along with the repeatable water absorption characteristics. **Chapter 4.2** discusses the novel method of utilizing the absorbed/swollen water as the active filler in obtaining the mechanical adaptability. To start with, the water swellability of the hydrophilic elastomer is tuned by varying the cross-link density. Quantitative and qualitative analysis of the absorbed water turned ice crystals have been investigated. Further, the morphology of the embedded ice particles (solidified water) at low temperature (below freezing temperatures) is analyzed using cryo-transmission electron

microscopy (cryo-TEM) and its interaction with polymer chain is also characterized by Fourier transform infrared (FTIR) spectroscopy. Ability of the absorbed water in exhibiting phase transition behavior and its effect on the mechanical properties at different temperatures (*i.e.*, mechanical adaptability) are discussed using DMA and stress–strain analysis. Finally, the extent of reversible/repeatable alteration of the mechanical properties and their schematic mechanism behind thermo-responsive mechanical adaptability are discussed. **Chapter 4.3** discusses the possibility of using polymorphic calcium sulphate as the active filler for obtaining mechanical adaptability. The methods and conditions involved in obtaining mechanical adaptability are discussed after the brief description of the composites containing as-prepared calcium sulphate filler. The phase transition induced morphology changes of the calcium sulphate filler particles present in the elastomer composites upon water and heat treatment are characterized by X-ray diffraction (XRD), Raman spectroscopy, scanning electron microscopy (SEM), and transmission electron microscopy (TEM) analysis. The effects of *in situ* morphology transformation on the mechanical properties (stress–strain and DMA) are presented in detail (*i.e.*, mechanical adaptability). Finally, the mechanism of adaptability is summarised in this sub-chapter.

Chapter 5 highlights the conclusions obtained from the discussed results and in addition the possible outlook for the future work is also presented here.

2 Literature review

2.1 Mechanically adaptive polymer composites

Mechanically adaptable polymer composites are a class of stimuli responsive polymer composites which can reversibly change its mechanical properties when it comes in contact with stimuli like temperature, electric field, light, water, solvents or ions. These composites are inspired from natural creatures like, the sea cucumber dermis which has the ability to rapidly and reversibly change the stiffness of their dermis (connecting tissue) when it is immersed in water^{4b}. One such type of sea cucumber species is *Cucumaria frondosa*, which exhibits a 10 fold modulus contrast (mechanical adaptability) within seconds and prevents itself from the potential threat. A series of studies were performed on the dermis of the sea cucumber and was found that the dermis exhibits a nanocomposite like structure consisting of rigid, high aspect ratio collagen fibrils dispersed in a viscoelastic matrix of fibrillin microfibrils¹⁷. The stiffness of the dermis depends on the ability of the adjacent collagen fibrils to transfer stress via transiently established interactions. These interactions between the collagen fibrils are modulated by the several locally secreted soluble glycoproteins in the living tissue based on the requirements. Stiparin, a constitutive glycoprotein of the extracellular matrix is reported to induce aggregation of the collagen fibrils causing the dermis to stiffen¹⁸. On the other hand, a second type of glycoprotein, softenin is secreted (when it comes in contact with water), which is usually called as stiparin inhibitor, reacts with stiparin and reduces the aggregation of the collagen fibrils, resulting in the soft nature of the dermis^{3, 12b}. These type of adaptive systems are attracting great interest not only for better understanding of the survival of organisms at their challenging times (by taking advantage of mechanical morphing), but also for material chemists, where the main aim is to develop smarter materials for the applications ranging from active dampening systems to soft robotics.

2.1.1 Mechanical adaptability triggered by different stimuli

Several array of materials and strategies have been combined to obtain mechanical property changes (adaptability) upon exposure to external stimuli. To realize the mechanical adaptability/switchability, researchers have exploited various mechanisms ranging from simple Joule's heating effect to the complicated reversible cross-linking mechanisms by using various stimuli like electricity, water, pH, temperature and others. Some of the important strategies will be discussed in this section, distinguished in the framework of external stimuli.

The passage of electricity through any resistive material will lead to rise in temperature/heat and this phenomenon is termed as Joule's heating. This generated heat (or temperature rise) in the polymer composite, has been utilized in obtaining phase transition (like melting/softening/glass transition) of the polymer/filler and thus altering the mechanical properties^{9b, 19}. One such example was demonstrated by Shan *et al.*^{2a} using a laser patterned conductive poly(propylene-co-ethylene) rubber (cEPM) embedded in an electrical and thermal insulating sheet of poly(dimethyl siloxane) (PDMS). When the temperature (developed due to the Joule's heating) exceeds the critical softening temperature of the cEPM ($T_s = 75\text{ }^{\circ}\text{C}$), the composites softens and reaches a tensile modulus of 1.5 MPa from 37 MPa. The potential application of the developed cEPM/PDMS composites as active tendons in artificial muscles was successfully demonstrated. Similarly, a conducting phase change material (rigid low melting point alloy, LMPA) embedded in PDMS matrix was developed and the large change in the stiffness is obtained by the melting of LMPA microstructure as a result of Joule's heating. Fast transition from rigid to soft states occurred in less than 1 s (stiffness change ratio of about 25) and at a low power of 500 mW. The ability of developed materials to function as strain sensors for measuring very precise strains was demonstrated^{2b}.

Auletta *et al.*^{8b} employed electrochemically reversible cross-links to prepare mechanically switchable composites on the application of electric potential. In this study, hydrogel based on sodium acrylate, sodium (4-styrene sulfonate) and poly(ethylene glycol diacrylate) was prepared and cross-linked with the help of Ferric chloride. The transition from Fe^{3+} to Fe^{2+} (redox driven switching) occurred in the cross-link, when the electric potential is applied. The initially formed Fe^{3+} state is found to be strongly interacting with the carboxylate groups on the polymer chain. When the electric potential is applied, oxidation takes place and Fe^{3+} state is replaced by weak to non-binding Fe^{2+} and thus their interaction is diminished. This has led to changes in mechanical property from 1.0 to 0.6 MPa. Further the addition of graphene oxide (GO) not only reinforced the hydrogel, but also enhanced the switchability and its rate (shown in Figure 2.1).

Chemical parameters like pH value or salt concentration can be utilized as stimuli in achieving chemo-responsive mechano-adaptability, especially in polyelectrolytes and supramolecular networks. A polyelectrolyte multilayer system consisting of oppositely charged poly(styrene sulfonate) (PSS) and poly(diallyldimethylammonium) (PDADMA) as individual layers yielded physically cross-linked structures with the help of electrostatic or ion pairing. The crosslinked (PSS/PDADMA) multilayer exhibited a maximum of 17 MPa (elastic

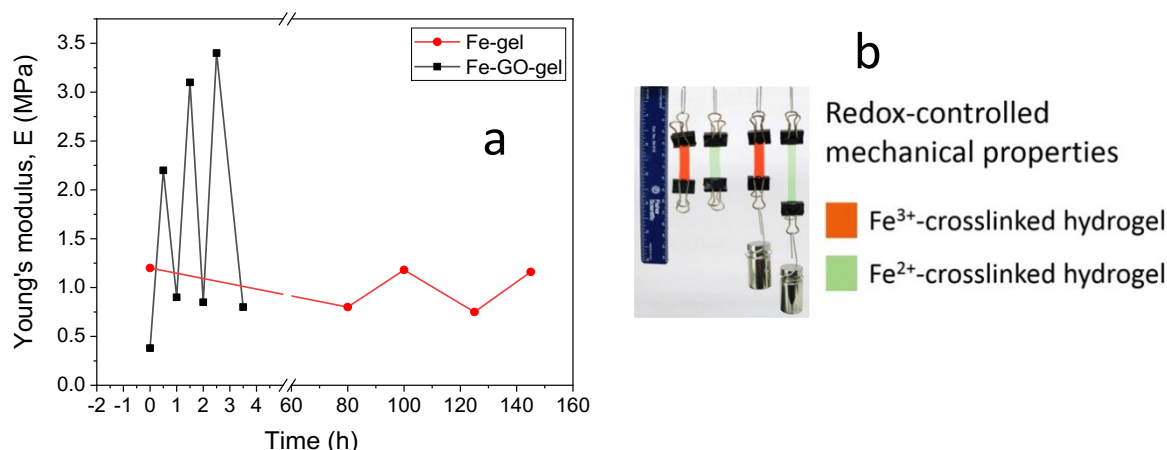


Figure 2.1 a) Cyclic studies of Fe crosslinked hydrogel when the electric potential is applied/removed. The enhanced rate and degree of switchability of graphene oxide dispersed hydrogels can also be observed here, b) Fe³⁺ crosslinked composite exhibited higher mechanical properties and the load carrying capabilities than the Fe²⁺ crosslinked hydrogel (adapted and redrawn with permission from^{8b}).

modulus) and the modulus change (switchability) was realized by exposing the PSS/PDADMA multilayer to the salt solution (sodium chloride solution) of varying concentration. The exposure to the salt solution weakened the cross-link between PSS and PDADMA, altering the cross-link density of the multilayer system, leading to the mechanical adaptability²⁰. Daigle *et al.*²¹ prepared a functional polymer, which is a linear copolymer of ethylene and diacetone acrylamide, exhibiting a crystallinity of about 45%. When the developed polymer is exposed to hydrazine gas, cross-linking occurred and further heating the polymer above its melting point (>130 °C), the crystallinity reduced to 10%. The lost crystallinity can be recovered by breaking the cross-link using ozonolysis process. This special polymer exhibiting two different states (crystalline and amorphous) when triggered upon action of simple chemicals can be utilized to prepare mechanically adaptive composites.

Biyani *et al.*²² synthesized a photo-reactive benzophenone derivatized cellulose nanocrystals (Bp-CNCs) and coumarin derivatized cellulose nanocrystals (Cou-CNCs) by reacting the hydroxyl groups present on the cellulose nanocrystals with 4- benzoylphenyl (6-isocyanatohexyl) carbamate and 7-coumaryl-(6-isocyanatohexyl) carbamate respectively. Then the synthesized materials were blended with poly(ethylene oxide-co-epichlorohydrin) (ECO) to obtain photo-responsive mechanically switchable polymer nanocomposites. On irradiation with 365 nm UV light, covalent bonds between Bp-CNCs/Cou-CNCs and the polymer chains are formed (confirmed by UV-visible absorption spectra, Figure 2.2a). This covalent bonding/cross-linking increased the tensile storage modulus from 222 MPa to 293 MPa and

199 MPa to 291 MPa for 10 wt-% Bp-CNCs and Cou-CNCs containing ECO nanocomposites respectively at room temperature (25 °C) as shown in Figure 2.2b.

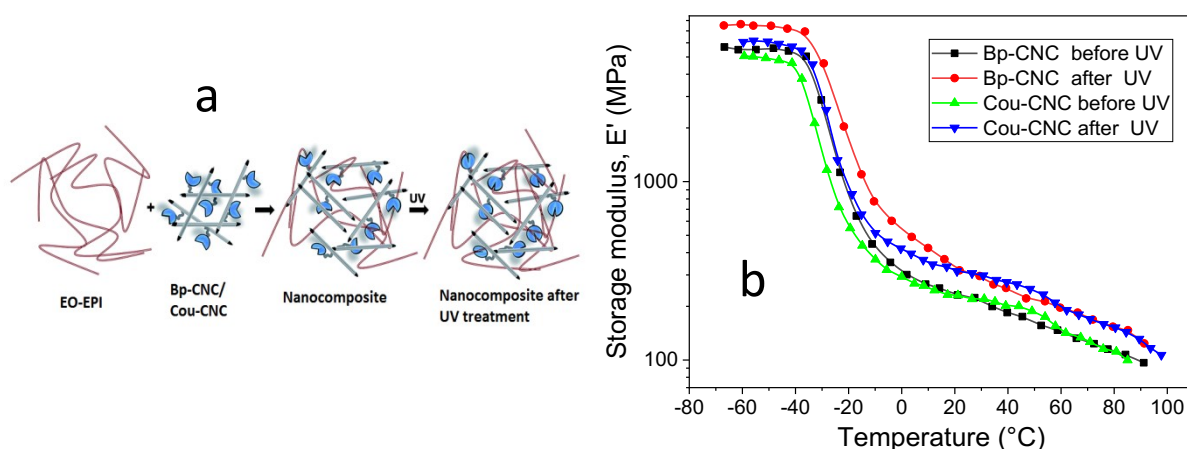


Figure 2.2 a) Schematic diagram of sample preparation and the mechanism behind the switchability (cross-linking between the polymer), b) temperature sweep analysis (DMA) of 10 wt-% Bp-CNC and Cou-CNC nanocomposites before and after UV irradiation. Enhanced modulus values after UV irradiation can be clearly seen (adapted and redrawn with permission from²²).

The bonding–debonding of polymer chains on the filler particles can be controlled under mechanical excitation (periodic deformation) to achieve responsive and adaptable composites¹¹. Poly(methyl methacrylate) (PMMA) is chosen as the polymer matrix due to its ability to interact with the hydroxyl groups on silica surfaces via hydrogen bonding. The mechanical properties of PMMA/silica composites strengthened with the increase in rest time during successive cyclic deformation, i.e., the deformed and rested sample exhibited higher elastic modulus than the undeformed initial sample. This unusual property is attributed to the enhanced entanglement of polymer chains at the polymer–filler interfaces (during the resting time after deformation), as evidenced from the Fourier transform infrared (FTIR) spectroscopy and small-angle neutron scattering (SANS) profiles. This type of dynamic mechanical reinforcement mechanism can be applied for designing mechanically responsive and adaptive composites which lack any responsive environment or constituents in the composites.

2.1.2 Water induced mechano-adaptive composites

In order to mimic the mechanically adaptable behavior of sea cucumber dermis using water as a stimulus, Shanmuganathan *et al.*²³ prepared a composite containing cellulose whisker and ECO/poly(vinyl acetate) (PVAc) with the help of special technique which is realized by three dimensional template approach. ECO/PVAc and cellulose nanocrystals (CNC) were chosen to

mimic the low modulus matrix (skin) and the nanofillers (collagen) present in the sea cucumber dermis (Figure 2.3a, b). The addition of CNCs has led to enhanced mechanical properties and this reinforcement is reported to be due to the formation of three dimensional filler networks present inside the polymer matrix (*hard state*). When the prepared samples are swollen in water, the absorbed water formed hydrogen bonding with the CNC particles resulting in the breakdown of the three dimensional filler networks responsible for the reinforcement. Thus the absorption of water has led to several times reduction in the stiffness of the composites (*soft state*). Further, the removal of water reverted the three dimensional filler networks to its reinforced initial hard state (Figure 2.3c).

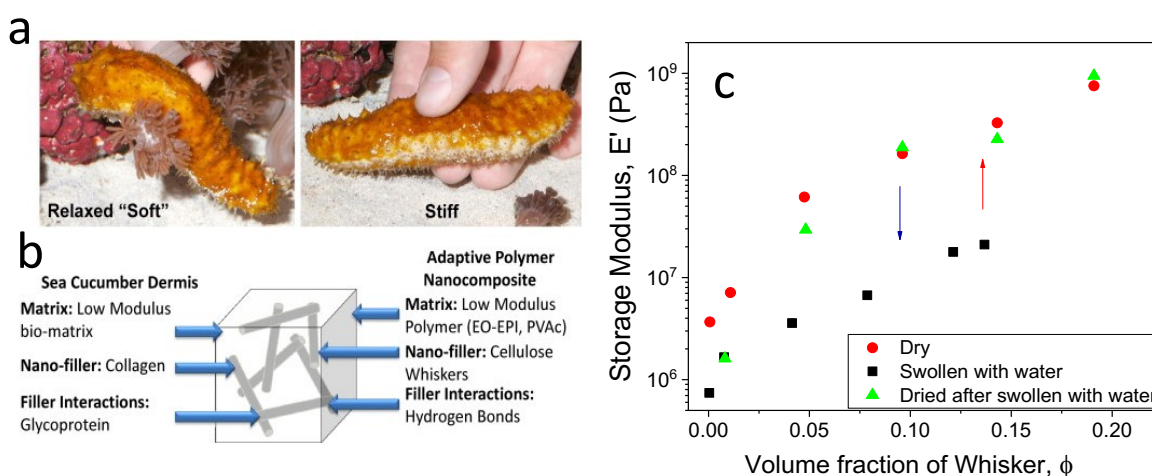


Figure 2.3 a) Mechanically adaptable behavior of sea cucumber dermis, b) material design for mimicking the sea cucumber dermis, c) results (mechanical switchability) obtained from the developed materials mimicking sea cucumber dermis (adapted and redrawn with permission from^{4a}).

Similar concept of formation/breakage of three dimensional filler (CNC) network upon the addition/removal of water has been explored in hydrophobic poly(styrene-co-butadiene) (SBR) and poly(1,3-butadiene) (BR) rubbers. These composites were prepared using three different approaches: solution casting, compression molding and template method. Interestingly, the hydrophobic polymer matrix (SBR) containing CNCs has also led to significant softening with the absorption of water. This clearly indicated the formation of hydrophilic channels by the polar CNCs within the hydrophobic SBR matrix. On the other hand, the rate and degree of mechanical switchability is found to be dependent on the fabrication method, for example, higher degree of switchability is displayed by the composites made from solution casting, followed by compression molding and template approach²⁴. Similarly, the source from which the CNCs are obtained, have significant impact in the mechanically switchable properties of the composites. CNCs obtained from tunicates (CNC-t) and the abundantly available cotton (CNC-c) were blended with poly(vinyl alcohol) (PVA)

and it was found that the CNC-t composites showed superior mechanical properties when compared to the CNC-c composites, which is attributed to the higher aspect ratio, polymer–filler interaction and the modulus of the filler material itself. Further, it was found that the large mechanical contrast between wet and dry states was observed for CNC-c containing composites than the CNC-t composites. This effect is attributed to presence of strong polymer–filler interaction in CNC-t composites compared to CNC-c composites, which restricts the breakage of three dimensional filler network²⁵.

Similar to cellulose nanocrystals, chitin nanocrystals also exhibited similar characteristics when solution casted with carboxylated poly(styrene-co-butadiene) rubber (XSBR). The addition of chitin nanocrystals has also led to the formation of percolating network within the XSBR polymer matrix and the exposure of this polymer film to water has led to the plasticization and breakdown of the percolating network leading to the mechanical switchability from 35 MPa to 5 MPa in less than 5 hours²⁶.

Similarly, Stone *et al.*²⁷ prepared an all-organic stimuli responsive polymer composites by incorporating an electrospun mat of PVA into the polymer matrix of PVAc/ECO using solution casting technique. The mechanical properties of the electrospun PVA/PVAc and PVA/ECO composites increased significantly with the addition of PVA filler mat. Both the PVAc and ECO composites exhibited significant modulus reduction when exposed to water. But only PVAc/PVA presented a reversible modulus reduction by a factor of 280 upon exposure to water, whereas ECO/PVA composites showed irreversible modulus reduction. This switchability (modulus reduction) is related to the variations in the polymer–filler interaction, filler–filler interaction and the filler crystallinity upon exposure to water²⁸. The incomplete recrystallization behavior of PVA mats as consequence of strong interaction between PVA and ECO was reported as the reason behind the irreversible switchable nature of ECO composites.

Like sea cucumber dermis, several natural materials also exhibit variable stiffness with the slight changes in temperature/humidity of the environment. One of the very well-known example is hemicellulose present in plants and wood. An abrupt loss in stiffness by almost three orders of magnitude from 8 to 0.01 GPa (Young's modulus of the composite) were reported^{6b, 29}. Another interesting example could be the spider silk where the modulus values varied from 10 GPa to 0.03 GPa at the highest humidity values³⁰. These stiffness/modulus changes were attributed to the ability of the absorbed water molecules to plasticize the polymer chains and thus leading to the early glass transition^{6a}.

Conversely, Musso *et al.*^{12a} developed a reactive composite (hydrogenated poly(nitrile-co-butadiene) rubber (HNBR)/cement) with the help of conventional elastomer processing technology, exhibiting water responsive mechanically adaptable properties. When hydrated for the first time, cement particles in the composite leads to the formation of calcium silicate hydrate gel and thus resulting in the enhanced stiffness from 30 MPa to 150 MPa. Additionally, post polymerization modification of nitrile groups (present in HNBR) to carboxylate anions (-COO^-) was confirmed by the FTIR analysis during the hydration process (shown in Figure 2.4). The ionic cross-linking between the newly formed carboxylate anion and the cations (Ca^{2+}) from the cement were formed when the composite is dried and thus resulting in enhanced modulus values from 150 to 400 MPa. Further when the composite is hydrated for the second time, the ionic cross-linking solvated and returned to its initial modulus of 150 MPa. This reversible formation/solvation of ionic cross-link between the carboxylate anion and the cations of the cement during dry/wet process has led to reversible mechanical adaptability between 150 MPa to 400 MPa^{12a, 31}.

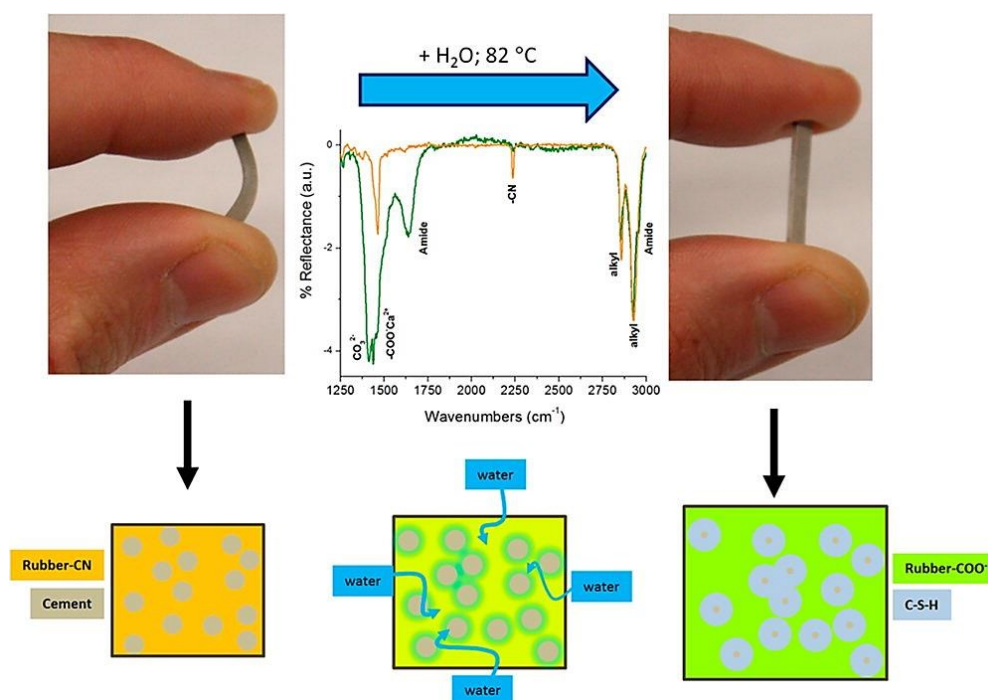


Figure 2.4 Development of strong and hard material from soft and flexible material using water as stimuli in HNBR/Cement composites. Comparison of FTIR analysis of dry and water swollen sample indicating the formation of carboxylate anion in the water-swollen sample. Also the morphology of the composite and the mechanism of mechanical adaptable process is also shown below (adapted with permission from³¹).

Similarly, magnesium oxide (MgO) can be used as novel water responsive reinforcing filler for HNBR composites³². The rubbery HNBR-MgO (40 vol-%) composite exhibits three times

higher storage modulus (80 MPa) on hydration, and on drying the modulus further increased to 200 MPa. This reinforcement is attributed to the conversion of micro-sized MgO in to nano-sized Mg(OH)_2 fillers upon hydration. The finer nano-particles are expected to have a higher contact surface area with the polymer and thus leading to higher reinforcement (modulus increase). On drying, the free water present in the composite evaporated and thus exhibited even higher properties^{12b}. Unfortunately, the higher transition temperature (Mg(OH)_2 to MgO) of about 400 °C restricted the reversible nature of mechanical adaptability process. In both the above cases, response time required for achieving higher adaptable state is very high (2 months for HNBR/MgO and 23 days for HNBR/Cement composites), which could possibly restrict their commercialization. The higher response time could be attributed to the poor water absorption capabilities of the hydrophobic rubber (HNBR) used in this study.

Comparison of few interesting and noteworthy research works regarding the mechanical adaptability explored in this review is listed in Table 2.1. This table indicates the attempts made by several researchers in obtaining mechanical adaptability using different stimuli and mechanism.

2.1.3 Possible future applications of mechanically adaptive systems

Smart materials that can alter its stiffness based on the environment could find applications in a wide range of fields from robotics to computing to architecture^{2b}. Some of the examples include:

- i) **Automotive design:** Switchable materials can be employed to improve both safety and comfort (for example: adaptive seating) which is generally a very contrasting feature for material scientists³³.
- ii) **Civil engineering:** Damages caused by natural calamities like winds and earth quakes can be reduced by changing the stiffness of the structure/material used in the buildings³⁴.
- iii) **Robotics:** Universal grippers for holding different type of materials³⁵, huge potential as adaptable skin material, artificial muscle, etc.
- iv) **Biomedical fields:** Stiffness changes in the catheters and endoscopes can be used to perform non-invasive surgeries with less tissue damage, reduced pain and greater efficiency³⁶, intra cortical implants which required to be stiff during the insertion and soften during the application (body fluids)³⁷, targeted drug delivery, etc.

Table 2.1 Materials, stimuli and strategies used in achieving mechanical adaptability throughout the literature survey: (AR-adaptability ratio)

Polymer	Filler	AR	Response Time	Stimulus	Mechanism	Ref
PDMS	cEPM	100	< 2 s	Electricity	Softening	2a
PDMS	LMPA	25	< 10 s	Electricity	Melting	2b
ECO PVAc	CNC	10^2 10^3	48 h	Water	Filler–filler, Polymer–filler interaction	4b
Hemicellulose	-	800	-	Temperature & moisture	Glass transition	6b
Polyurethane	-	10^3	100 s	Temperature	Glass transition	9a
PMMA	Silica	2	-	Strain	Filler-polymer interaction	11
HNBR	Cement	10	23 d	Water	Phase transition (filler)	12a
HNBR	MgO	100	48 d	Water	Phase transition (filler)	12b
PSS/DAAM	-	20	-	Salt (NaCl)	Reversible cross-linking	20
SBR	Cellulose	150	5–6 d	Water	Filler–polymer interaction	24
ECO/PVA	PVA mat	150 280	15 min 20 min	Water	Filler–polymer interaction	28b
Spider silk	-	330	-	Temperature & moisture	Glass transition	30
Polyurethane foams	Wax	10^2	-	Temperature	Melting/self- healing	38

v) **Aerospace:** Adaptable wings in aerospace fields which can lead to reduced fuel costs and noise during take-off and landings³⁹.

vi) **Smart tires:** Rigidity/modulus of the tires can be varied to modify the size of the contact patch, which in turn can be used to adapt to wet, uneven, slippery and normal conditions⁴⁰.

One of the areas where these types of materials find immediate application is vibration control. For example, cyclic stiffness modulation occurring at the helicopter blade root can be used to significantly reduce the vibrations in the helicopter⁴¹. In this context, adaptive elastomer composites finds application in mounts, dampers, buffers, etc⁴².

Mechanically switchable composites can be widely used for sensors (strain sensors, humidity sensor, displacement sensors) and actuators^{2b, 9b}. More specifically, these materials could be used in designing deployable structures, microfluidic systems, etc.

2.2 Water absorption in elastomer composites

In general, most of the rubbers are hydrophobic in nature and so the rubber compounds are expected to absorb very low amount of water (<5%). Even these low amount of water absorbed by the rubber compounds are mainly due to the presence of microdefects and polar additives (accelerators, activators and other fillers like clay, whiting, barytes) present in the composites⁴³. Rubber compounds when exposed to water for extended period of time and at high temperatures may absorb very large amount of water. Briggs *et al.*⁴⁴ studied the effect of temperature on the water absorption of the rubber compounds and reported that the rate of water absorption increased with the temperature and it was found that almost 40% of water was absorbed at 160 °C in the absence of oxygen. Similarly, water absorption can be enhanced by adding hydrophilic fillers like silica, cellulose and other bio-based fillers like rice husk, starch, hemp, sisal fibers, etc⁴⁵. The presence of polar moieties on these fillers absorb significant amount of water and the use of silane coupling agent slightly reduced the water absorbing ability of the fillers. The water absorbed by adding hydrophilic fillers are found to be always less than 20%.

Generally, in most of the conventional applications, water absorption by the elastomer composites are seen as disadvantageous as it reduces the mechanical properties of the composites⁴⁶. But for some special applications like water sealing or prevention of water leakage, water absorption or more precisely water swelling become very important. In general, water absorption is a term used to indicate the water uptake, while swelling is a more scientific term used to indicate the expansion/relaxation of polymer chain caused due to the absorption of water. But in most of the cases, the words swelling and absorption are interchangeably used.

In this work, the focus is given on preparing and utilizing elastomer composites which can absorb/swell significant amount of water for adaptive applications, thus the state of the art involving elastomer composites which can absorb significant amount of water will be discussed more in this section.

2.2.1 Strategies used for developing water swellable elastomer composites

The water swellability of the rubber composites can be improved by mixing the hydrophobic rubbers with water absorbent materials such as poly(acrylic acid) (PAA), PVA, starch and others. Compatibilisers and other fillers are used to compensate the marked polarity difference between the hydrophobic rubbers and the water absorbent resins. Such water swellable elastomer composites exhibited extremely high degree of swelling (1000% by weight) with high rate. Different combinations of rubbers, water absorbent resins, and compatibilisers are used to prepare water swellable elastomer composites and are briefly discussed in the Table 2.2.

Table 2.2 Combination of rubbers, water absorbent resins, and compatibilisers used for preparing water swellable elastomer composites

Rubber	Water absorbent resin	Compatibilisers/fillers	Water swelling %	Ref
PDMS	PAA (60 phr)	Aminopropyltriethoxysilane	600	47
Poly(cis-1,4 isoprene) (NR)	Cassava starch grafted polyacrylamide (20 phr)	Poly(ethylene oxide) (PEO)(10 phr), Trimethylolpropane trimethacrylate (5 phr)	400	48
Chloroprene	Sodium polyacrylate (50 phr)	PEO (10 phr)	700	49
SBR	Sodium polyacrylate (40 phr)	Poly(ethylene oxide)-block-poly(butyl acrylate) (20 phr), Poly(ethylene glycol) (15 phr)	1800	50
Poly (epichlorohydrin)	Cross-linked polyacrylate (100 phr)	Poly(vinyl alcohol)-graft-poly(butyl acrylate)	900	51
Poly(ethylene) (30phr)/poly(nitrile -co- butadiene) (70 phr)	Sodium polyacrylate (70 phr)	Chlorinated polyethylene (6 phr)	960	52
Poly(ethylene-co-propylene-co-ethylidene norborene)(EPDM)	Cross-linked polyacrylate (30 phr)	Silica (30 Phr)	650	53

Though the prepared elastomer composites exhibited significant water swelling abilities, several shortcomings are reported during the water swelling experiments which limits their commercialization^{47, 54} and are:

- 1) Separation/leaching of water absorbent resin from the composites occurred upon contact with water for a long period of time. This has led to the reduced degree and rate of swelling in the consecutive water swelling cycles.
- 2) The mechanical properties of water swollen and dried elastomer composites decreased significantly when compared to the non-swollen elastomer composites due to the formation of holes/pores as a result of the loss of water absorbent resins, even after the addition of compatibilisers (Figure 2.5).

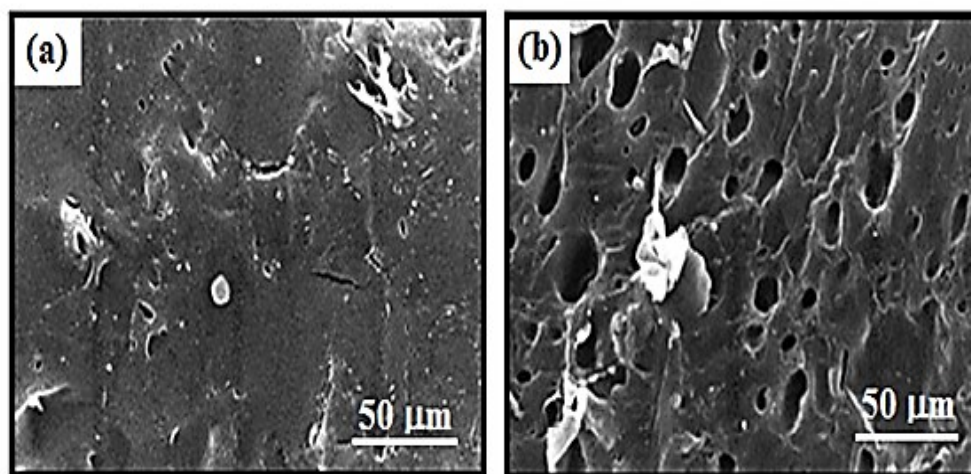


Figure 2.5 SEM images of NR/sodium polyacrylate vulcanisates (with PEO as compatibilisers): a) before and (b) after water immersion. The loss of water absorbent resin from the elastomer composites leading to holes/pores is shown in the image (adapted with permission from⁴⁸).

These limitations occur due to the poor compatibility between the water absorbent resin and the hydrophobic elastomer even after the addition of compatibilisers. There have been a lot of researches being carried out extensively to solve these incompatibility issues. Nakamura *et al.*⁵⁵ elucidated that separation of water absorbent resins can be reduced, when the water absorbent resin is homogeneously dispersed along with water soluble resins (like PEO, poly(vinyl pyrrolidone), hydroxyethyl cellulose) in the elastomer composite.

The compatibility between the water absorbent resin and the elastomer matrix is said to be improved, when the water absorbent resin (sodium acrylate NaAA/lithium acrylate LiAA) is formed *in situ* during the mixing process with rubber⁵⁶. The *in situ* polymerization of the NaAA/LiAA in the chlorinated polyethylene elastomer (CPE) was initiated by the addition of

peroxide and was confirmed with the help of FTIR. More than 200% of water absorption was observed at 50 phr loading of the *in situ* formed NaAA/LiAA in the composite (Figure 2.6a). The mechanical properties of the elastomer composites containing *in situ* formed water absorbent resin improved with the addition of the NaAA/LiAA, which was found to be due to the increased ionic cross-link density with the increase of NaAA/LiAA content. Even after the *in situ* preparation of water absorbent resins, the mechanical properties (tensile strength) of the water swollen-dried composites were very low, compared to the dry composites and this contrast increased with the filler content (LiAA) as shown in Figure 2.6b. This once again indicates the leaching of the water absorbent resins.

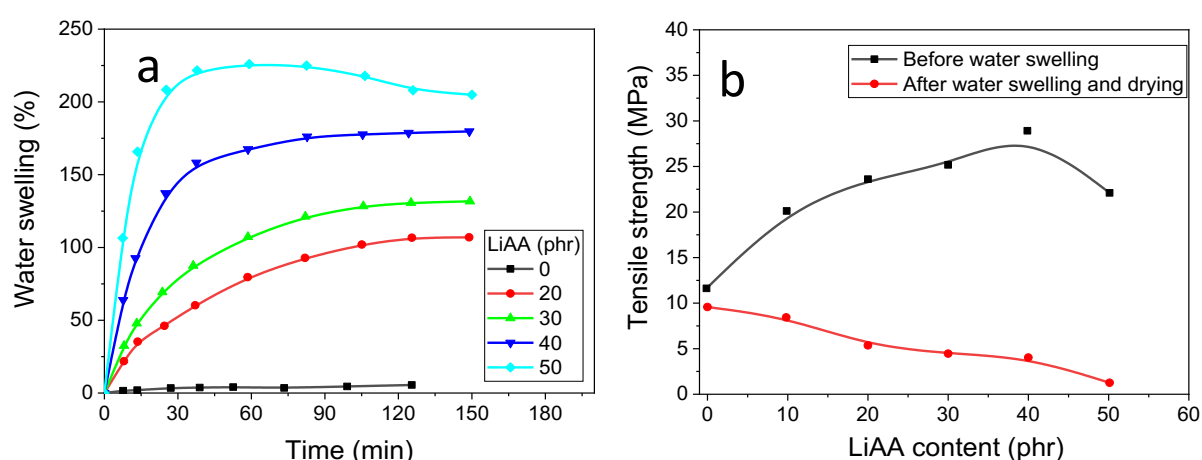


Figure 2.6 a) Water absorption characteristics and b) mechanical properties of CPE-LiAA containing composites before and after water swelling process (adapted and redrawn with permission from^{56a}).

Amphiphilic polymers are synthesized by grafting the water absorbent resin on the elastomer matrix chemically and are used as compatibilisers for the water swellable blends⁵⁷. An amphiphilic polymer i.e., chlorinated poly(ethylene)-graft-poly(ethylene glycol) (CPE-g-PEG) was synthesized based on the reaction between the chlorine in CPE and sodium salts of PEGs. The developed amphiphilic polymer CPE-g-PEG was used as compatibiliser to improve the compatibility between CPE rubber and the poly(acrylic acid-co-acrylic amide) (P(AA-AM)) resin. The addition of amphiphilic graft co-polymer improved not only the mechanical property, but also the water swelling characteristics of the elastomer composites (Figure 2.7a). More importantly, a significant increase in water swelling ability during the consecutive swelling cycles were obtained for the compatibilized system compared to the uncompatibilized CPE/P(AA-AM) composites (shown in Figure 2.7b), indicating the decreased loss of the water absorbent resin with the addition of amphiphilic polymer.

The concept of interpenetrating polymer networks (IPNs) has been used to control the phase morphology of the immiscible polymer blends and this technology has been investigated for the preparation of compatible and stable water swellable elastomer composites. Riyajan *et al.*⁵⁸ prepared a semi-interpenetrating polymer network (semi-IPNs) consisting of epoxidised poly(cis-1,4 isoprene) (ENR) and PVA with maleic anhydride as a cross-linking agent. The addition of maleic anhydride reduced the crystalline content and cross-linked with the PVA in the semi-IPN films. Semi-IPNs exhibited good mechanical properties, thermal stability and high water swelling ratio. SEM images showed no phase separation indicating the compatibility between ENR and PVA networks present in the semi-IPNs.

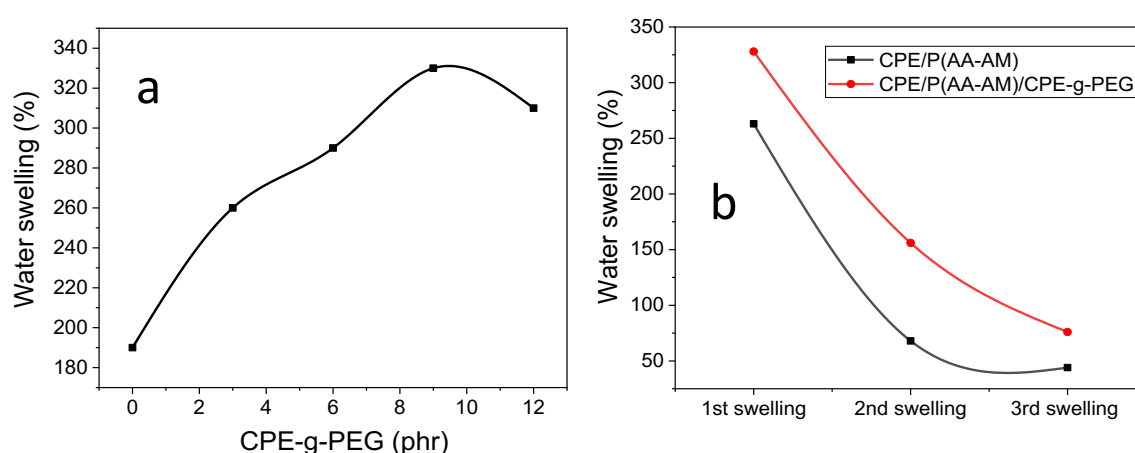


Figure 2.7 a) Effect of amphiphilic compatibilisers (CPE-g-PEG) on the water swelling ratio, b) Water swelling abilities after three consecutive cycles of CPE/P(AA-AM) composites (adapted and redrawn with permission from^{57b}).

Similarly Peng *et al.*⁵⁹ developed interpenetrating polymer networks composed of gelatin hydrogel and thermoplastic polyurethane elastomer with stable mechanical and water swelling property. But, still approximately 10% and 50% loss of the hydrogel was found at room temperature (RT) and 37 °C, respectively after 30 days of immersion in water.

Though several compatible and stable water swellable systems have been developed, the loss (leaching) of water absorbent resin from the elastomer matrix is still reported and has been a major concern in this aspect.

2.2.2 States of water present in the polymers

Water absorbed by hydrophilic polymers exhibits different thermodynamic properties when compared to bulk water⁶⁰. This unusual behavior is attributed to the strong interaction of water molecules with the polar groups present in the hydrophilic polymer. The absorbed water in the hydrophilic polymer can be classified into three types: non-freezable bound water,

freezable bound water (also called intermediate water) and free water⁶¹. Initially, the water molecules get confined between the polymer layers due to its strong interaction with the polar groups of the hydrophilic polymer and are termed as non-freezable bound water. Further addition of water exhibits weak interaction with the hydrophilic group providing freezable characteristics and is termed as freezable bound water. More addition of water gets isolated and is termed as free water (Figure 2.8a). Generally non-freezable bound water does not exhibit any detectable phase transition over the range of temperatures, whereas both free water and freezable bound water exhibit melting points at different temperatures: the crystals of freezable bound water melt at temperatures less than 0 °C and the ice crystals from the free water melts at or above 0 °C⁶². Ping *et al.*⁶² confirmed the presence of different states of water in PVA by using differential scanning calorimeter (DSC) analysis (Figure 2.8b). From Figure 2.8b, one can understand that 10% and 24% water absorbed composites does not show any phase transition, which confirms the presence of non-freezable bound water. At 37% and 54% water absorption, a melting close to 0 °C is identified and this indicates the presence of both non-freezable bound water and freezable bound water, whereas at 59% water absorption, two melting occurs: one below and one above 0 °C indicating the presence of all three types of water (i.e., non-freezable bound water, freezable bound water and free water). At very large water absorption like 83%, both the melting peaks merged to form a broad melting peak around 0 °C, once again indicating the presence of all three types of water.

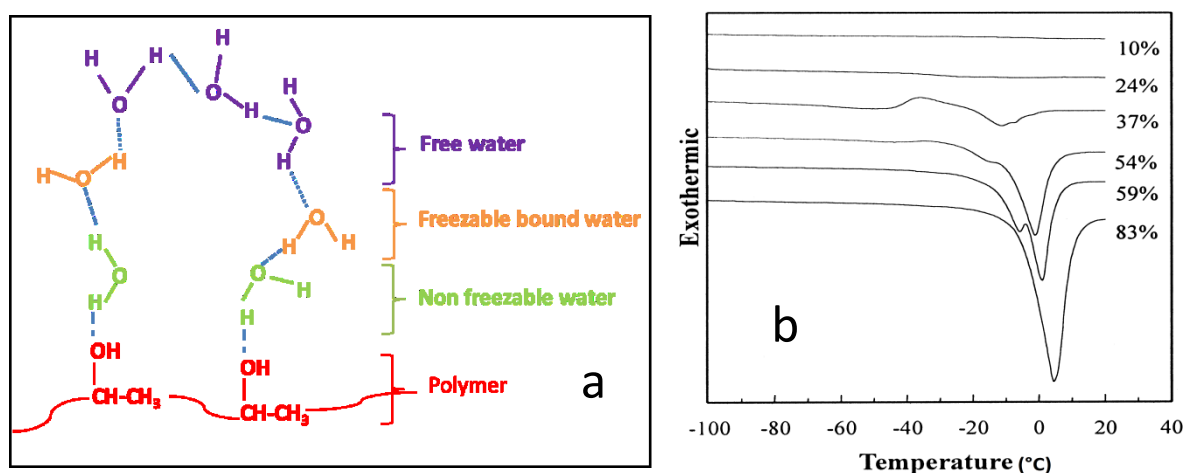


Figure 2.8 a) Schematic drawing showing the position of different types of water present in the swollen polymer, b) DSC curves of the polymer composites containing different water content, explaining the different states of water (adapted with permission from⁶²).

Several other works confirmed the similar behavior of water in other polymers like cellulose, starch, lignin, PAA, poly(vinyl pyrrolidone), etc⁶³. Guan *et al.*^{63c} studied the interaction between water and polymer in four different polymers (PAA, poly (acrylic-co-maleic acid),

poly(sodium acrylate), poly(vinyl methyl ether)) using FTIR and DSC. Formation of hydrogen bonds was confirmed as the reason behind the strong interaction between water and the polar groups in the hydrophilic polymers (non-freezable water). The amount of non-freezable and freezable bound water is found to be dependent only on the chemical structure of the polymer (like hydroxyl, carbonyl, and carboxyl groups). The average numbers of non-freezable water molecules absorbed by the hydroxyl and amide groups present in the hydrophilic polymers are 1 and 4.2 respectively. Similarly, the size of alkaline group associated with the carboxyl group in the hydrophilic polymer also plays a huge impact in water absorption, where larger the alkaline group size, higher would be the absorbed water⁶².

2.2.3 Effect of water absorption on the thermal and mechanical properties

Water absorbed in hydrophilic polymers acts as plasticizer affecting the mechanical and thermal properties (like glass transition temperature). Hodge *et al.*⁶⁴ employed positron annihilation lifetime spectroscopy (PALS) and nuclear magnetic resonance (NMR) to analyze the mechanism of plasticization of water-swollen PVA. The PALS data indicates that the absorption of water increases the size of free volume cavities of the polymer. Solid state NMR data confirmed the lubrication effect of the absorbed water, thus promoting the chain mobility and reducing the polymer-polymer interaction. Further, it was proposed that the non-freezable type of water present in the polymer is majorly responsible for the plasticization rather than the freezing type of water⁶⁵. As a result of plasticization, the polymer exhibited a marked decrease in the glass transition temperature as indicated by the DSC, DMA studies. Several polymers or more specifically food materials are reported to exhibit huge decrease in T_g of about 20–60 °C with the absorption of water. The plasticizing ability (decrease in glass transition temperature) of water in the hydrophilic polymer is found to be in agreement with the polymer-diluent theory (Gordon-Taylor/Kelly Bueche equations) and follows the same principle/mechanism like any other organic plasticizers⁶⁶. Reimschuessel *et al.*⁶⁷ elucidated the decrease in the glass transition temperature of hydrophilic polymers (nylon 6, nylon 6,6, poly(vinyl pyrrolidone)) until the critical concentration of the water is reached. This critical concentration is related to the amount of water required for complete interaction with all accessible polar groups present in the polymer (Figure 2.9).

Mostly, it is believed that water is absorbed only in the amorphous region and the crystalline regions remain unaffected by water at room temperature. Contrastingly, Roos *et al.*⁶⁸ studied different type of food materials like sucrose, lactose and fructose and reported that the effect

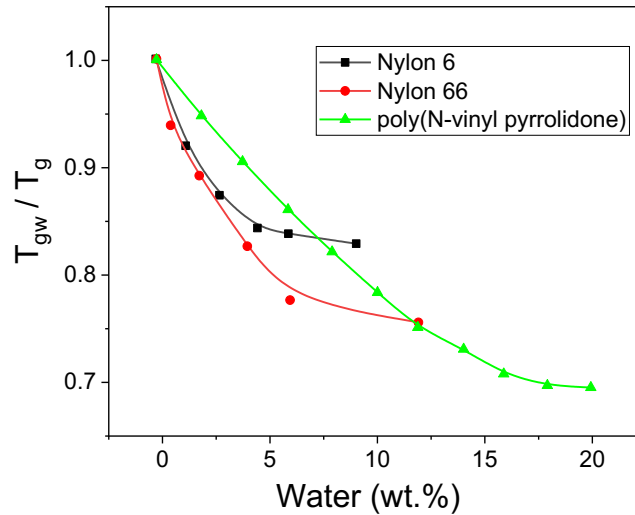


Figure 2.9 Effect of water absorption on the variation of glass transition temperature T_g for different hydrophilic polymer showing the plateau T_{gw} after the critical water content (T_g , T_{gw} – glass transition temperature of initial sample and water absorbed sample respectively) (adapted and redrawn with permission from⁶⁷).

of moisture not only reduces the glass transition temperature, but also the crystallization and melting temperatures were significantly decreased. Similarly, Hodge *et al.*⁶⁹ demonstrated that the crystalline fractions in poly(vinyl alcohol) decreased with the addition of water with the help of X-ray diffraction (XRD) analysis (Figure 2.10). The investigations indicated that water diffusion initially occurred at the amorphous region and then slowly diffused in to the crystalline/amorphous interface and finally reaching the crystalline region and as a result, the polymer becomes totally amorphous. Additionally, Iwamoto *et al.*⁷⁰ used Raman spectroscopy and confirmed the destruction of the crystalline regions by water, using the variations in amorphous and crystalline bands at 1124 cm^{-1} and 1147 cm^{-1} respectively.

The plasticization and the reduction in crystallinity by the absorbed water are expected to vary the mechanical properties of the composites. Water sorption is found to deteriorate the material's mechanical properties, such as the modulus of elasticity, stress at break and produce changes in yield/deformation mechanisms⁷¹. A significant deterioration of the mechanical property is observed for polymers with high hydrophilicity⁷². The reduction in mechanical properties depends on the amount of absorbed water. For example, Peresin *et al.*⁷³ studied the effect of humidity on the mechanical properties of electrospun PVA fiber mats reinforced with cellulose nanocrystals. The reduction in the tensile strength was found to be 80% when the humidity of the environment changed from 10% to 80% RH. Several natural polymers like cellulose, hemicellulose, starch and other synthetic polymers like poly(vinyl pyrrolidone) are found to exhibit tremendous reduction (more than 100 times) in modulus/

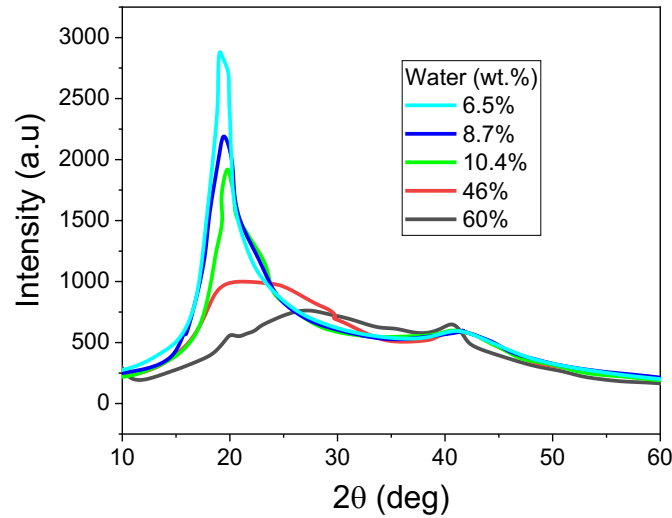


Figure 2.10 XRD analyses of poly(vinyl alcohol) containing different amounts of water. The image indicates the reduction of crystallinity with water absorption (adapted and redrawn with permission from⁶⁹).

stiffness when the polymer is exposed to moisture. The drop in mechanical properties can be slightly reduced by the addition of filler, which in turn reduces the water absorption capabilities⁷⁴.

2.2.4 Kinetics of diffusion of water in the hydrophilic polymers

The kinetics of the water swelling process is an important phenomenon to be considered when designing water swellable compounds. In general, it is accepted that swelling occurs by two steps which includes diffusion of water molecules into the structure of the polymer and the relaxation of the polymer chains leading to the swelling/expansion of the polymer composite. The behavior or kinetics of swelling varies depending on which step dominates the process, in other words, the slowest step. In case of diffusion being the dominating mechanism of the water swelling process, the Fick's second law holds applicable and is expressed by⁷⁵

$$\frac{\partial C}{\partial t} = D_c \frac{\partial^2 C}{\partial x^2} \quad 2.1$$

Where C is the concentration of the diffused liquid/water at time t and at the position x , and D_c is the diffusion co-efficient/constant. On integrating, we get

$$M_t = M_\infty \left[1 - \frac{8}{\pi^2} \sum_{j=0}^{\infty} \frac{1}{(2j+1)^2} \exp\left(-\frac{D_c(2j+1)^2\pi^2}{4h^2} t\right) \right] \quad 2.2$$

Where M_t , M_∞ , h are the weight of the absorbed water at time t , equilibrium weight of the swollen water and the thickness of the sample respectively.

When the polymer chain relaxation rate is comparable to or much lower than the diffusion mechanism, then the swelling behavior is considered non-Fickian in nature, Berens *et al.*⁷⁶ defined it as a relaxation controlled transport mechanism and derived a differential equation:

$$\frac{dM_t}{dt} = k_r(M_\infty - M_t) \quad 2.3$$

where k_r is the relaxation rate constant. On integrating, we get

$$\frac{M_t}{M_\infty} = 1 - e^{-k_r t} \quad 2.4$$

Mechanism of water swelling is found to be dependent on the pH and temperature of the swelling medium. Bumsang *et al.*⁷⁷ evaluated the dynamic swelling behavior of anionic poly(methacrylic acid) based hydrogel and reported that the water swelling mechanism changed from Fickian to non-Fickian when the pH of the swelling medium changed above 7. Similarly Robert *et al.*⁷⁸ studied the influence of cross-link density on the water swelling mechanism using HEMA (2-hydroxyethyl methacrylate) cross-linked with small amounts of ethylene glycol dimethacrylate (EGDMA) and found that the mechanism changed from Fickian to non-Fickian as the cross-link density increased from 0.007 to 0.124 mol EGDMA/mol HEMA. Yao *et al.*⁷⁹ studied the swelling kinetics of glutaraldehyde cross-linked chitosan based interpenetrating polyether hydrogels and established that the degree of acetylation, cross-link density, electrolyte composition, temperature and gel composition all plays a major role in defining the kinetics/mechanism of water swelling process. On the other hand, addition of hydrophilic fillers in to the hydrophobic polymer matrices like polypropylene exhibited Fickian diffusion behavior, which might be due to its low water absorption ability and its restricted relaxation behavior⁸⁰.

2.2.5 Application of water swellable elastomer composites

These types of water swellable elastomer composites have been widely used in oil field as well as mining and civil engineering applications. In civil engineering and construction industries, the water swellable components are used for caulking, sealing of gaps, preventing water leakage from pipe or block connections, preservation of airtightness in machinery and apparatus, isolation of open and cased holes and more specifically used in underground

installations such as subways, metros, retaining dams, impounding reservoirs, etc. Swellable elastomer composites can also be used in self-healing sealing systems (Figure 2.11a)⁸¹. In oil industries, swell packers made of swellable elastomers are utilized during the zonal isolation, well completion, stimulation, underbalanced drilling operations, etc. Zonal isolation achieved with the help of swellable elastomers was found to be more effective than the conventional perforating and cementing techniques (Figure 2.11b)⁸².

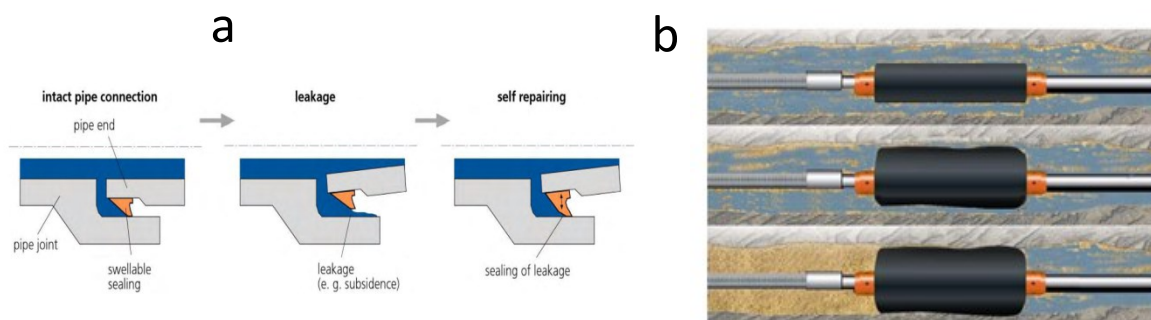


Figure 2.11 a) Self-healing seals (fundamental principle of the sealing system), b) Zonal isolation by elastomer swell packers (adapted with permission from⁸¹⁻⁸²).

2.3 Calcium sulphate and its polymorphic transition

In this work, the functional filler exhibiting polymorphism (structural phase transition) have been explored to develop mechanically adaptable elastomer composites. Polymorphism is defined as the ability of a solid material/mineral to exist in more than one form or crystal structure. Even though several materials exhibit polymorphism, there are only few materials which exhibit significant mechanical property difference with the structural phase transition. Calcium sulphate is one such material and is specifically chosen in this work due to its polymorphic characteristics in presence of water.

Calcium sulphate (CaSO_4) is one of the abundantly available materials in the natural environment, not only in the earth; its presence has also been detected in Mars⁸³. Calcium sulphate has been widely used in construction, ceramics and medical industries. It has been found to exist in several crystal structures and are mainly classified based on the level of hydration: anhydrite (CaSO_4), hemihydrate ($\text{CaSO}_4 \cdot 0.5 \text{H}_2\text{O}$) and dihydrate ($\text{CaSO}_4 \cdot 2 \text{H}_2\text{O}$)⁸⁴. Calcium sulphate hemihydrate and dihydrate are popularly known as ‘plaster of Paris’ and ‘gypsum’ respectively. Only insoluble anhydrite and dihydrate phases are available from nature and on the other hand, the hemihydrate and anhydrite (soluble) are being industrially manufactured by heating the dihydrate to high temperatures. Two types of hemihydrates are

formed based on the method of calcination/heat treatment process: α -hemihydrate (α - $\text{CaSO}_4 \cdot 0.5 \text{H}_2\text{O}$), β -hemihydrate (β - $\text{CaSO}_4 \cdot 0.5 \text{H}_2\text{O}$) obtained from the wet and dry calcination process respectively. Heat treating the respective hemihydrates at higher temperature (120-220 °C) could lead to their respective soluble anhydrides (α , β , hexagonal). Further exposing the soluble anhydride to temperatures above 220 °C and 1180 °C could lead to sparingly soluble anhydrides (II, orthorhombic) and insoluble anhydrites (I, cubic) respectively. The polymorphs of the calcium sulphate could be visualized from Figure 2.12. Industrially, calcium sulphate can also be prepared by mixing sulphuric acid with calcium chloride in an aqueous saturated solution⁸⁵. Calcium sulphate has also been produced as a by-product in large quantities during flue gas desulphurization and phosphoric acid, calcium fluoride, zinc sulphate production process.

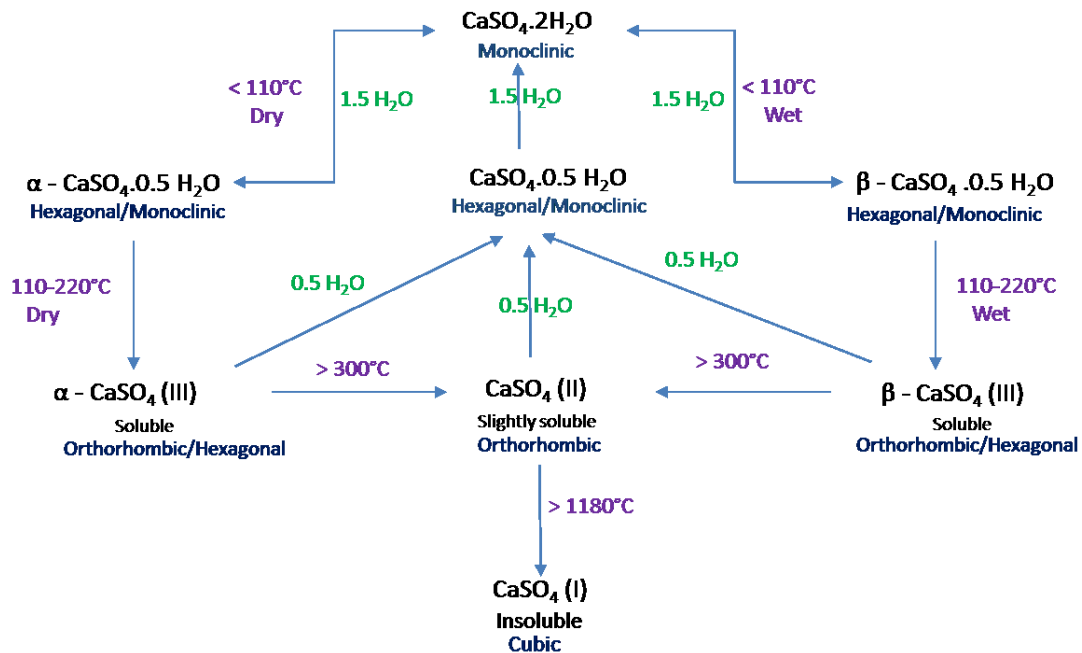


Figure 2.12 Calcium sulphate and its polymorphs (adapted with permission from⁸⁶).

One of the unique properties of calcium sulphate exploited in designing mechanically adaptive composites is its ability to harden in water. This hardening process occurs due to the phase transition of calcium sulphate from hemihydrate/anhydrite to dihydrate (gypsum) crystal structure when it comes in contact with water. This phase transition process leads to the formation of highly porous material with a relatively large internal surface consisting of interlocking crystals in the form of rods and needles, which results in significant enhancement in the compression strength and other mechanical properties⁸⁶. This formation of gypsum crystal is believed to occur via three stage process: initially the nanocrystalline hemihydrate particles are precipitated and then the precipitated nanocrystals assembled to form elongated

aggregates along their 'c- axis' and finally transforms into the dihydrate or gypsum form⁸⁷. Similarly, Saha *et al.*⁸⁸ indicated the possibility of the formation of amorphous particles as an intermediate phase before reorganizing themselves into crystalline gypsum within tens of seconds. It is reported widely that the presence of little amount of organic acids like citric or malic acids can retard the hardening process and radically change the mechanism of setting/hardening process⁸⁹. Water/powder ratio is found to have significant effect in achieving higher strength from the hardening process, as higher ratio of water could lead to dissolution and a lower ratio could lead to incomplete calcium sulphate transformation process.

Song *et al.*⁹⁰ demonstrated the possibility of generating different morphology (like rods, sheets, fibers) and sizes of gypsum nanocrystals by varying the concentration of organic solvent in the saturated solution. Similarly Wang *et al.*⁹¹ tuned the aspect ratio of the nanocrystals from long and slim hexagonal rods to fat and short hexagonal columns by varying the concentration of calcium chloride in the calcium sulphate saturated solution (Figure 2.13).

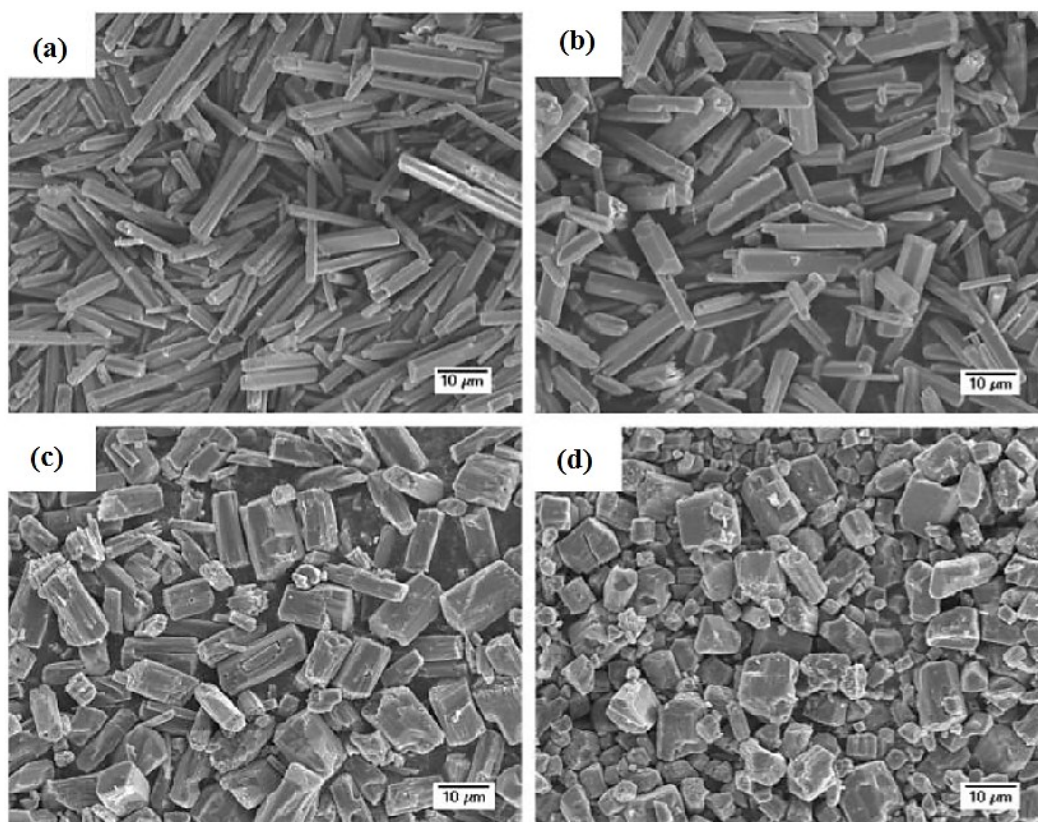


Figure 2.13 SEM images of nano CaSO_4 crystals synthesized using various concentrations of calcium chloride: a) 35.5 wt-%, b) 31.5 wt-%, c) 27.5 wt-%, d) 23.5 wt-% (adapted with permission from⁹¹).

Due to the polymorphic nature of calcium sulphate, gypsum (dihydrate) can be transformed to hemihydrate by solvothermal recrystallization process leading to α -hemihydrate⁹² or by heating at higher temperature (~ 120 °C) in dry state to obtain β -hemihydrate. Some organic acids like adipic acid, citric acid, and tartaric acid can be mixed with calcium sulphate saturated solution for obtaining hemihydrate at lower temperatures (< 90 °C). Additionally, the temperature and kinetics of this transformation process can be varied by altering the partial pressure, pH, type of salt and its concentration in the solution, and also the calcination method (vacuum oven, autoclave or hot air oven)⁹³. Ball *et al.*^{93b} studied the kinetics of dehydration of calcium sulphate between 80 °C and 150 °C at varying partial pressures of water vapour between 10^{-5} and 45 mm and reported the extremely complex nature of calcium sulphate dihydrate dehydration process: diffusion mechanism controls the dehydration process above 110 °C and below which both the nucleation and boundary control mechanism plays a vital role. Similarly, anhydrite (soluble) could be obtained from gypsum at relatively higher temperatures and this dehydration process occurs through the formation of hemihydrate first and then the anhydrite phase. Azimi *et al.*⁹⁴ studied the mechanism of gypsum-anhydrite transformation process at different temperatures and reported that transformation occurs through different mechanism at low and high temperatures. Below 100 °C, the anhydrite is directly obtained with no intermediate hemihydrate formation, whereas above 100 °C, the transformation occurs through the formation of intermediate hemihydrate. This transformation process (gypsum-anhydrite) can be accelerated by adding salts, temperature, chloride and sulfate in the saturated solution⁹⁴ similar to gypsum-hemihydrate transformation process. Thus, it can be concluded that, the crystal system of calcium sulphate exhibits reversible transition (polymorphic) characteristics between them when it comes in contact with water and heat.

Despite the abundant availability, CaSO_4 has not been used in rubber/polymer industry due to its water absorbing ability. Very few publications were identified utilizing CaSO_4 as filler in polymer composites. Even in those reports, stable and insoluble CaSO_4 anhydrite (I) were used to prepare polymer composites⁹⁵. This is the first time, to my knowledge, where a meso-stable CaSO_4 is being mixed with rubbers and its polymorphic structure is altered *in situ* and investigated in details for developing mechanically adaptable elastomer composites.

3 Experimental

3.1 Materials

3.1.1 Polymers

In this work, a special grade of epichlorohydrin rubber and ethylene oxide based polyether copolymer was used to obtain water responsive/swellable elastomer composites.

3.1.1.1 Poly(ethylene oxide-co-epichlorohydrin-co-allyl glycidyl ether) (GECO)

GECO, a special type of epichlorohydrin rubber which is a terpolymer of ethylene oxide (EO), epichlorohydrin (CO), and allyl glycidyl ether (AGE) was used. GECO rubber is chosen in this study, due to the presence of polar groups present in the backbone of the polymer chain, which is expected to absorb water to a certain extent (20–30%) and also could lead to enhanced compatibility with the water swellable resin. This particular grade of GECO was kindly supplied by Zeon Chemicals and is sold under the trade name Hydrin T3108. The chemical structure and its specifications are shown in Figure 3.1 and Table 3.1.

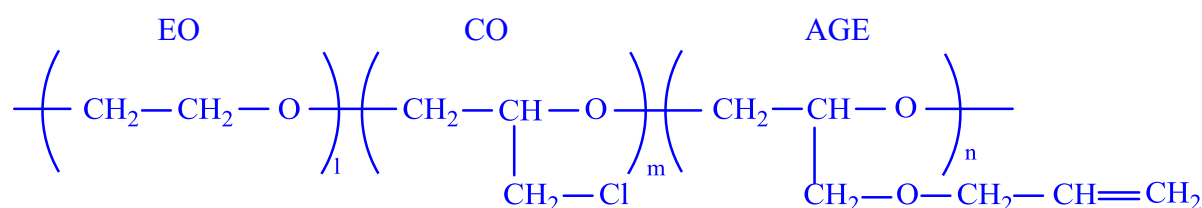


Figure 3.1 Chemical structure of GECO (Hydrin T3108)

Table 3.1 Specifications of GECO (Hydrin T3108)

Polymer properties	Quantity
Ash (%)	<1.0
Moisture (%)	<1.0
Chlorine (%)	18.1–20.1
Mooney viscosity M_L (1+4) @ 100 °C	40–54
AGE content (%)	6.2–8.2
Specific gravity (g/cm ³)	1.26

3.1.1.2 Poly(ethylene oxide-co-propylene oxide-co-allyl glycidyl ether) (GEPO)

GEPO, a terpolymer of ethylene oxide (EO), propylene oxide (PO), allyl glycidyl ether (AGE), was kindly supplied by Zeon Chemicals and is sold under the trade name Zeospan 8030. This particular water swellable resin (GEPO) was chosen due to its similar structure with the elastomer matrix GECO, which inturn is expected to produce compatible/miscible elastomer composite. The chemical structure and its specifications are shown in Figure 3.2 and Table 3.2.

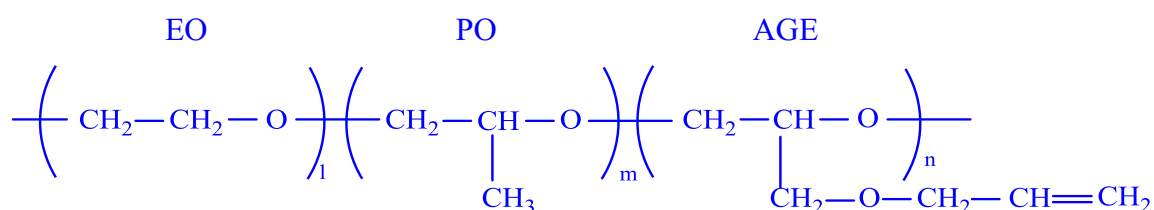


Figure 3.2 Chemical structure of GEPO (Zeospan 8030)

Table 3.2 Specifications of GEPO (Zeospan 8030)

Polymer properties	Quantity
Ash (%)	<1.0
Moisture (%)	<3.0
AGE content (%)	10.5–11.0
Specific gravity (g/cm ³)	1.16

3.1.2 Fillers

3.1.2.1 Calcium sulphate (CaSO₄)

Calcium sulphate was supplied by Acros Organics, Belgium. The obtained calcium sulphate is 99% anhydrous and slightly soluble in water. The specific gravity is 2.96 g/cm³ and its melting point is around 1400 °C. The average particle size is 45 μm (volume mean diameter). 50% and 90% of the material was found to be larger than 37 and 5 μm respectively.

3.1.2.2 Other curing ingredients

Zinc oxide (99.5% purity) and stearic acid (97% purity) was obtained from Acros Organics, Belgium and other vulcanisation accelerators like tetramethyl thiuram disulfide (TMTD) and mercapto benzothiazole disulfide (MBTS) were obtained from Lanxess, Germany. Sulphur (S) was obtained from Fisher Scientific GmbH, Germany.

3.2 Preparation of rubber composites

In general, the preparation of rubber composites consists of three different steps. Initially, the raw rubber is mixed with different ingredients and then the prepared rubber compound is subjected to rheometer to determine the optimum molding conditions and at last, the rubber compound is molded to obtain rubber composites.

3.2.1 Compounding and mixing

In general, compounding is a very important step in preparing rubber composites and it involves selecting and mixing the right proportion of rubber and other ingredients, meeting not only the performance properties, but also, processing and cost requirements for rubber products. The rubber compounding formulation used in this work is shown in Table 3.3. All the materials are expressed in parts per hundred rubber (phr). In this work, two stages of mixing were carried out. Initially the raw rubber was mixed with fillers in internal mixer and then the curatives were mixed in two roll mill.

Table 3.3 Compounding formulation

Materials	GECO	GEPO	CaSO ₄	TMTD	MBTS	S
100 GECO (SC1)	100	–	–	2.5	1	1
75/25 GECO/GEPO	75	25	–	2.5	1	1
50/50 GECO/GEPO	50	50	–	2.5	1	1
25/75 GECO/GEPO	25	75	–	2.5	1	1
100 GEPO	–	100	–	2.5	1	1
SC2 (GECO)	100	–	–	0.5	0.5	0.5
SC3 (GECO)	100	–	–	0.25	0.25	0.25
75/25/10 GECO/GEPO/CaSO₄	75	25	10	2.5	1	1
75/25/30 GECO/GEPO/CaSO₄	75	25	30	2.5	1	1
75/25/50 GECO/GEPO/CaSO₄	75	25	50	2.5	1	1
100/50 GECO/CaSO₄	100	–	50	2.5	1	1
50/50/50 GECO/GEPO/CaSO₄	50	50	50	2.5	1	1
25/75/50 GECO/GEPO/CaSO₄	25	75	50	2.5	1	1
100/50 GEPO/CaSO₄	–	100	50	2.5	1	1

(*All the compound contains 3 phr of ZnO and 2 phr of Stearic acid).

3.2.1.1 Internal mixer

Rubber, activators (ZnO, stearic acid) and filler (CaSO_4) were mixed in an internal mixer (Haake Rheomix, Thermo Electron GmbH, Karlsruhe, Germany) at a temperature of 70 °C at 60 rpm (Figure 3.3a). Banbury type rotors were used for the mixing process and are shown in Figure 3.3b. Generally, for the compounds containing calcium sulphate filler, the mixing was performed for 8 min. The other compounds without fillers were mixed for ~4–5 min. The dump temperature was found to be less than 110 °C. Then the prepared masterbatch compound was removed from the internal mixer and allowed to cool at room temperature.

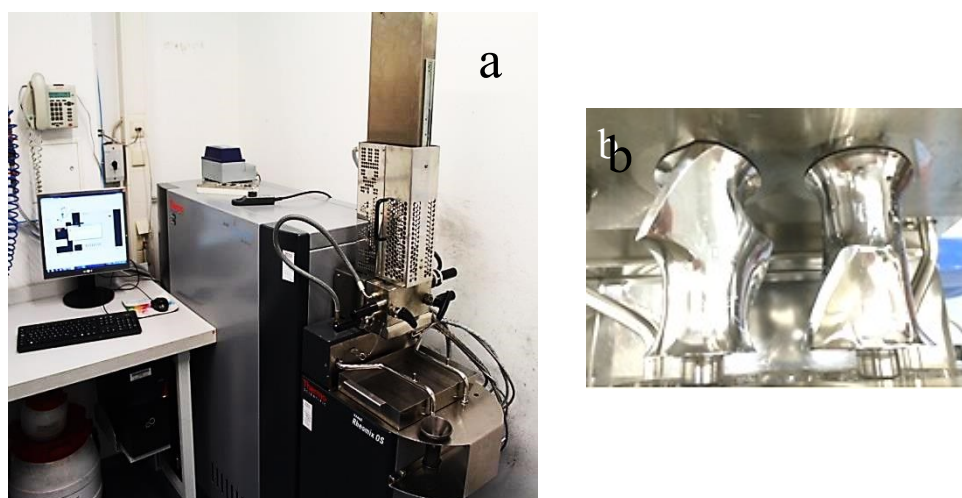


Figure 3.3 a) Internal mixer (Haake Rheomix), b) Banbury rotors

3.2.1.2 Two roll mill

The rubber compound (masterbatch) from the internal mixer was mixed with curatives in an open two roll mill (Polymix 110L, size: 203 × 102 mm², Servitec GmbH, Wustermark, Germany) and is shown in Figure 3.4(a, b). The mixing was carried out at 70 °C with a friction ratio of 1:1.2 between the front and back roll. The curing additives like MBTS, S, and TMTD were sequentially added to the masterbatch. The mixing was followed by homogenization and sheeting out the finished rubber compound, the whole process took 10 min. The nip gap was initially 0.5 mm during the addition of curatives and then reduced to 0.3 mm to homogenise and distribute the filler particles in the rubber matrix.

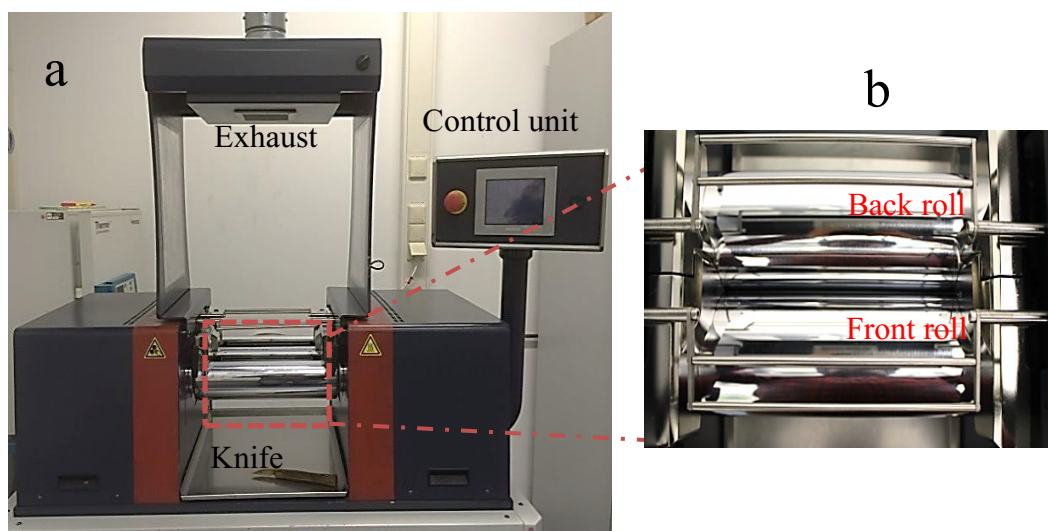


Figure 3.4 a) Two roll mill and b) top view of the front and back rolls.

3.2.2 Curing study and molding

The rubber compound obtained from two roll mill was allowed to mature for 24 h. Then the compounded mass (~5 g) was subjected to rheometer (SIS-V50, Scarabeus GmbH, Germany, Figure 3.5) to determine the time and temperature required for vulcanisation process (optimum curing times). The isothermal time sweep mode was applied at 160 °C with a frequency of 1.67 Hz and the generated torque was recorded. From this torque-time curve, the optimum curing time (t_{c90}), scorch time (t_{s2}) and curing kinetics data were calculated.

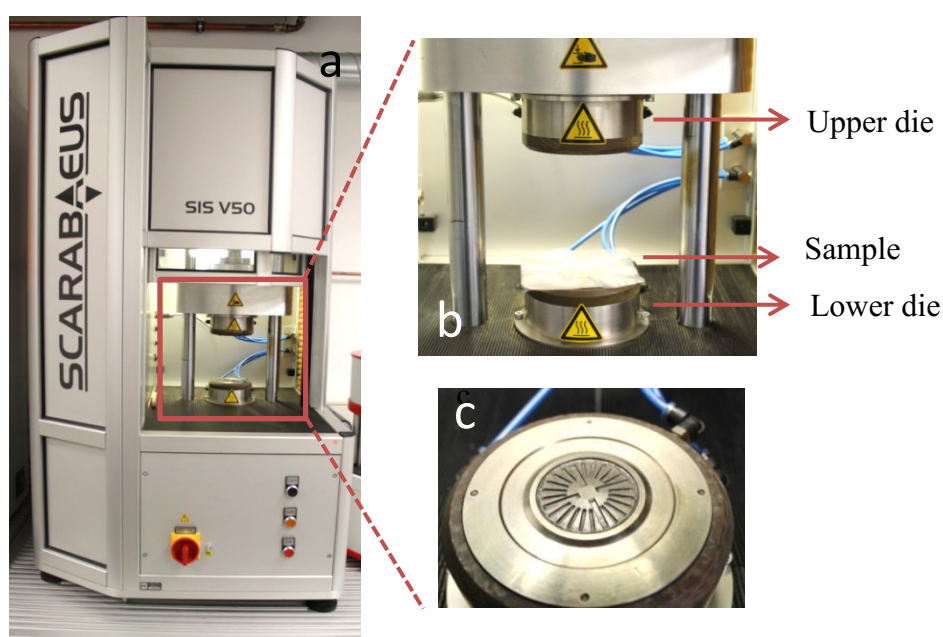


Figure 3.5 a) Moving die rheometer (Scarabeus SIS-V50), b) upper and lower dies, c) die design

To produce molded sheets from the rubber compound, the matured rubber compound was initially warmed in the two-roll mill. Then the required amount of sample was weighed (based on the density of the compound) and placed in the pre-heated mold. The rubber compound was molded and subsequently cured by a compression molding machine. Fontijne Holland, Model TP400, a typical compression molding machine operated by an electrically heated hydraulic press was used and is shown in Figure 3.6a. The rubber compound was cured at 160 °C and 150 kN with their corresponding optimum cure times (t_{c90}) obtained from rheometer. The thickness of the compression mold was 2 mm (b). After molding, it was made sure that samples were wrapped in plastic bags to avoid the moisture uptake.



Figure 3.6 a) Compression molding machine, b) mold (2 mm)

3.3 Characterization

3.3.1 Water swelling studies

The water swelling/absorption characteristics were performed using immersion/gain method. The measurements were performed using a square sample (10 mm × 10 mm) with a thickness of 2 mm. Firstly, the weight of the dry sample was recorded (W_d). Then the sample was immersed in deionized water (Milli-Q, Millipore GmbH, Darmstadt, Germany). The immersed sample was removed from water (after some time) and weighed after wiping the surface water by blotting with tissue paper (W_{dw}). This process was carried out till the equilibrium weight was achieved. The effect of water swelling at different temperatures were measured by placing the sealed bottles containing water and samples in a hot air oven at 30, 50, 70, 90 °C respectively. The degree of water swelling (DS) was calculated as

$$DS (\%) = \frac{(W_{dw} - W_d)}{W_d} \times 100 \quad 3.1$$

3.3.2 Thermal analysis (DSC and TGA)

Differential scanning calorimetry (DSC) was carried out for select samples using Q2000 V24.11 Build 124, TA instruments, USA coupled with an auto-sampler by varying temperature from -90 to $+90$ °C at a scanning rate of 10 K/min under nitrogen atmosphere (Figure 3.7a).

Thermogravimetric analysis (TGA) was carried out using TGA Q500 V20.13 Build 39, TA instruments, USA. The sample was placed in the platinum pan and heated till 600 °C under nitrogen atmosphere and then changed to oxygen/air atmosphere till 900 °C (Figure 3.7b).

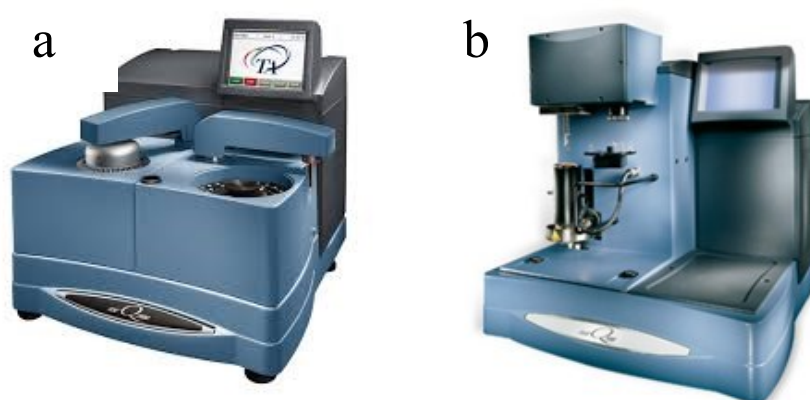


Figure 3.7 a) Differential scanning calorimeter (DSC Q2000), b) thermogravimetric analysis (TGA Q500)

3.3.3 Dynamic mechanical analysis (DMA)

Dynamic mechanical analysis was performed using dynamic mechanical thermal spectrometer in temperature, time and amplitude sweep modes. The standard rectangular specimen ($35 \times 10 \times 2$ mm³) punched out from the prepared rubber sheet was used for all modes of measurement. In case of temperature sweep, Eplexor 150 N (Gabo Qualimeter, Ahlden, Germany) was used in tension mode. The isochronal frequency of 10 Hz, dynamic load at 0.2% strain and static load at 1% strain was applied and the storage modulus (E'), loss modulus (E'') and loss factor ($\tan \delta$) were recorded in the temperature range of -80 °C to $+80$ °C at the heating rate of 2 K/min. In case of time sweep and amplitude sweep, Eplexor 2000 N (Gabo Qualimeter, Ahlden, Germany) was used in tension mode (Figure 3.8a, b). In case of amplitude sweep, the storage modulus (E'), loss modulus (E'') and loss factor ($\tan \delta$) were recorded at a particular temperature (-20 °C/ 60 °C), isochronal frequency of 10 Hz and static load of 60% with varying dynamic load from 0.01–30%. Similarly, time sweep analysis was

performed for 20 min with a dynamic load of 0.2% strain, static load at 1% strain and an isochronal frequency of 10 Hz.

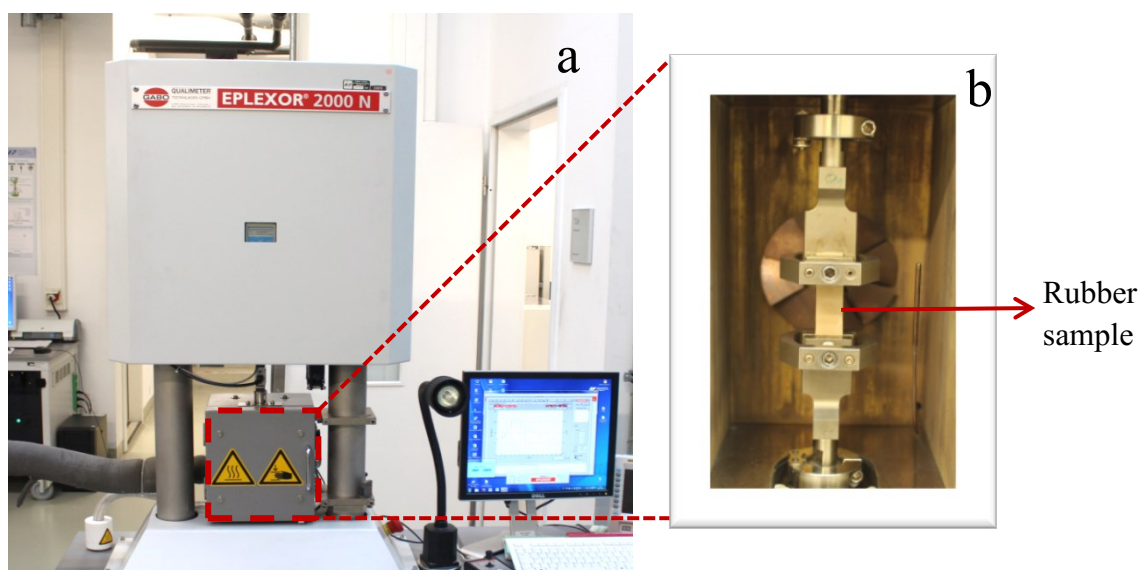


Figure 3.8 a) Dynamic mechanical analyzer (Eplexor 2000N) with tensile clamp, (b) view of the clamps inside the test chamber (highlighted by red dotted box)

3.3.4 Stress–strain studies

Stress–strain studies were performed with the help of Zwick universal testing machine (model 1456, Z010, Ulm Germany) and is shown in Figure 3.9. Dumbbell shaped specimens were punched from the molded rubber composite sheet and the tensile tests were carried out at particular temperatures in tension mode with a cross head speed of 200 mm/min^{-1} .

From the tensile studies, Young's modulus, tensile strength (TS) and elongation at break values (EB) were measured. Young's modulus values are generally associated with the linear regime (slope) of the stress–strain curves and for rubbers, it occurs in the low deformation range (below 2–5% of elongation), while the tensile strength was measured as the stress required to break the rubber sample.

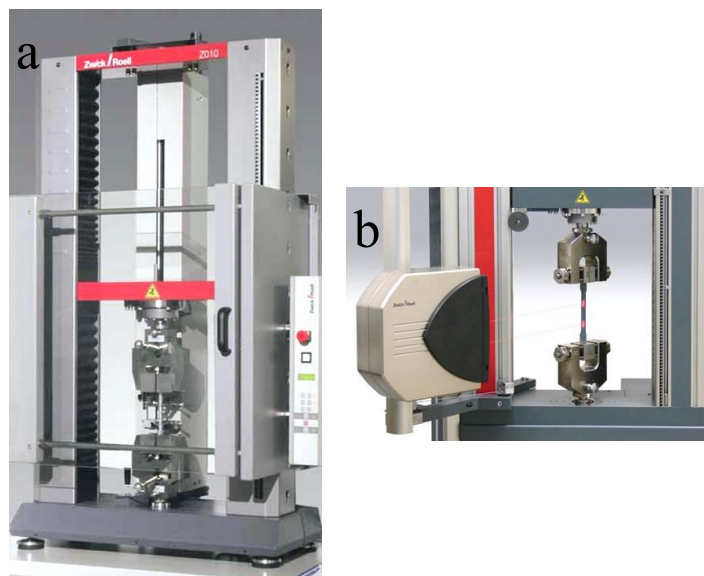


Figure 3.9 a) Zwick 1456 Universal testing machine, b) typical optical extensometer

3.3.5 Fourier transform infrared spectroscopy (FTIR)

FTIR spectroscopic analysis was performed using an evacuated Vertex 80v FTIR spectrometer (Bruker, Germany) equipped with an Mercury cadmium telluride detector and a Golden Gate Diamond ATR unit (attenuated total reflection, SPECAC) (Figure 3.10). ATR-FTIR spectra of dry and water-swollen elastomers were recorded within the range of $4000\text{--}600\text{ cm}^{-1}$. Every spectrum was obtained with 4 cm^{-1} spectral resolution and 100 scans per spectrum. Before comparison, spectra were normalized onto the stretching vibration band of the methylene group around 2867 cm^{-1} (internal reference approach⁹⁶).



Figure 3.10 Vertex 80v FTIR spectrometer (Bruker, Germany) equipped with an Mercury cadmium telluride detector and a Golden Gate Diamond ATR unit

3.3.6 Morphological analysis

3.3.6.1 Scanning electron microscopy (SEM)

The morphology of fillers in the elastomer composites were observed using scanning electron microscopy (Zeiss Ultra Plus, Carl Zeiss Microscopy GmbH, Jena, Germany) and is shown in Figure 3.11a. Rubber specimens were cut into thin films and ~2 nm of platinum was sputter coated on the surface and placed into the SEM chamber for imaging.

3.3.6.2 Transmission electron microscopy (TEM)

The morphology of filler particles in the filled composites were also analyzed by transmission electron microscopy (TEM). Ultrathin sections of the rubber composites were cut by ultra-microtome (Ultracut UC7, Leica Microsystems GmbH, Germany) at $-100\text{ }^{\circ}\text{C}$ and the images were captured by Libra 120 transmission electron microscope (ZEISS, Oberkochen, Germany) with an acceleration voltage of 200 kV (Figure 3.11b).

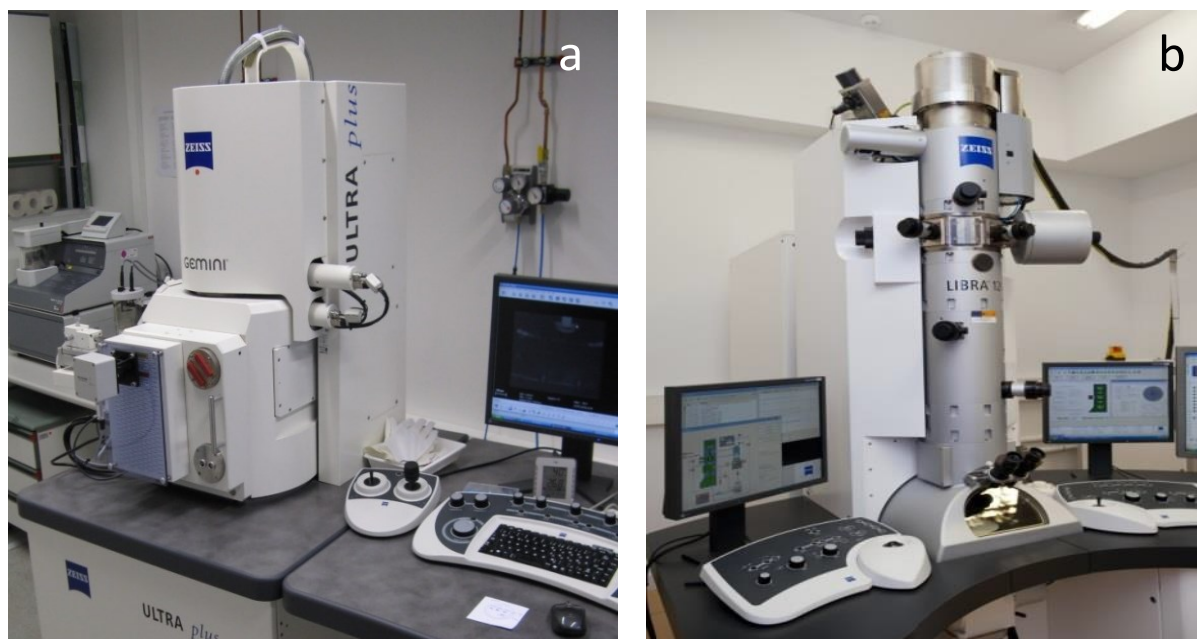


Figure 3.11 a) Zeiss Ultra Plus SEM machine, b) Libra 120 TEM machine

3.3.6.3 Cryo-transmission electron microscopy (cryo-TEM)

Cryo-transmission electron microscopy (cryo-TEM) is used for imaging frozen-hydrated specimens at cryogenic temperatures. A small sample was cooled down to $-160\text{ }^{\circ}\text{C}$, mounted on an ultra-microtome chamber and flooded with dry nitrogen at a temperature of $-160\text{ }^{\circ}\text{C}$. Approximately 120 nm thick section was cut with a diamond knife (knife temperature -160

°C) and transferred onto a cooled TEM grid. The grid was transferred under liquid nitrogen into a cryo-TEM holder (Gatan 626, Gatan Inc., USA) and inspected in TEM at -170 °C.

3.3.7 X-ray diffraction (XRD)

XRD was employed to obtain information regarding the phase transition behavior of the calcium sulphate filled composites. A Seifert XRD 3003 θ/θ (GE Inspection Technologies/Seifert-FPM, Freiberg, Germany) with $\text{CuK}\alpha$ radiation was used in transmission mode and is shown in Figure 3.12. The experiments were performed in the wide angle range from 5 – 50° , with an increment of 0.05° . The measurement time for the intensity at each angle was 15 s. Bragg's law was employed to calculate the crystal structures and is shown in Eq.3.2.

$$n\lambda_i = 2d \sin\theta \quad 3.2$$

Where d is the distance between crystal lattices, θ is the angle between incident beam and planes, λ_i is the wavelength of the incident wave/light and n is an integer.



Figure 3.12 X-ray diffraction instrument (Seifert XRD 3003 θ/θ)

3.3.8 Raman spectroscopy

Raman spectroscopy was utilized to confirm the phase transition achieved during hydration (water treatment) and dehydration (heat treatment) process of the CaSO_4 filled composites and is shown in Figure 3.13. Raman spectra was recorded using the Confocal Raman Microscope alpha 300 R (WITec GmbH, Ulm, Germany) equipped with a laser with an excitation wavelength of 785 nm and a laser power of 200 mW.

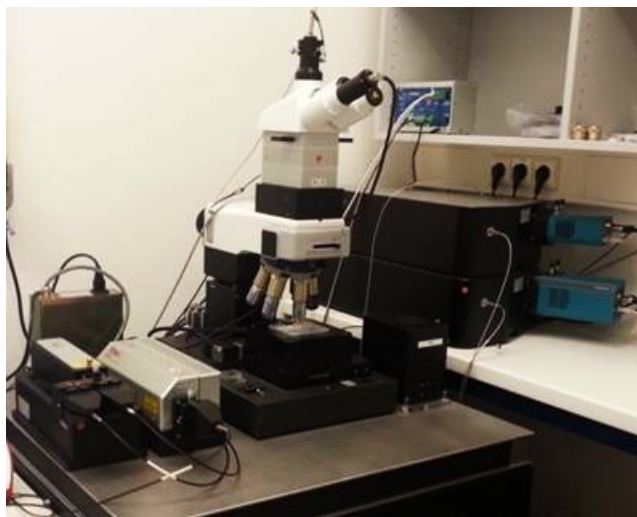


Figure 3.13 Raman spectrometer with microscope (Alpha 300 R+)

Samples were measured with a 20× objective for an integration time of 0.5 s for a single scan in the wavelength region from 200 to 3500 cm^{-1} . For each spectrum 200 accumulations were done.

4 Results and discussions

4.1 Development of novel water swellable elastomer composites based on GECO/GEPO

Water swellable elastomer composites were introduced in the late 1970s and have been widely used for water-stopping applications, packers and zonal isolation in civil engineering applications⁸¹⁻⁸². Most of the literature and commercialized materials utilized the mechanical blending of water swellable resin/hydrogels with the hydrophobic elastomer matrices along with compatibilisers^{54, 97}. These materials displayed poor compatibility between the hydrogel and the hydrophobic rubber, which resulted in poor mechanical properties. More importantly, the hydrogels/water absorbent resins were separated/leached from the composites during water swelling process, which led to poor repeatable characteristics. Therefore, in this chapter, an attempt has been made to prepare compatible/miscible water swellable elastomer blends which exhibits repeatable water swellable properties.

In this work, commercially available polyether based elastomer ethylene oxide-chlorohydrin-allyl glycidyl ether terpolymer (GECO) is used along with the structurally similar polyether based polymer resin ethylene oxide-propylene oxide-allyl glycidyl ether terpolymer (GEPO). Compatibility, water swellability and the reusability of the developed GECO/GEPO blends are explored in this chapter within the scope of the study.

4.1.1 Miscibility of the polymer blend (GECO/GEPO) systems

4.1.1.1 Curing study

GECO, GEPO and their different blend ratios (100/0, 75/25, 50/50, 25/75, 0/100) were prepared based on the formulation shown in Table 3.3 and their curing characteristics are shown in Figure 4.1. Figure 4.1 clearly indicates that both the neat hydrophilic elastomer GECO and hydrophilic polymer GEPO can be effectively cured independently by the sulphur/accelerator system. The higher torque value and the cure rate of the GEPO compared to GECO can be attributed to the higher amount of allyl glycidyl ether (AGE, cure-site monomer) present in GEPO. The addition of GEPO in the GECO/GEPO blends enhanced the torque values and the blends (75/25, 50/50, 25/75) showed torque values in between those of the individual polymer compounds. The intermediate torque values indicate the possibility of miscibility/compatibility between the polymers in the blend. The similar structure and cross-

linking mechanism of the polymers suggests the possibility of co-vulcanisation between two polymers in the blend.

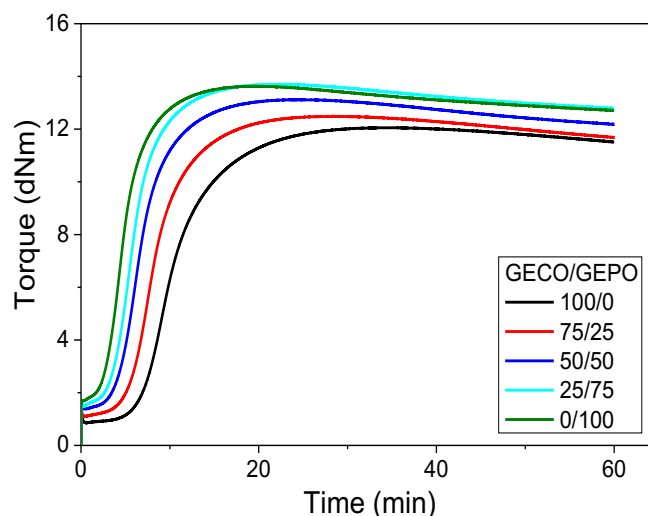


Figure 4.1 Cure characteristics of different GECO/GEPO blends using moving die rheometer operated at 160 °C.

4.1.1.2 DSC analysis

DSC is one of the potential methods to determine the miscibility of the polymer blends. DSC curves (second heating) of the different GECO/GEPO blends are shown in Figure 4.2a from which the glass transition temperature (T_g) and melting temperature (T_m) can be obtained.

The neat GECO and GEPO showed T_g values around -44.9 °C and -54.4 °C respectively. Figure 4.2a shows that upon blending GEPO and GECO, a single T_g is obtained and is positioned between the T_g 's of the individual polymers. The T_g of 75/25, 50/50 and 25/75 GECO/GEPO blends are around -48 , -48.5 and -50 °C respectively. It is well established in literature⁹⁸, that any two polymers are said to be miscible with each other if they show a single and intermediate T_g between two individual polymers. Hence the prepared blend system (GECO/GEPO) is said to be miscible in all proportions. When the polymers in the blend has closer T_g , they tend to display a broad single T_g and is sometimes misinterpreted as miscible system. However, in our case, closer T_g values of GECO and GEPO, did not cause any difficulty in yielding prominent sharp single glass transition temperature for the blend system.

To further support the miscibility based on the glass transition temperature, the melting behavior of all the blends were analyzed from the Figure 4.2a and tabulated in Table 4.1. GEPO showed a broad melting behavior between -20 °C and 60 °C, which indicates the

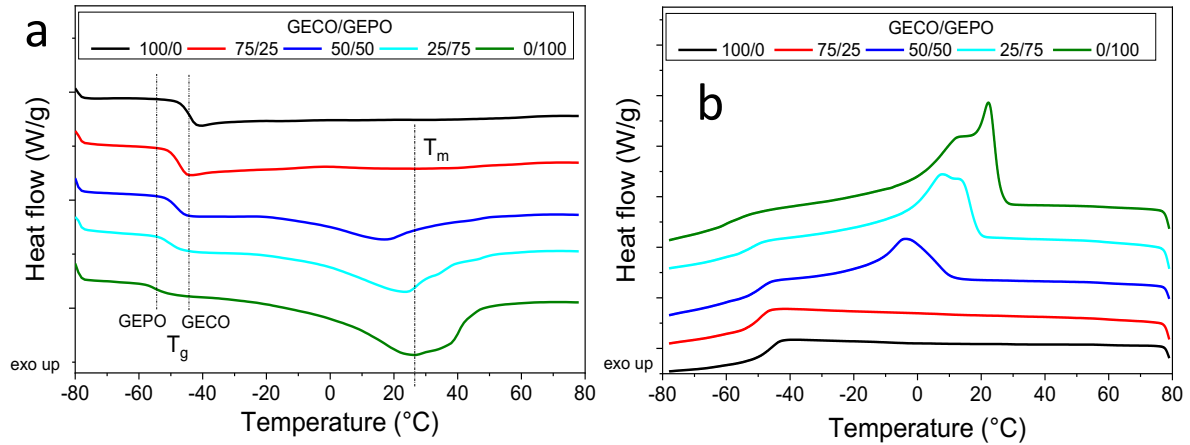


Figure 4.2 DSC curves: a) heating curve, b) cooling curve (recrystallization studies). A single glass transition temperature and the semi-crystalline nature of the GECO/GEPO blends were evident from the Figure.

Table 4.1 DSC profile of the GECO/GEPO blends

GECO/GEPO	T_g (°C)	T_m (°C)	X_c (%)	Theoretical X_c (%)
100/0	-44.89	-	-	-
75/25	-47.97	-	1.1	6.25
50/50	-48.46	17.26	9.36	12.5
25/75	-50.04	23.65	16	18.75
0/100	-54.36	26.33	24.3	-

semi-crystalline nature of the polymer. This broad melting region of GEPO may contain more than one melting peak, which might be due to the presence of different types of crystal structure. The different crystal structures of GEPO can be understood from the two distinct crystallization peaks observed in the cooling curve (Figure 4.2b). The melting enthalpies and the melting temperatures (T_m) were calculated from the area under the curve and the maximum of the endothermic peak respectively. The degree of crystallinity (X_c) present in the blend system can be calculated from the following equation.

$$X_c = \frac{\Delta H_{m,blend}}{\Delta H_{PEO}^0} \quad 4.1$$

where $\Delta H_{m,blend}$ and ΔH_{PEO}^0 are the melting enthalpies per gram of blend and 100% crystalline PEO (213 J/g⁹⁹) respectively. Since the GEPO terpolymer contains 85% of PEO, it's obvious that crystallinity arises from PEO phase present in the GEPO terpolymer.

The degree of crystallinity present in the neat GEPO polymer was found to be ~25% (which is close to the data provided by the polymer producer). Upon blending GECO with GEPO, melting/crystalline regions can be observed clearly in GEPO rich blends (*i.e.*, 50/50 and 25/75 blends) and is found to be insignificant in the 75/25 blend system. The degree of crystallinity obtained from the DSC analysis for the 25/75, 50/50 and 75/25 GECO/GEPO blends (16, 9.4, 1.1% respectively) are found to be lower than the theoretical crystallinity values (18.75, 12.5, 6.25% respectively). The reduced crystallinity in the GECO/GEPO blend indicates the possibility of diffusion of GECO polymer chains into the GEPO crystalline regions. Similarly, the peak melting temperature of 50/50 and 25/75 GECO/GEPO blends reduced to 16.7 °C and 23.7 °C respectively, when compared to 26.1 °C for the neat GEPO. According to Nishi and Wang¹⁰⁰, the depression in melting point of the crystalline phase can be used as an indication of miscibility between the amorphous polymer (GECO) and the semi-crystalline polymer (GEPO) in the blend system.

To further understand the miscibility between two polymers, several basics models are employed to predict the glass transition temperature of the different polymer blends. The equation used to predict the dependence of blend composition on the glass transition temperature of miscible blends are mostly empirical or have been derived from thermodynamic or free volume concepts. The simplest of them is the Fox equation, given as¹⁰¹

$$\frac{1}{T_g} = \frac{\varphi_1}{T_{g1}} + \frac{\varphi_2}{T_{g2}} \quad 4.2$$

Where φ_i , T_{gi} represents the weight fraction and glass transition temperature of the individual polymers used in the blend and T_g is the glass transition temperature of the blend (1 is used for polymer having lower T_g).

Further, Gordon-Taylor anticipated the possibility of enthalpy changes occurring during the mixing process and hence introduced a parameter k_{GT} ($= \Delta C_{p1} / \Delta C_{p2}$) to the Fox equation by assuming T_{g2}/T_{g1} close to unity and the modified equation is written as follows¹⁰².

$$T_g = \frac{\varphi_1 T_{g1} + k_{GT} \varphi_2 T_{g2}}{\varphi_1 + k_{GT} \varphi_2} \quad 4.3$$

where ΔC_{pi} is the difference in specific heat between the rubbery and glassy states at T_{gi} . However, k_{GT} is considered as real fitting parameter obtained from the experimental data.

Kwei¹⁰³ extended the Gordon-Taylor equation by introducing the quadratic term $q\varphi_1\varphi_2$ to deduce the strength of intermolecular interactions between the polymers in the blend.

$$T_g = \frac{\varphi_1 T_{g1} + k_{KW} \varphi_2 T_{g2}}{\varphi_1 + k_{KW} \varphi_2} + q\varphi_1 \varphi_2 \quad 4.4$$

Here, both k_{KW} , q are treated as fitting parameters obtained from the experimental data and the value of q is assumed to be proportional to the number of specific interactions between the polymers in the blend. Similar to Gordon Taylor equation, the parameter k_{KW} in the Kwei equation is also considered as volume additivity constant.

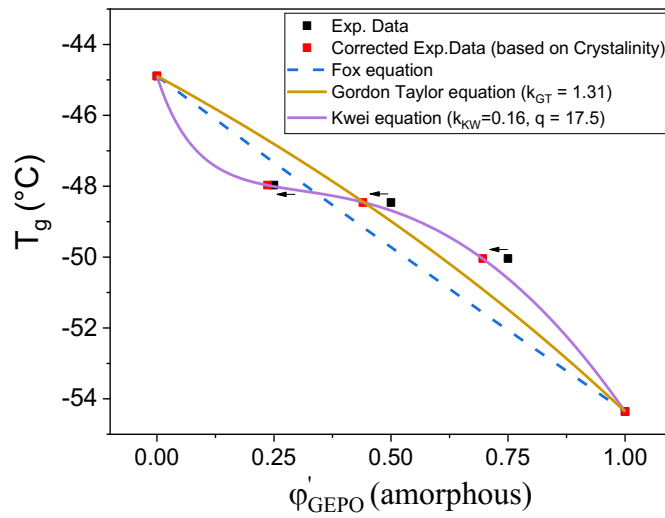


Figure 4.3 Model fitting of glass transition prediction equations of the different GEPO/GEPO blends against the weight fraction of GEPO phase in the GEPO/GEPO blends corrected based on blend crystallinity (φ'_{GEPO}) (black symbols denote the actual experimental data, plotted as a function of the overall weight fraction of GEPO in the blend and the arrow marks indicate the shift in the weight fraction).

Since the above blend system exhibits crystalline melting regions as shown in the Figure 4.2a, it is expected that the miscibility might be occurring only in the amorphous phase of the polymer blends containing amorphous (GECO) and semi-crystalline polymer (GEPO). In such cases, it makes sense to recalculate the weight fraction of the polymer blends by considering only the amorphous regions of the polymers in the blend. The weight fraction of the amorphous GEPO phase (φ'_{GEPO}) was calculated/corrected based on the blend crystallinity ($\varphi'_{GEPO} = \frac{\varphi_{GEPO} - X_{c,blend}}{1 - X_{c,blend}}$)¹⁰⁴ and is plotted against the glass transition temperature in Figure 4.3, where $X_{c,blend}$ is the degree of crystallinity in the GEPO/GEPO blend.

The experimental T_g values of GEPO/GEPO blends were fitted with the Fox, Gordon-Taylor, Kwei equation and are shown in Figure 4.3. In this figure, it is observed that the experimental

values of 75/25 blends showed a slight negative deviation, while the 50/50, 25/75 blends showed significant positive deviation from the Fox equation. Similarly, Gordon Taylor equation which takes into account the volume additivity of the polymer blends also poorly fitted the experimental data. Generally, positive deviation is expected due to the strong interaction between the polymers in the blend¹⁰⁵. In order to confirm the presence of strong interaction between the polymers in the blends, Kwei equation was utilized and found to perfectly fit with k_{KW} and q values around 0.16 and 17.5 respectively. The positive q values indicate the presence of specific interactions between GECO and GEPO in the blend. Based on the literature, q value of 17.5 is considered to be moderate and hence suggests a moderate interaction between the polymers in the blend.

From the above studies, the single glass transition temperature, depression in melting point and reduction in degree of crystallinity obtained for all the blends confirmed the miscibility of GECO/GEPO blend in all proportions. Additionally, specific interaction between GECO and GEPO were characterized by the Kwei equation and suggests the possibility of co-vulcanisation between them. More specifically, it can be concluded that, the developed GECO/GEPO blends comes under the category of miscible amorphous–semi-crystalline polymer blend system, due to the presence of crystalline domains.

4.1.1.3 Dynamic mechanical analysis (DMA)

Temperature sweep experiments in DMA can be used to detect glass transition temperatures (T_g) and other secondary segmental motions very precisely¹⁰⁶ similar to DSC. In DMA, T_g of the elastomer is often predicted from the temperature of maximum (peak) loss factor ($\tan \delta$) or maximum loss modulus (E''). DMA (Temperature sweep) was employed to further confirm the single T_g /miscibility of the GECO/GEPO polymer blends (observed from DSC measurements) and is shown in Figure 4.4a-c. Figure 4.4a, b clearly showed that addition of GEPO in to GECO has resulted in a single glass transition ($\tan \delta$ and E'' peak), which was found to be between the glass transition temperatures of GECO and GEPO. It is also interesting to note that the T_g values of GECO, GEPO and their blends obtained from DMA ($\tan \delta$ and E'' peak values) were found to be slightly different from DSC values. This could be attributed to the different principle/experimental conditions involved in DMA and DSC for measuring T_g . Similarly, GECO/GEPO blends showed intermediate $\tan \delta$ peak height values between GECO and GEPO (Figure 4.4a). Single glass transition (positioned between GECO

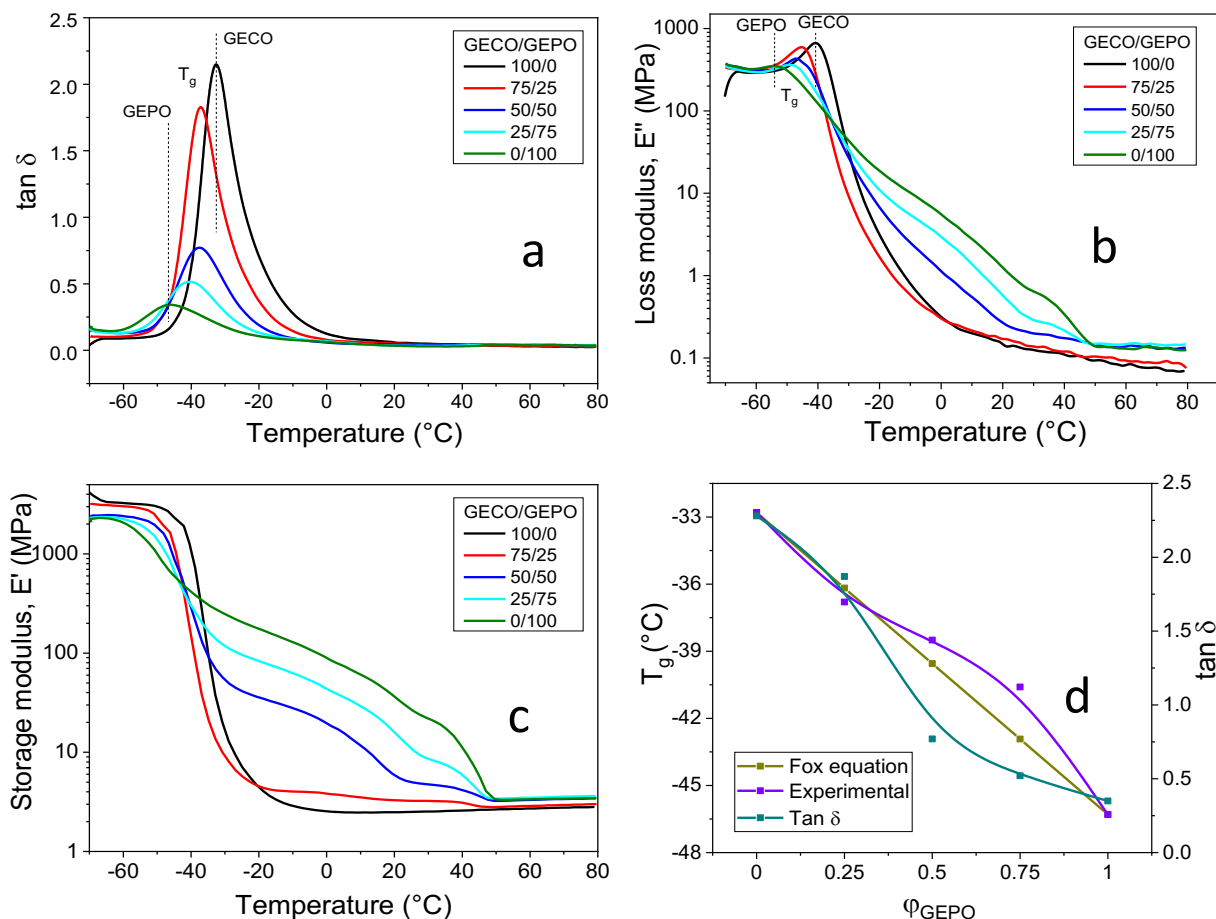


Figure 4.4 Dynamic mechanical analysis of GECO/GEPO blends: temperature dependence of a) Loss factor ($\tan \delta$), b) loss modulus (E''), c) storage modulus (E'), and d) effect of GEPO content (ϕ_{GEPO}) on T_g and $\tan \delta$ peak height values.

and GEPO) and the intermediate $\tan \delta$ peak height values of GECO/GEPO blends obtained from DMA, once again confirms the miscibility of the GECO/GEPO blends in all proportions. The T_g obtained from $\tan \delta$ is compared with the Fox equation and is shown in Figure 4.4d. Similar to DSC results, slight negative deviation for 75/25 blends and significant positive deviation for 25/75 and 50/50 GECO/GEPO blends were obtained in DMA.

Storage modulus values of GECO/GEPO blends against temperatures are shown in Figure 4.4c. Semi-crystalline nature of GEPO can be comprehended from the decreasing storage modulus values between -20 °C to 50 °C. The elastomeric plateau is observed after the melting of crystalline region beyond 50 °C. This melting transition of the semi-crystalline GEPO can also be clearly seen in the 50/50 and 25/75 blends, which was found to be negligible in the 75/25 GECO/GEPO blend. To summarize, the results obtained from DMA studies confirm the miscibility of GECO/GEPO blends in all proportions with the formation of amorphous–semi-crystalline polymer blend systems.

4.1.1.4 Mechanical properties: stress–strain characteristics

Stress–strain properties of the GECO/GEPO composites were measured at room temperature (20 °C) and are shown in Figure 4.5a. The neat GEPO exhibited higher stress–strain properties compared to GECO, due to its crystalline nature at room temperature (DSC results, Figure 4.2a). Blending of GEPO with GECO has led to an increase in Young's modulus, tensile strength and decrease in elongation at break values (Figure 4.5b). Blending of GEPO in GECO has led to 30, 90 and 158% improvement in Young's modulus for 75/25, 50/50 and 25/75 GECO/GEPO blends respectively. All the blends showed intermediate mechanical properties between those of the individual polymers. This once again confirms the miscibility of GECO/GEPO blend in all proportions. GECO, GEPO and its blends exhibited very low tensile properties from application point of view. This could be compensated by the addition of reinforcing fillers.

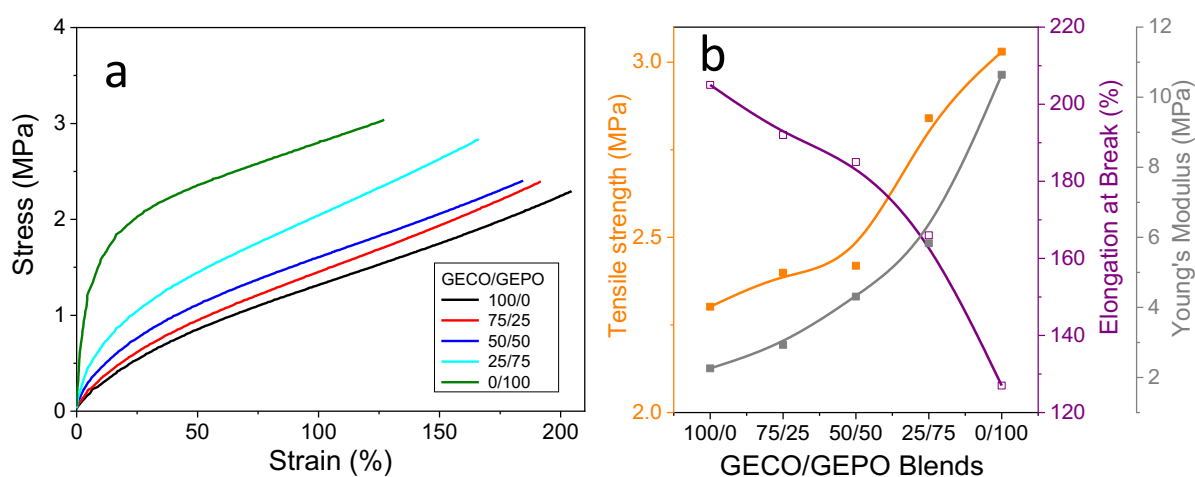


Figure 4.5 a) Stress–strain curves of GECO, GEPO and their blends, b) comparison of all the mechanical properties with varying GECO/GEPO blend ratios.

4.1.2 Water absorption behavior of GECO/GEPO blends

The water absorption/swelling behavior of the GECO/GEPO blends were measured using weight-gain method and is shown in Figure 4.6a. The neat GECO rubber absorbed ~20% which could be considered high compared to other commercial elastomers, while the hydrophilic polymer resin GEPO absorbed a maximum of about 430%. The blending of GEPO in GECO enhanced the water swelling degree to around 75, 160 and 275% for the 75/25, 50/50 and 25/75 GECO/GEPO blends respectively (Figure 4.6b). GECO, GEPO and its blends showed similar water absorption behavior: *i.e.*, an initial increase in water absorption, followed by the plateau indicating the achievement of equilibrium water swelling abilities (Figure 4.6a). The achievement of equilibrium water swellability (plateau curves)

indicates that there is no loss of hydrophilic particles during the water swelling process. It is also interesting to note that all the GECO/GEPO blends achieved equilibrium rapidly in less than 12 hours.

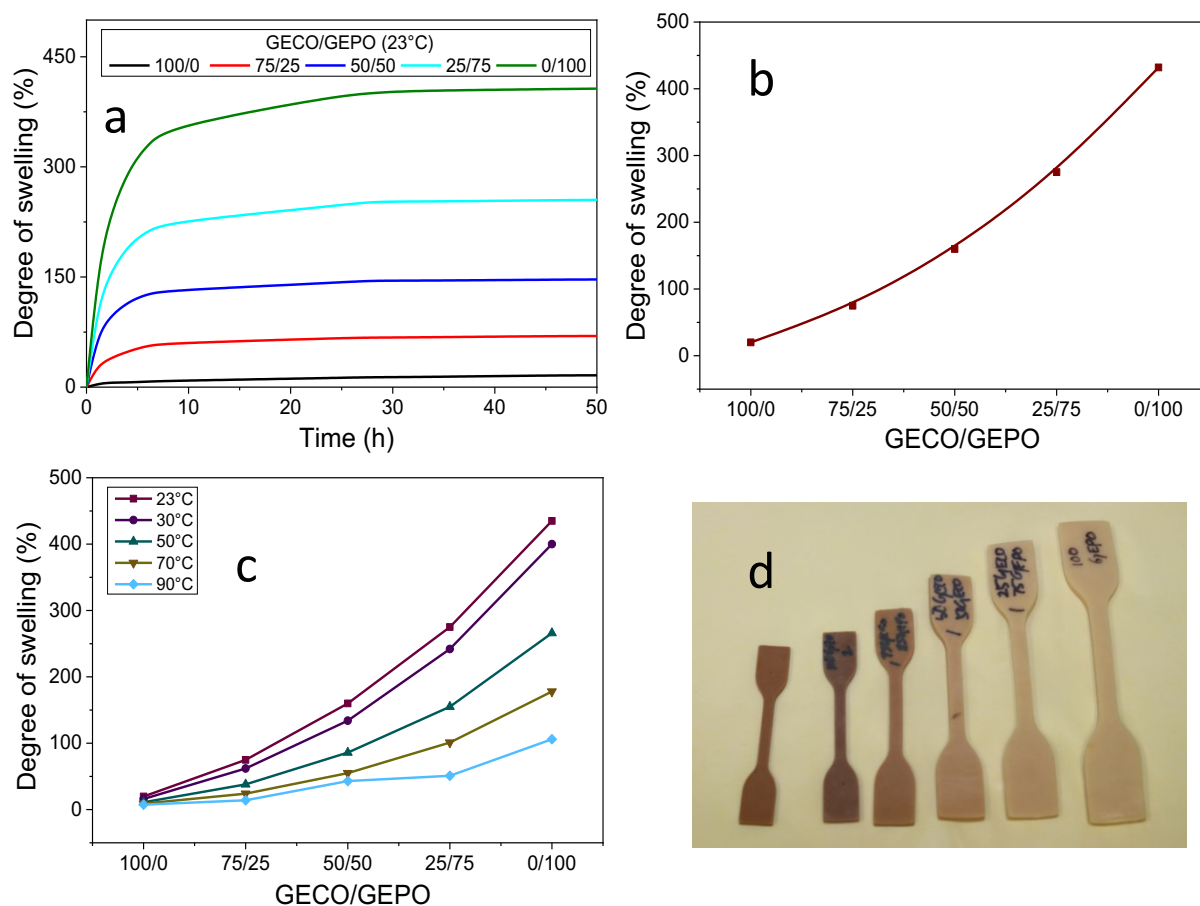


Figure 4.6 Water absorption characteristics of different GECO/GEPO blends against a) time (at 23 °C), b) blend ratio (GECO/GEPO), c) temperature and (d) images of water-swollen samples compared with dry sample (from left, Dry, 100/0, 75/25, 50/50, 25/75, 0/100 GECO/GEPO).

The effect of temperature on equilibrium water swelling is shown in Figure 4.6c. GECO/GEPO blends exhibited decreased water swelling ratio with the increase in temperature. This might be due to the reduced hydrophilic nature of GEPO at higher temperatures. This needs to be studied extensively to explain such a phenomenon, but this is not under the scope of our study. An image of the water-swollen samples is shown in Figure 4.6d. The image indicates that the stable water swellable elastomer composites were developed with very minimal weight loss and smooth surface after swelling.

4.1.2.1 Mechanism and kinetics of water swelling

The mechanism and kinetics of water swelling in GECO, GEPO and their blends were analyzed from Figure 4.6a. Generally, water transport in polymer is classified as Fickian, relaxation controlled (non-Fickian) or anomalous. The shape of the curve: initial sharp increase in water absorption followed by the saturation; indicate the possibility of Fickian diffusion¹⁰⁷ in GECO/GEPO blends. However, the different mechanisms of diffusion/water transport can be distinguished using the simple empirical equation, also called as power law¹⁰⁸

$$\frac{M_t}{M_\infty} = kt^r \quad 4.5$$

where M_t , M_∞ are the weight of the absorbed water at time t and the equilibrium weight of the swollen water. While r is the swelling exponent used to indicate the mechanism of the water swelling process and k is a characteristic constant representing the interaction between polymer and water. Power law constants (k , r) were obtained from the linear regimes in the logarithmic plot of $\frac{M_t}{M_\infty}$ vs t and are tabulated in Table 4.2.

Table 4.2 Power law exponents of water absorption process

GECO/GEPO	k	r	R^2
100/0	0.03	0.89	0.99
75/25	0.11	1.0	0.99
50/50	0.15	1.01	0.96
25/75	0.11	1.13	0.97
0/100	0.086	1.24	0.97

Peppas *et al.*¹⁰⁸ derived for thin films, $r < 0.5$ corresponds to Fickian type of diffusion, while $r > 1$ indicates the relaxation controlled type and $0.5 < r < 1$ implies the anomalous transport. Except GECO (100/0), all the GECO/GEPO blends exhibited $r \geq 1$ in the region of $\frac{M_t}{M_\infty} < 60\%$, indicating the possibility of relaxation controlled water transport mechanism. On the other hand, GECO showed $r < 1$ indicating the possibility of anomalous transport mechanism.

According to Hopfenberg and Berens⁷⁶, Fickian and relaxation process occurs independently in the water transport/swelling process and thus the total absorbed water can be written as

$$M_t = M_{t,F} + M_{t,R} \quad 4.6$$

$$\frac{M_t}{M_\infty} = \Psi_F \left(\frac{M_t}{M_\infty} \right)_F + \Psi_R \left(\frac{M_t}{M_\infty} \right)_R \quad 4.7$$

$$\frac{M_t}{M_\infty} = \Psi_F \left[1 - \frac{8}{\pi^2} \sum_{j=0}^{\infty} \frac{1}{(2j+1)^2} \exp \left(-\frac{D_c(2j+1)^2 \pi^2}{h^2} t \right) \right] + (1 - \Psi_F)[1 - \exp(-k_r t)] \quad 4.8$$

Where $M_{t,F}$, $M_{t,R}$, M_t indicate the water uptake from the Fickian, relaxation mechanism and total water uptake respectively. Ψ_F, Ψ_R represent the relative contributions of Fickian and relaxation mechanism to the equilibrium water absorption process respectively. D_c , h , k_r are the average diffusion coefficient, thickness of the polymer sample and relaxation rate constant respectively. F and R indicate the Fickian and relaxation mechanism respectively.

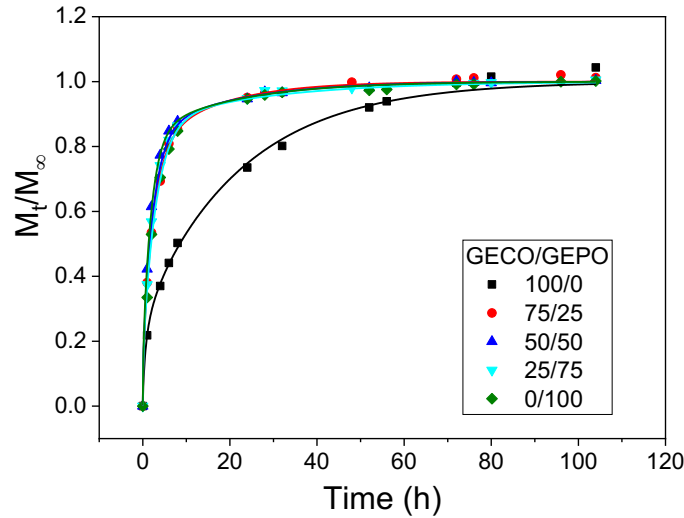


Figure 4.7 Water swelling (experimental data) fitted by Hopfenberg-Berens model. The symbol, lines represent the experimental data and the fitted curves respectively.

The experimental data perfectly fitted the Hopfenberg–Berens model (Figure 4.7) and the fitting parameters (Ψ_F , D_c , k_r , Ψ_R) are shown in Table 4.3. The values of Ψ_F and Ψ_R around 0.8–0.9 and 0.1–0.2 confirms the contribution of both Fickian and relaxation mechanism for the total water absorption of GE/CO, GE/PO and their blends. The higher value of Ψ_F suggests the dominance of Fickian diffusion mechanism over the total water uptake (equilibrium water absorption). The lower value of Ψ_R implies the possibility of relaxation mechanism occurring

only at higher $\frac{M_t}{M_\infty}$ values as seen in several other materials¹⁰⁹. This has been further confirmed from Figure 7.1(Appendix), where the Fickian diffusion equation fits perfectly the experimental data till $\frac{M_t}{M_\infty} = 0.8$ and above which poor fit is observed.

Table 4.3 Fickian and relaxation constants derived from Hopfenberg-Berens equation.

GECO/GEPO	Ψ_F	$D_c \times 10^6$ (mm²/s)	k_r	Ψ_R ($1 - \Psi_F$)
100/0	0.89	4.94	1.452	0.11
75/25	0.79	45.4	0.064	0.21
50/50	0.84	56.4	0.050	0.16
25/75	0.84	46.1	0.050	0.16
0/100	0.87	36.7	0.034	0.13

The diffusion coefficient values indicate that the rate of diffusion followed the order of 50/50 > 25/75 > 75/25 > 0/100 > 100/0 GECO/GEPO blends. D_c values are found to increase with the addition of GEPO in the blend till 50 phr and after which a slight decrease is noticed. The initial increase in diffusion coefficient is expected due to the increase in the hydrophilic nature (GEPO) of the composite. But the slightly decreased D_c values above 50 phr of GEPO in the composites could be attributed to the presence of crystalline regions in the blend system. It is needless to say that the crystalline regions offer resistance to the diffusion of the water molecules and thus reducing the rate of diffusion¹¹⁰.

To summarize, the power law equations explained the possibility of relaxation controlled water transport mechanism and the Hopfenberg-Berens equation clearly distinguished the water absorption contributions from the Fickian (80–90%) and relaxation mechanism (10–20%). From this study, it can be concluded that the initial part of the water absorption curves exhibited Fickian diffusion mechanism followed by relaxation controlled water absorption at higher water contents.

4.1.3 Effect of water swelling on thermal and mechanical properties

4.1.3.1 Retention of crystal structure during water swelling process: DSC analysis

DSC analyses of dry (D) and water swollen-dried samples (DWD) were performed for the GECO/GEPO blends and their ability to retain the crystal structure after water swelling is shown in Figure 4.8. It has to be noted here that the water-swollen samples were dried at room temperature for 24 h and then exposed to 50 °C for 3 h before the measurement and so, the possibility of some undried bound water molecules present in the DWD sample should not be neglected. From the DSC studies, it is clear that DWD samples exhibited a positive shift in peak melting point and onset melting temperature compared to the Dry (D) samples (Table 4.4). On the other hand, DSC cooling curves (Figure 4.8b) indicated the broad crystallization behavior of D samples (50/50, 25/75 and 0/100) being replaced by sharp crystallization behavior in DWD samples. However, it is interesting to note that very slight changes in percent crystallinity of the 50/50, 25/75 blends were obtained after the water swelling process, where as significant reduction is obtained for 75/25 GECO/GEPO blend. Glass transition temperature of both dry (D) and swollen-dried (DWD) samples of all the blends are observed to have almost similar values.

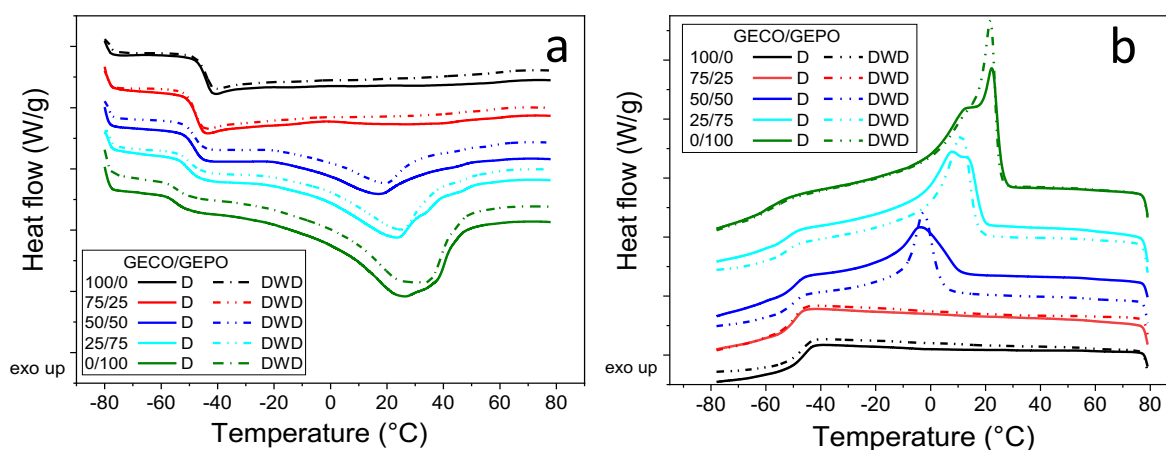


Figure 4.8 DSC analyses of dry (D) and water swollen–dried (DWD) samples of GECO/GEPO blends: a) heating curve, b) cooling curve. Very slight alteration in the recrystallization behavior of the GECO/GEPO blends with water absorption is illustrated.

Table 4.4 DSC analyses of GEICO/GEPO blends before (D) and after water swelling process (DWD)

GEICO/GEPO	Dry (D)			Swollen-dried (DWD)		
	T_g (°C)	T_m (°C)	X_c (%)	T_g (°C)	T_m (°C)	X_c (%)
100/0	-44.9	-	-	-45.0	-	-
75/25	-48.0	-	1.1	-48.2	-	0.7
50/50	-48.5	17.3	9.4	-48.3	19.7	9.3
25/75	-50.0	23.7	16.0	-49.8	25.2	15.7
0/100	-54.4	26.3	24.3	-54.0	33.9	24.1

To summarize, it is clear that the DWD samples almost retained their crystal structure even after the water swelling process. More specifically, slight difference in the melting profile and the crystallization behavior is detected and is only expected to have slight difference in the mechanical properties of the GEICO/GEPO blends.

4.1.3.2 Retention of mechanical properties: DMA (Temperature sweep)

DMA analyses of different GEICO/GEPO blends are shown in Figure 4.9. Three types of samples are shown for each blend system: D – Dry sample as prepared, DW – Water-swollen sample (sample contains equilibrium water content), DWD – water swollen and dried sample.

DWD samples are expected to have similar mechanical properties compared to D samples for commercial applications. As expected, 100 GEICO composites exhibited almost similar values of D samples. Surprisingly, slightly higher storage modulus values are observed for 75/25 GEICO/GEPO composites (Figure 4.9b). This could be attributed to the reduced crystallinity and its consequent depression in the melting region (Table 4.4), leading to the enhanced storage modulus values above 40 °C. On the other hand, the blends of DWD samples containing 50 phr or more GEPO (50/50, 25/75, 0/100) exhibited slight reduction in the storage modulus values between 20 and 50 °C (compared to D samples, Figure 4.9c-e). This could be attributed to the alteration of the crystal structure during/after the swelling process, as characterized from DSC studies (Figure 4.8).

All the DW samples (containing water) except 75/25 GEICO/GEPO exhibited a decrease in storage modulus values when compared to dry (D) samples (Figure 4.9c-e). This is obvious due to the presence of large amount of water in the swollen samples acting as plasticizer in the

composites, which can be confirmed from the decrease in glass transition temperature (temperature at $\tan \delta$ peak (inset)) of the composite.

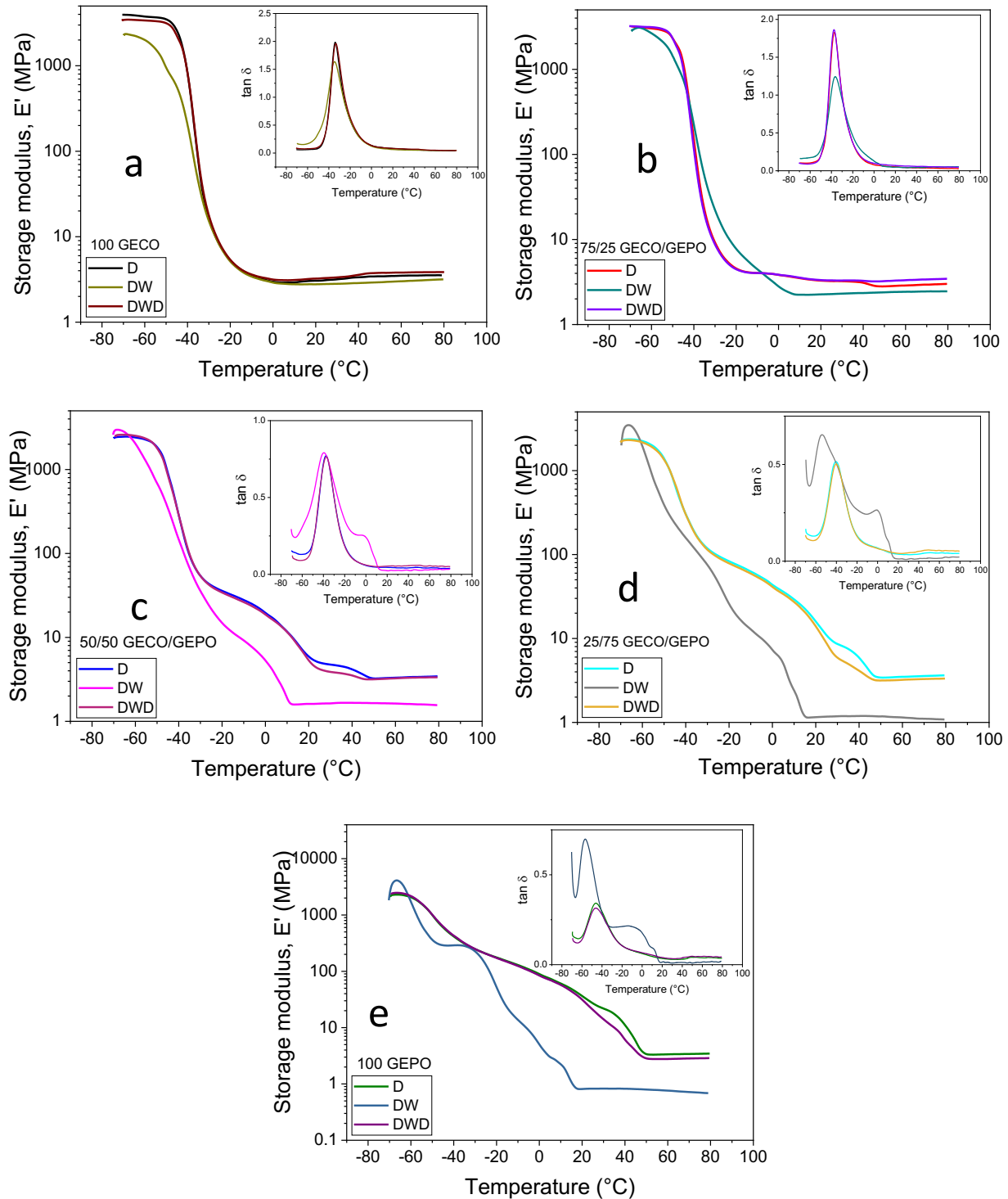


Figure 4.9 Dynamic mechanical analysis of GECO/GEPO blends when the sample is dry as prepared (D), Water-swollen (DW) and the water swollen-dried (DWD): a) 100 GECO, b) 75/25 GECO/GEPO, c) 50/50 GECO/GEPO, d) 25/75 GECO/GEPO, e) 100 GEPO.

On the contrary, 75/25 GECO/GEPO DW composites exhibited higher modulus between T_g and $-5\text{ }^{\circ}\text{C}$ compared to the initial dry (D) samples. This enhancement in modulus below $0\text{ }^{\circ}\text{C}$ could be due to the formation of solid ice crystals (from absorbed water) and its tendency to act as reinforcing filler below $0\text{ }^{\circ}\text{C}$, which can be confirmed by the decrease in the $\tan \delta$ peak height (Figure 4.9b, inset). This reinforcement effect is replaced by the plasticizing effect at higher temperatures, as the ice crystals melts at $0\text{ }^{\circ}\text{C}$ and thus the modulus decreases above $0\text{ }^{\circ}\text{C}$. This concept of switching the ability of fillers to reinforce/plasticize has been explored in this work for designing mechanically adaptable composites and will be discussed in detail in the next chapter. Conversely, it is also expected that the ice crystals formed in the other blends systems (50/50, 25/75, 0/100 GECO/GEPO) in the region below $0\text{ }^{\circ}\text{C}$ to have produced a reinforced composite. However, a decrease in storage modulus is observed and this might be due to the dominance of plasticizing effect of the non-freezable bound water over the reinforcement effect of the *in situ* formed ice crystals. More precisely, it is expected that the non-freezable bound water molecules has diffused in to the crystalline domains, leading to the destructions of crystalline region and thus exhibiting lower modulus.

4.1.3.3 Retention of mechanical properties after water swelling: Tensile properties

Stress–strain properties of the D and DWD samples of GECO, GEPO and their blends are tabulated in Table 4.5. DWD samples almost retained the stress–strain characteristics of D samples. More specifically, tensile strength (TS) of the DWD samples of 100/0 and 75/25 GECO/GEPO are slightly higher than the dry (D) samples. On the other hand, 50/50, 25/75, and 0/100 GECO/GEPO blends exhibited slightly lower tensile strength than the initial dry sample. This is in trend with the DMA results (storage modulus values of the blends). Generally, no conclusion could be derived from the elongation at break (EB) values of D and DWD samples and it could be very difficult to explain in such complicated polymer blend systems.

Table 4.5 Retention of mechanical properties in water swollen and dried (DWD) composites

GECO/GEPO	Before water swelling (D)		After water swelling (DWD)	
	TS (MPa)	EB (%)	TS (MPa)	EB (%)
100/0	2.29	204	2.32	193
75/25	2.40	192	2.68	210
50/50	2.42	185	2.32	216
25/75	2.85	167	2.72	221
0/100	3.1	230	2.9	225

4.1.4 Cyclic water swellable characteristics

Cyclic water swellable characteristics of the developed GECO/GEPO blends were studied for three swelling cycles and are shown in Figure 4.10. A weighed dry (W_d) sample was immersed in water till the equilibrium weight was achieved and then the sample was removed from water and weighed (W_{dw}) after removing the surface water. The sample was allowed to dry at room temperature (24 °C) for 48 hours and exposed to 50 °C for 3 hours to remove the bound water and then weighed again (W_{dwd}). The same process was repeated for second and third water swelling cycles.

The leaching of hydrophilic polymers/resin from the elastomer composites has been reported as the primary reason behind poor repeatable characteristics^{54, 56a}. In this work, the leaching/removal of the hydrophilic polymers (GEPO) from the GECO/GEPO blends were evaluated by measuring the weight difference ($(W_d - W_{dwd})/W_d \times 100$) before (D) and after the swelling-dried (DWD) process for three cycles and is represented as weight loss (%) in Figure 4.10a. The neat GECO exhibited very low weight loss (<2%), whereas GEPO showed substantial weight loss characteristics (<5%) and their blends showed weight loss in between those of the individual polymers after three swelling cycles. The observed weight loss might be due to the loss of the low molecular weight polymer/unreacted fillers/curatives present in the composites like ZnO, stearic acid, TMTD, MBTS, and S. This observed weight loss of <5 % is very low when compared to water swellable composites reported in literature (>20%)^{56b, 79, 97b} and hence the composite is expected to have stable and repeatable water swellable characteristics. Thermogravimetric analysis (TGA) is additionally employed to evaluate the

loss of hydrophilic polymer during the water swelling process in the GECO/GEPO blends and is shown in Figure 4.10b. Both the D and DWD samples of GECO/GEPO blends showed almost similar weight loss characteristics with temperature. This once again indicates no or very little removal of hydrophilic materials in the blend after water swelling process.

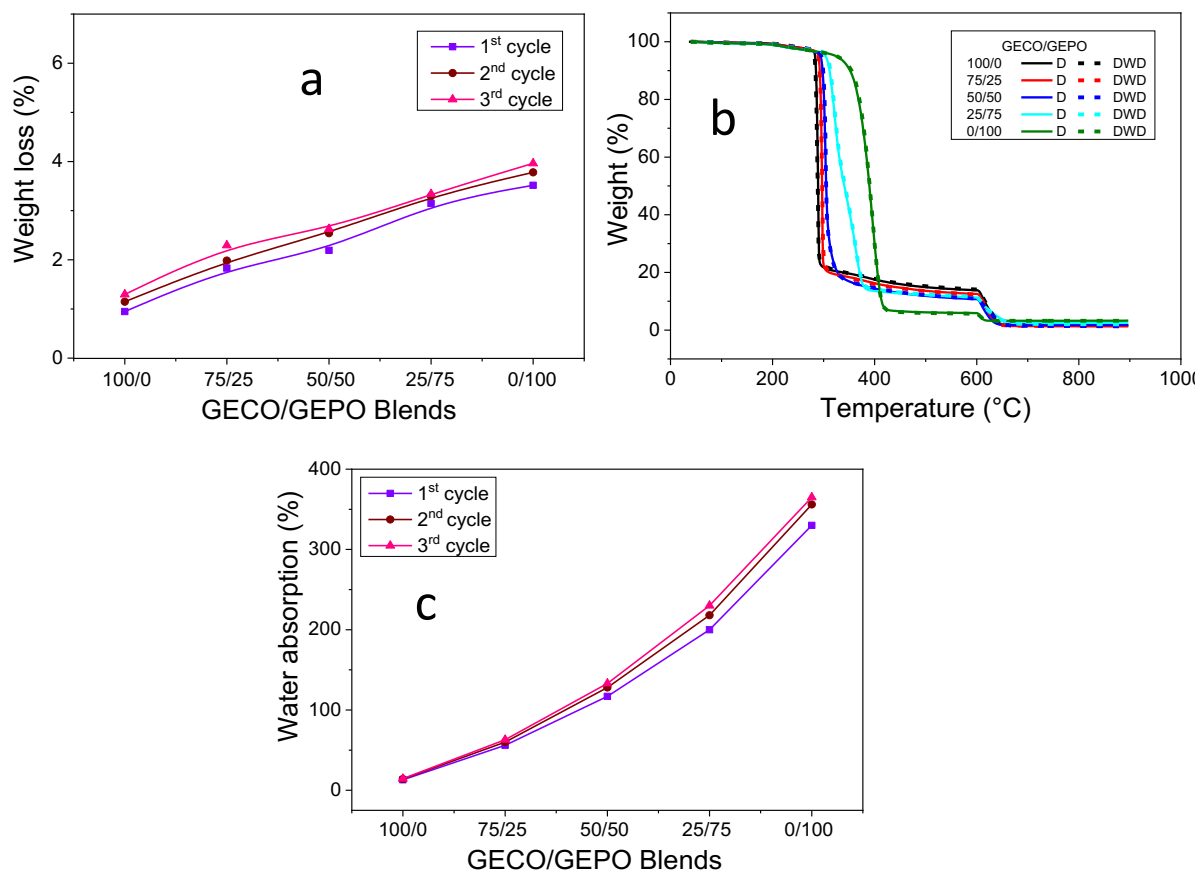


Figure 4.10 a) Weight loss analysis of the GECO/GEPO blend samples after few cycles of water swelling, b) TGA of GECO/GEPO blends before (D) and after water swelling-dried (DWD) samples, c) repeatable water swelling characteristics of the GECO/GEPO blends.

Equilibrium water swelling/degree of swelling (i.e., $(W_{dw} - W_d)/W_d \times 100$) of all the blends for three cycles are studied and is shown in Figure 4.10c. Equilibrium swelling studies showed almost similar results for first, second and third cycles for all the GECO/GEPO blends. More specifically, a slight increase in water swellability is observed with swelling cycles and it might be due to the changes in the crystal structure during the water swelling process or minor changes in the environmental conditions like temperature, pressure, etc. Similar water absorption characteristics even after three cycles of water swelling confirmed the stable and repeatable water swellable characteristics. To summarise, the developed GECO/GEPO blends exhibited stable and repeatable water swellable characteristics.

4.2 Thermo-responsive mechano-adaptable composites based on solid–liquid phase transition of absorbed water.

In this chapter, mechanical adaptability is achieved by temperature induced phase transition process, i.e., the ability of certain materials to change its phase from solid to liquid at low temperatures. More specifically, phase change materials, which undergo solid to liquid transition at lower temperatures ($<100\text{ }^{\circ}\text{C}$) can be employed as a functional filler in attaining the temperature dependent mechanically adaptable elastomer composites. Some of the well-known examples of phase change materials are paraffins, salt hydrates, eutectics, etc. One of the widely available and cheapest phase change material used in our day to day life is water/ice. By imbibing water inside the elastomer, the ice crystals can be formed at temperatures less than $0\text{ }^{\circ}\text{C}$ and can be transformed in to liquid water at higher temperatures ($>0\text{ }^{\circ}\text{C}$). This solid–liquid transition is expected to provide different mechanical properties before and after the transition and thus leading to temperature induced mechanical adaptability.

Since water cannot withstand the processing conditions of an elastomer, it has to be incorporated in to the elastomer composites after the vulcanisation process. The same process of water swelling used in the previous chapter has been employed here. The reinforcing ability of water (ice) at low temperature followed by the plasticizing ability at high temperatures, as observed in the DMA analysis of 75/25 GECO/GEPO DW sample (Figure 4.9b) is expected to tune the mechanical properties around $0\text{ }^{\circ}\text{C}$. The slight crystalline melting (Figure 4.9b) around $0\text{ }^{\circ}\text{C}$ for 75/25 GECO/GEPO is expected to complicate the interpretation of the adaptability process. Hence the neat GECO compounds, which is completely amorphous, is used in this study. But in case of 100 GECO (DW), the formation and melting of ice crystals (around $0\text{ }^{\circ}\text{C}$) cannot be perceived from the DMA analysis (Figure 4.9a). This is anticipated due to the low water absorption capability of the prepared GECO composites.

In order to improve the water absorption characteristics, cross-link density of GECO can be reduced by decreasing the amount of accelerator/sulphur present in the rubber compound. SC1 the same compound as 100 GECO (used in the previous chapter), SC2 containing 0.5 phr of S and 0.5 phr of TMTD, and SC3 containing 0.25 phr of S and 0.25 phr of TMTD were prepared (Table 3.3) and its rheological characteristics (torque-time curve) are shown in

Results of this chapters are published in ACS Omega 2 (2), 363-371, 2017

Figure 7.2 (Appendix), indicating higher cross-link density for $SC1 > SC2 > SC3$. Figure 4.11 shows that the reduction of curatives/cross-link density has led to the increase in water swellability and a maximum of ~40% of water is absorbed by SC3 composite (containing very less curatives). So, the SC3 composite is chosen for further studies and is hereafter abbreviated as GECCO.

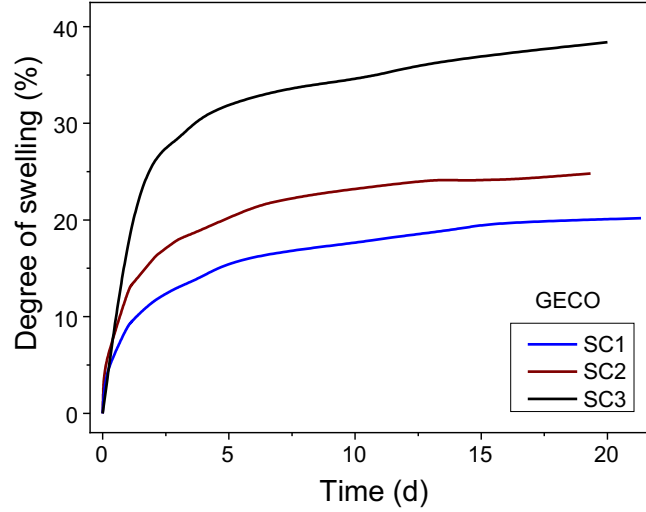


Figure 4.11 Water absorption characteristics of GECCO with varying curative content. The composite (SC3) containing slight amount of S/TMTD exhibited higher water absorption characteristics.

4.2.1 Quantitative analysis of *in situ* formed ice crystals

GECCO (SC3) absorbs water to a maximum of ~40% of its initial weight (of the dry sample) and reaches 90% of its swelling capacity in 4–5 days (Figure 4.11). Due to the different states of water present in the composites (non-freezable bound water, freezable bound water and freezable free water), only a part of absorbed water can be frozen to form ice crystals below 0 °C (section 2.2.2). The amount of freezable and non-freezable water can be quantified from the endothermic ice melting profile of the swollen elastomers using differential scanning calorimetry (DSC). The heating curves of the dry GECCO and its 2, 7, and 20 days water-swollen composites are shown in Figure 4.12. The broad endothermic peak, obtained around 0 °C, is attributed to the combined melting of the free and freezable bound water¹¹¹.

It is assumed that the total absorbed water (W_t) is the sum of freezable (W_f) and non-freezable water (W_{nf}). The freezable water (W_f) includes the fractions of both free water and freezable bound water in the polymer.

$$W_t = W_{nf} + W_f \quad 4.9$$

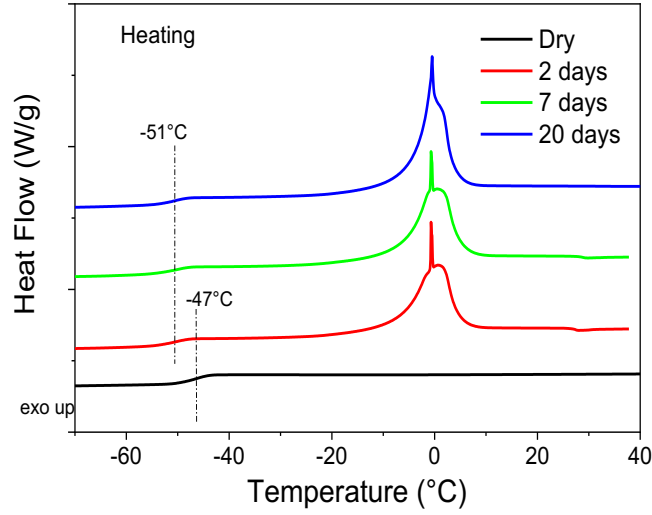


Figure 4.12 DSC analyses of Dry, 2, 7, and 20 days water-swollen samples. Melting of ice crystals formed in water-swollen samples can be visualized in the temperature around 0 °C.

The amount of freezable water can be obtained from the following equation (assuming the melting enthalpies of the different types of water (free and freezable bound water) to be same)

$$\frac{W_f}{W_d} = Q \frac{\Delta H_{ws}}{\Delta H_{bw}} \quad 4.10$$

Where W_d , W_w are the weight of the dry and water swollen sample respectively, ΔH_{ws} is the enthalpy of the water swollen elastomer, and ΔH_{bw} is the enthalpy of bulk water, which can be taken as ~ 330 J/g, The melting enthalpies of different crystal structures of ice are assumed to be same during the calculation, so the calculated values of freezable water/ice crystals are expected to have a standard deviation of about 5%⁶² (lowest for tetragonal ice crystals, 312 J/g, and highest for hexagonal ice crystals, 334 J/g). The ice-melting enthalpies (ΔH_{ws}) were obtained by integration of the peak areas of the DSC curves (Figure 4.12) of water-swollen GECO composites. Q , the swelling ratio of the swollen sample, can be written as $Q = \frac{W_{dw}}{W_d}$.

The vol- % of the filler (ice crystals) present in the GECO composites can be quantified using the following equation:

$$\begin{aligned} & \text{Vol- \% of the filler(ice crystals)} \\ &= \frac{\text{vol. of freezable water}}{\text{vol. of dry composite} + \text{vol. of total absorbed water}} \times 100 \end{aligned} \quad 4.11$$

Based on the calculations from the above equations, volume percent (*vol-%*) of the ice crystals (filler) with respect to the total volume of the sample were calculated and is shown in Table 4.6. From Table 4.6, it can be understood that, with the increase in the absorbed water/days of swelling, more freezable water molecules are formed (W_f), indicating the increased volume of the ice crystals formed inside the elastomer composites. Approximately 21.2, 23.7 and 25.4 *vol-%* of ice crystals are formed *in situ* the elastomer composites by immersing the prepared sample in water for 2, 7, and 20 days respectively. It is also important to note that 70–80% of the absorbed water has been transformed to ice crystals.

Table 4.6 DSC melting profile and volume percentage of the filler (ice crystals) formed in GECCO composites

Water swollen time (days)	DS ($(W_{dw}-W_d)/W_d$) (%)	Enthalpy ΔH (J/g)	Freezable water (W_f/W_d) (%)	Vol-% of the ice crystals that act as filler in GECCO composites (%)
Dry	-	-	-	--
2	26.8	56.7	81.6	21.2
7	33.5	61.5	73.2	23.7
20	38.4	66.3	74.2	25.4

Additionally, from Figure 4.12, the glass transition temperature (T_g) of the water-swollen composites can be obtained and it is expected that absorption of water reduces the glass transition temperature. Initially, a 4 °C drop in T_g (–47 to –51 °C) is observed for 2 days swollen sample and further increase in water content/days of water swelling did not have any impact on the glass transition temperature. This is in accordance with the several works indicating the levelling of T_g after the limiting water content is reached^{67, 112}. This behavior is attributed to the formation of solid ice crystals (below 0 °C) after certain threshold of water absorption is achieved. Nevertheless, initial 4 °C drop in T_g is attributed to the plasticizing effect caused by the non-freezable bound water present in the composites.

Thermogravimetric analysis (TGA) of dry and 20 days samples were studied and are shown in Figure 4.13. 20 days water-swollen GECCO samples exhibited a two stage decomposition process. The first decomposition process completed around 180 °C with a loss of 28% and is expected due to the evaporation of water (which is in accordance with the swelling studies). The second decomposition occurs due to the polymer degradation and appeared around 325–

335 °C. Surprisingly 5 °C rise in polymer degradation temperature is observed for 20 days water-swollen sample, indicating formation of a more stable compound when treated with water (derivative plot, inset). This might be due to the presence of some unevaporated bound water molecules confined to the polymer chains till the degradation temperature of the polymer.

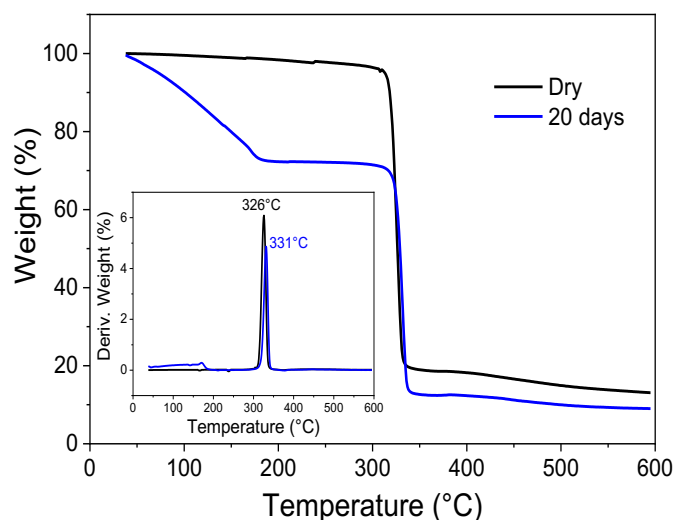


Figure 4.13 Thermogravimetric analysis of dry and 20 days water-swollen sample. Derivative weight of the GECO -water composites as a function of temperature (inset).

4.2.2 Characterization of the filler (ice crystals) morphology

4.2.2.1 Morphology of the *in situ* formed ice crystals using cryo-TEM

Cryo-transmission electron microscopy was utilized to visualize the morphology of ice crystals formed at freezing temperatures inside the water-swollen GECO composites. Cryo-TEM images of 20 days water-swollen GECO composites are shown in Figure 4.14. Roughly spherical to oval shaped ice crystals are observed and are found to be uniformly distributed in the GECO matrix (Figure 4.14a). The dark regions in the images are identified as ice crystals condensed due to humidity on the surface of the specimen. 20 days water-swollen sample was freeze dried *in situ* during the cryo-TEM imaging process and is shown in Figure 4.14b. Sublimation of ice crystals occurred during the freeze drying process and has led to the formation of pores (holes) in the composites. This formation of pores confirms the presence of solid ice crystals inside the water-swollen GECO composites before the freeze drying process.

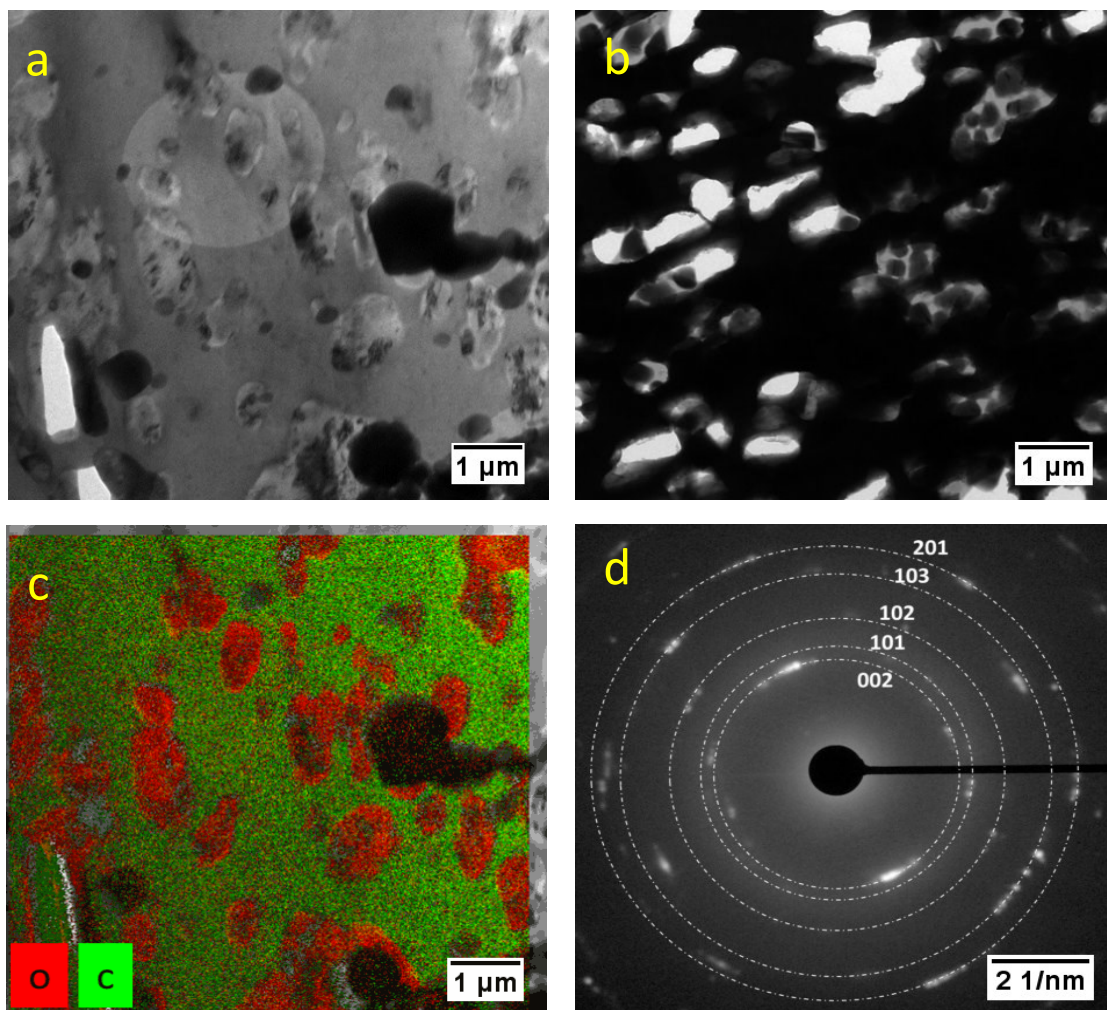


Figure 4.14 a) *In situ* formation of ice crystals are observed in cryo-TEM image of water-swollen GECO sample, b) freeze drying process leading to the formation of holes in the composites indicating the presence of ice crystals, c) EFTEM, Elemental mapping of carbon and oxygen over a), d) selected area electron diffraction (SAED) image of GECO-ice crystals composite. The indexed rings correspond to hexagonal crystal structure of ice.

Elemental mapping was carried out using energy filtered transmission electron microscopy (EFTEM) to establish the chemical composition of the water-swollen composites and is shown in Figure 4.14c. The red and green areas indicate the oxygen present in solid ice and the carbon present in the polymer respectively. The oxygen rich areas (red) confirmed the formation of solid ice crystals. It is also important to note that the oxygen present in the GECO polymer backbone can also be identified, as red dots in the green rich areas. Selected area electron diffraction (SAED) pattern of water-swollen GECO composites were analyzed and is shown in Figure 4.14d. A ring and spot pattern is obtained and is attributed to the polycrystalline nature of ice crystals. The obtained patterns are indexed as (002), (101), (102), (103), (201) planes that confirmed the hexagonal crystal structures of ice and is found to be in accordance with literature¹¹³.

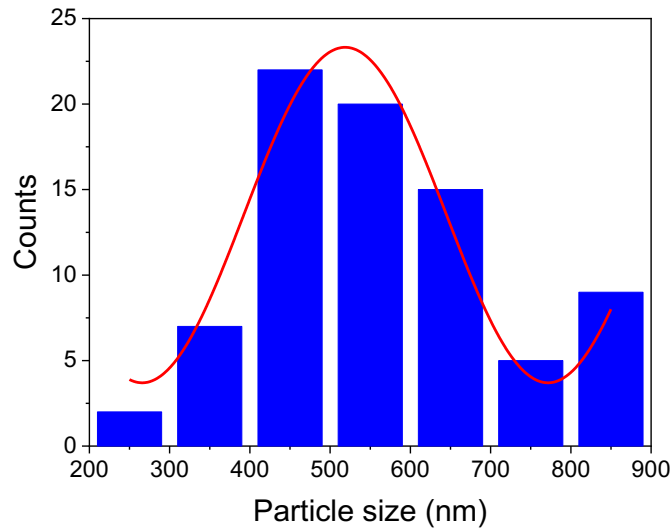


Figure 4.15 Particle size distribution of ice crystals from cryo-TEM images

The particle sizes of the ice crystals were measured from the cryo-TEM images by assuming the ice crystal to be spherical in nature and are shown in Figure 4.15. The particle sizes of the ice crystals varied from 200–1100 nm. The average particle size of the ice crystals is found in the range of 400–600 nm, which is considered as ideal for achieving reinforcement in the polymer composite.

4.2.2.2 Filler networking using amplitude sweep (DMA)

The amplitude (strain) sweep analysis was performed using DMA at $-20\text{ }^{\circ}\text{C}$ to evaluate the filler–filler interactions of the *in situ* formed ice crystals filled GECO composites and are shown in Figure 4.16. The measurements were performed after holding the sample at $-20\text{ }^{\circ}\text{C}$ for 30 min, so that the stable crystals can be formed. Dry GECO composites exhibited dynamic strain independent storage modulus value, which is typically expected for unfilled composites. On the other hand, a nonlinear dependence of storage modulus on dynamic strain is observed for the water-swollen samples and is attributed to the so called Payne effect, which is based on the destruction of the filler–filler network with respect to strain¹¹⁴. A stronger Payne effect was observed with the higher volume fraction of ice crystals inside the rubber. This confirms the existence of filler networks of *in situ* formed ice crystals in the water-swollen GECO composite.

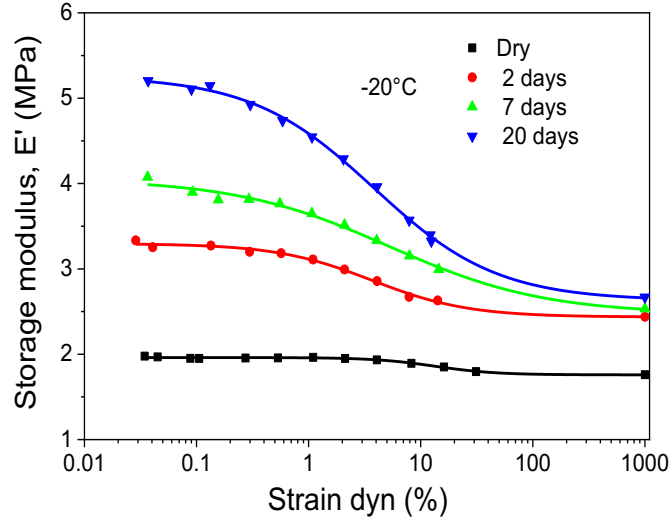


Figure 4.16 Storage modulus (E') as a function of dynamic strain at $-20\text{ }^{\circ}\text{C}$. The data for high strains are extrapolated for hydrodynamic reinforcement from the dry GECCO. Solid dots and lines represent experimental values and fitted (Kraus equation) curves respectively.

The in-depth analysis of Payne effect has been carried out based on the agglomeration-deagglomeration mechanism of the filler proposed by Kraus¹¹⁵.

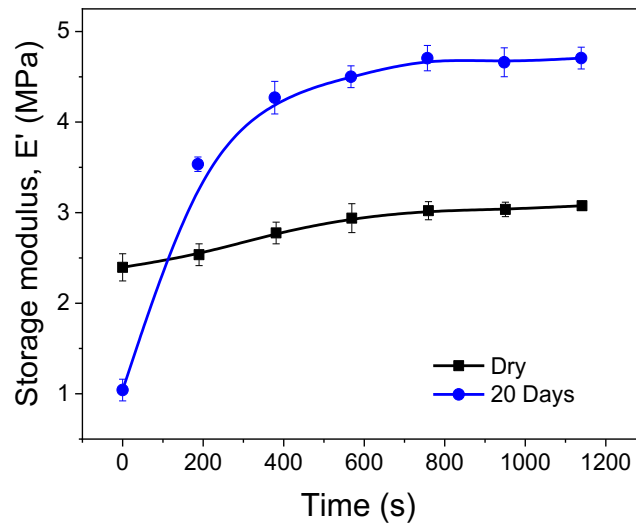
$$\frac{E'(\gamma) - E'_{\infty}}{E'_0 - E'_{\infty}} = \frac{1}{1 + \left(\frac{\gamma}{\gamma_c}\right)^{2m}} \quad 4.12$$

Where, $E'(\gamma)$ is the modulus of the composite at the given strain γ , $E'(\gamma) = E'_{\infty}$ at very large strains; $E'(\gamma) = E'_0$ at very low strain (γ_0); γ_c is the critical strain, at which the magnitude of $E'_0 - E'_{\infty}$ becomes half, and is largely dependent on the nature and type of the polymers, fillers, and their state of the dispersion in soft elastomer matrix; m is a strain sensitivity constant, which depends on specific fractal dimensions of the fractal agglomerate structures of the fillers and the mechanism of filler–filler contact breakage. The experimental datas are fitted with the above equation (Figure 4.16) and the values of γ_c and m are shown in Table 4.7. In Table 4.7, almost similar values of γ_c can be observed, which might indicate the similar type of rubber-filler and filler–filler interactions. The value of m decreased with higher amount of *in situ* formed ice crystals. The m values of several carbon black filled rubber composites were studied in literature and is found to be independent of the type and nature of the carbon black (reported value is ~ 0.6 ¹¹⁶). While the decreasing value of m in the present case indicates the possibility of formation of different morphologies of the ice crystals for different days in the water-swollen GECCO samples.

Table 4.7 Amplitude sweep analysis of the water-swollen samples at $-20\text{ }^{\circ}\text{C}$: values derived from Kraus model.

Sample (Days)	Critical strain γ_c (%)	Exponent (m)
2	3.67	1.58
7	3.62	1.01
20	3.85	0.79

The reinforcing character of the ice crystals, developed during the phase transition of water to ice, can be visualized using the time sweep analysis at $-20\text{ }^{\circ}\text{C}$ and is shown in Figure 4.17. Time sweep analysis was performed by measuring the storage modulus as a function of time with a constant static (1%) and dynamic load (0.2%) at $-20\text{ }^{\circ}\text{C}$. The measurement started as soon the temperature was reached. The modulus of the dry rubber is found to be almost independent of time. However, the remarkable increase in storage modulus is observed with time for the water containing GECO sample (20 days). This modulus enhancement can be used to visualize the phase transition process (formation of ice crystals) of water (filler) and its interaction with the polymer.

**Figure 4.17 Time sweep analysis of dry and 20 days water-swollen GECO samples. Phase transition of water to ice crystals and their reinforcing efficiency can be observed from this study.**

4.2.3 Polymer–filler interaction

Attenuated total reflection-Fourier transform infrared (ATR-FTIR) spectra of dry and 20 days water-swollen GECO composites were analyzed at room temperature (RT) to study the possible interaction between water and polymer and are shown in Figure 4.18a. The water-

swollen sample (20 days) exhibited intensive broad bands of both stretching and deformation vibrations of hydroxyl groups (water) at 3415 and 1639 cm^{-1} respectively¹¹⁷, indicating the presence of water in the composite. GECCO being highly polar in nature, is expected to have strong interaction with the water molecules, usually resulting in a remarkable band shift of the ether group at 1088 cm^{-1} . But the 20 days water-swollen sample exhibited a very weak band shift of about 4 cm^{-1} , which is close to the spectral resolution. It is important to note that even the dry composite exhibited weak bands in the spectroscopic water regions such as 3415 and 1639 cm^{-1} . This indicates traces of moisture already present in the dry GECCO composite. It is expected that the moisture could be absorbed from the environment during handling or storage conditions (it was roughly measured to be around 3–5% after storing in RT for 20 days).

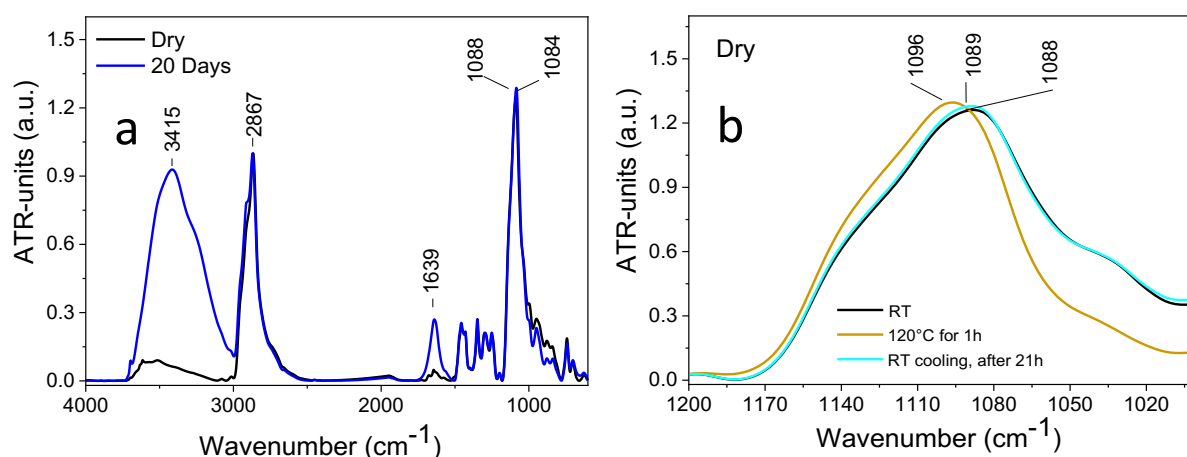


Figure 4.18 ATR-FTIR spectra of GECCO composites: a) Dry and 20 days water-swollen GECCO sample, b) FTIR spectra at room and elevated temperatures: Dry sample at RT, after 1h treatment at 120 °C, after cooling back to RT and in 21 hours at RT.

In order to confirm the strong intermolecular hydrogen bonding between ether groups of the GECCO polymer and water molecules, temperature dependent ATR-FTIR spectroscopy of dry sample was studied. Figure 4.18b shows the FTIR spectra of the dry sample (RT), sample heated to 120 °C for 1 hour, and the 21 hour cooled sample after heating to 120 °C. It is found that after heating the sample to 120 °C (removal of the absorbed water), a remarkable band shift ($\sim 8 \text{ cm}^{-1}$ shift) of ether group to higher wavenumber (1096 cm^{-1}) is observed. When the sample is brought back to room temperature and tested after 21 hours, the ether band returned to lower frequencies (1089 cm^{-1}) similar to untreated dry (RT, 1088 cm^{-1}) samples, indicating the absorption of moisture at RT.

One can conclude from the FTIR measurements that, the dry sample was already bonded with water molecules (absorbed from the air), explaining the weak shift of ether band regardless of

water amount, even for the 20 days water-swollen sample. To summarize, a significant band shift of 12 cm^{-1} (20 days – 1084 cm^{-1} , dry sample without moisture – 1096 cm^{-1}) is obtained indicating the strong hydrogen bonding between the ether group of GECO and the water molecule. Based on the FTIR studies, a probable interaction between the ether group of GECO and the hydrogen from the water molecules is schematically shown in Figure 4.19.

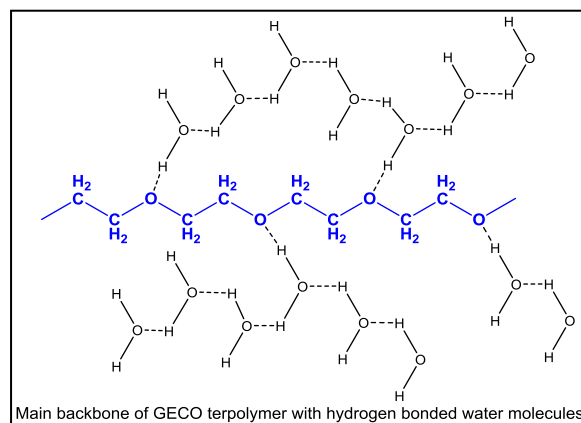


Figure 4.19 Schematic representation of intermolecular hydrogen bonding between water molecules and polymer chains in the GECO composite.

Molecular dynamics simulations are exploited to study the probable molecular arrangements of the polymer and water molecules and the simulations were performed using ChemBio3D 14.0, PerkinElmer, MM2 optimization and is shown in Figure 4.20. To maintain simplicity, polymer molecules containing 7 polyoxyethylene repeating units were simulated with 15 water molecules and the resulting conformation is shown in Figure 4.20. The figure established the possibility of polymer chains enclosing a cluster of water molecules, indicating a strong hydrophilic character of the GECO polymer.

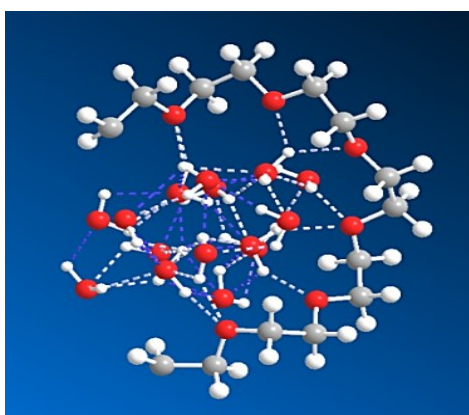


Figure 4.20 Molecular dynamics simulation of the polymer and water system (red - oxygen, gray – carbon, white – hydrogen atom, dashed lines: blue – intramolecular bonding in water, white – intermolecular hydrogen bonding between polymer and water).

4.2.4 Mechanical adaptability analysis

4.2.4.1 Stress–strain properties

Stress–strain properties were studied in tension mode at two different temperatures (in order to examine the mechanical adaptability) at $-20\text{ }^{\circ}\text{C}$ and $+20\text{ }^{\circ}\text{C}$ and are shown in Figure 4.21a. The samples were maintained at the respective temperatures for 30 min before the stress–strain measurements, so that the stable crystals can be formed. At $-20\text{ }^{\circ}\text{C}$, the 20 days water-swollen samples showed higher mechanical properties than the dry samples. Young's modulus (E) values of the 20 days water-swollen samples remarkably increased from 1.45 (for the dry sample at $-20\text{ }^{\circ}\text{C}$) to 3.14 MPa (*hard state*). However, at $+20\text{ }^{\circ}\text{C}$, water containing samples (20 days) showed poor mechanical properties as the Young's modulus values dropped from 0.6 (for the dry sample at $+20\text{ }^{\circ}\text{C}$) to 0.03 MPa (*soft state*). The presence of hydrogen bonding between the *in situ* formed ice crystals and the polymer chains (as understood from FTIR) is expected to be reason behind the reinforcement at low temperature ($-20\text{ }^{\circ}\text{C}$). On the other hand, at temperatures above $0\text{ }^{\circ}\text{C}$, the solid ice crystals melt and act as a plasticizer, thus reducing the mechanical properties.

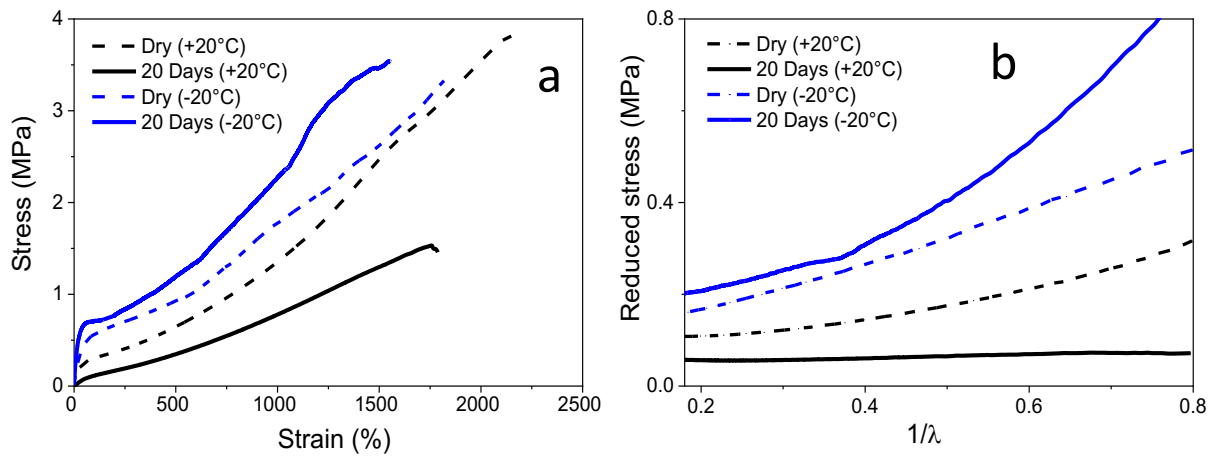


Figure 4.21 a) Stress–strain properties establishing the adaptability of 20 days water-swollen samples at $-20\text{ }^{\circ}\text{C}$ and $+20\text{ }^{\circ}\text{C}$ compared to dry samples, b) Mooney-Rivlin plot of the dry and 20 days water-swollen GECO composites at different temperatures.

The polymer–filler interaction and the reinforcement characteristics can be understood by applying stress–strain values to the phenomenological expression proposed by Mooney and Rivlin¹¹⁸

$$\frac{\sigma}{\lambda - \lambda^{-2}} = 2(C_1 + C_2\lambda^{-1}) \quad 4.13$$

where σ is the applied stress, λ is the extension ratio and C_1 , C_2 are the Mooney-Rivlin (MR) constants. The Mooney-Rivlin plots of dry and 20 days water-swollen GECO composites are shown in Figure 4.21b. C_1 and C_2 values can be obtained from the analysis of linear regime in the reduced stress ($\frac{\sigma}{\lambda-\lambda^2}$) vs $1/\lambda$ plot. Further the cross-link density (ν) can be calculated from C_1 with the following expression $2C_1 = \nu k_B T$ where ν is cross-linking density, k_B is the Boltzmann constant and T is temperature and is shown in Table 4.8. The cross-link density of 20 days water-swollen GECO samples showed slight decrease at 20 °C and slight increase at -20 °C, compared to dry sample. The increase in cross-link density indicates the formation of polymer–filler network through hydrogen bonding. The reduced cross-link density at 20 °C might probably indicate the decrease in entanglement of the polymer chains due to the plasticizing ability of water molecules.

Table 4.8 Cross-link density values obtained from Mooney-Rivlin equations

Sample designation	C_1	C_2	Cross-link density (ν) mol/cm ³
Dry @ RT (20°C)	0.05302	0.226	4.35 x 10 ⁻⁵
20 days @ RT (20°C)	0.04316	0.0336	3.54 x 10 ⁻⁵
Dry @ -20°C	0.06034	0.5131	5.73 x 10 ⁻⁵
20 days @ -20°C	0.06711	0.5946	6.38 x 10 ⁻⁵

The volume fraction of the ice crystals acting as filler particles can be calculated approximately using the Young's modulus values obtained from the stress–strain experiments (–20 °C) with the help of hydrodynamic equation proposed by the Chen and Acrivos for hard spherical particles¹¹⁹.

$$\frac{E}{E_0} = 1 + 2.5 \phi + 5.0 \phi^2 \quad 4.14$$

Here, E , E_0 are the Young's modulus of water-swollen and dry GECO samples, ϕ is the volume fraction of the *in situ* formed ice crystals. The volume fraction of *in situ* formed ice crystals is calculated to be around 29 vol-% which is very well in accordance to the DSC study (~26 vol-%).

4.2.4.2 Dynamic mechanical analysis

Dynamic mechanical behavior of water-swollen GECCO composites were studied as a function of temperature and is shown in Figure 4.22. Water absorption by the GECCO composite has led to enhanced storage modulus values in the temperature range of $-37\text{ }^{\circ}\text{C}$ to $0\text{ }^{\circ}\text{C}$. For example, at $-20\text{ }^{\circ}\text{C}$, storage moduli values of 2, 7, and 20 day swollen GECCO composites are about 67% (5 MPa), 167% (8 MPa), and 333% (13 MPa) higher than those of the dry GECCO composites (3 MPa) respectively, forming the *hard state* (Figure 4.22a). The *in situ* formation of ice crystals below $0\text{ }^{\circ}\text{C}$ is expected to interact with polymer chains, by forming hydrogen bonds with the oxygen present in the polymer backbone, resulting in ice crystal reinforced composites. At $0\text{ }^{\circ}\text{C}$, a crossover point in the storage modulus has been observed; the storage modulus of the water filled GECCO composites decreased with the increase in water content (swelling time) compared to dry GECCO composite. The storage modulus at $+20\text{ }^{\circ}\text{C}$ of 2, 7 and 20 days water-swollen GECCO composites are about 41% (1 MPa), 45% (0.94 MPa), and 64% (0.62 MPa) lower than the dry GECCO composite (1.7 MPa) (Figure 4.22a), leading to the *soft state*. At $20\text{ }^{\circ}\text{C}$, it is expected that the ice crystals are melted and liquid water acts as a plasticizing agent, leading to decreased storage modulus values.

The glass transition temperature (T_g) of the elastomer is often predicted from the temperature of maximum loss factor ($\tan \delta$) or maximum loss modulus (E''). The T_g obtained from $\tan \delta$ values remained unaltered at $-37\text{ }^{\circ}\text{C}$ with the increase in water content inside the elastomer composite (Figure 4.22b), which is in contrast with the DSC analysis. On the other hand, T_g measured from E'' curves exhibited significant negative shift of about $\sim 2\text{ }^{\circ}\text{C}$ for the 2 days swollen sample, however, no change is detected with further swelling (Figure 4.22c). The results (T_g) from the E'' curves are found to follow the same trend as DSC results. Several authors¹²⁰ proposed that T_g obtained from maximum loss modulus (E'') values to be a more consistent indicator of the segmental motion of the polymer chains and the maximum loss tangent values ($\tan \delta$) could be used to better understand the polymer–filler interaction. The loss factor as a function of temperature is shown in Figure 4.22b. It is noticed that the $\tan \delta$ peak height reduced with the higher amount of water/ice crystals. This reduction in $\tan \delta$ maximum confirms the interaction of ice crystals with the polymer chains. Further, the decrease in the $\tan \delta$ values above $0\text{ }^{\circ}\text{C}$, once again confirms the plasticizing effect of the liquid water present inside the GECCO composites. Additionally, the melting of ice crystals can also be inferred from the small peaks around $0\text{ }^{\circ}\text{C}$.

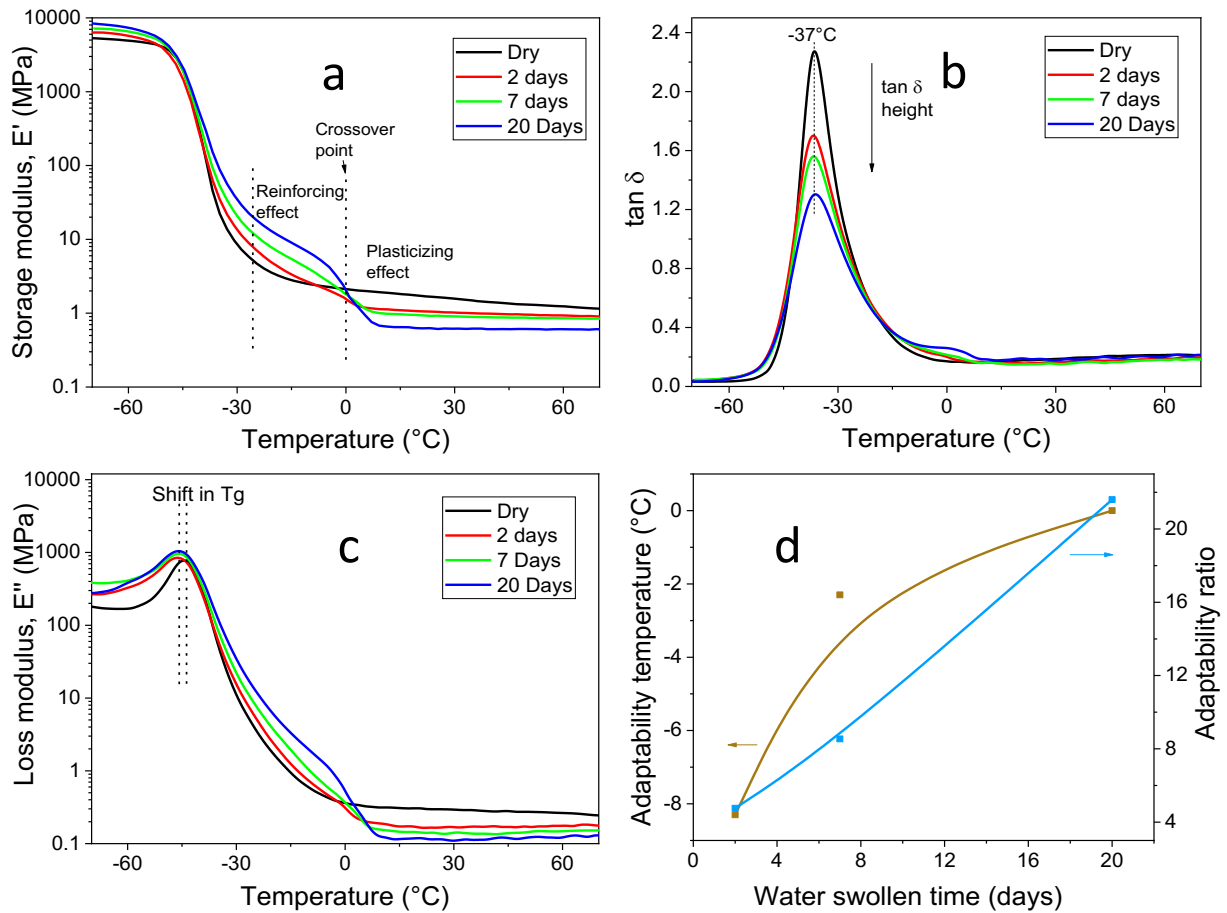


Figure 4.22 Dynamic mechanical analyses of water-swollen GECO composites: a) storage modulus (E'), b) loss factor ($\tan \delta$), c) loss modulus (E'') as a function of temperature with different days water-swollen GECO samples, d) adaptability ratio and temperature as a function of water swollen time (water content).

Adaptability temperature is defined as the temperature at which the crossover occurs from reinforcing to plasticizing ability of the filler (water) present in the composites. The crossover point can be identified by comparing the storage modulus values of water containing sample with respect to the dry composite. In other words, the adaptability temperature is related to the peak melting temperature of the fillers (ice crystals). Figure 4.22d, indicates higher adaptability temperatures with the increase in *in situ* formed ice crystals (days of water absorption). The lower melting temperature of the ice crystals in 2 days swollen samples indicate that the majority of ice crystals are formed from freezable bound water⁶². Similarly, adaptability ratio can be defined as the ratio of modulus at lower temperature (-20 $^{\circ}\text{C}$) (*i.e.* reinforced state) to the modulus at higher temperature (20 $^{\circ}\text{C}$) (*i.e.* plasticized state). Here again, it is found that higher water content/days of water swelling could lead to higher degree of adaptability. Adaptability ratio as high as 20 is achieved for the 20 days water-swollen sample. So, it can be concluded that the adaptability temperature and degree could be easily tuned by varying the filler content (ice crystals) in the polymer composites via swelling time.

A cyclic temperature sweep was carried out to understand the reversible nature of the solid to liquid phase transition inside the elastomer composites. The storage modulus as function of temperature (heating and cooling cycles) for 7 days water-swollen sample is shown in Figure 4.23a. In the first heating cycle, the phase transition occurred around 0 °C, while in the cooling cycle, the phase transition occurred around –14 °C. Similar difference in the melting and freezing temperatures of water/phase change materials has been reported in DSC elsewhere¹²¹ and the reason is not well understood. In the second heating, the storage modulus curve followed the first heating cycle and this indicates a reversible temperature-dependent mechanical performance of the rubber sample. The noted slight difference in the first and second cycle could be due to the Mullins effect and the loss of water at higher temperatures (Figure 4.23b).

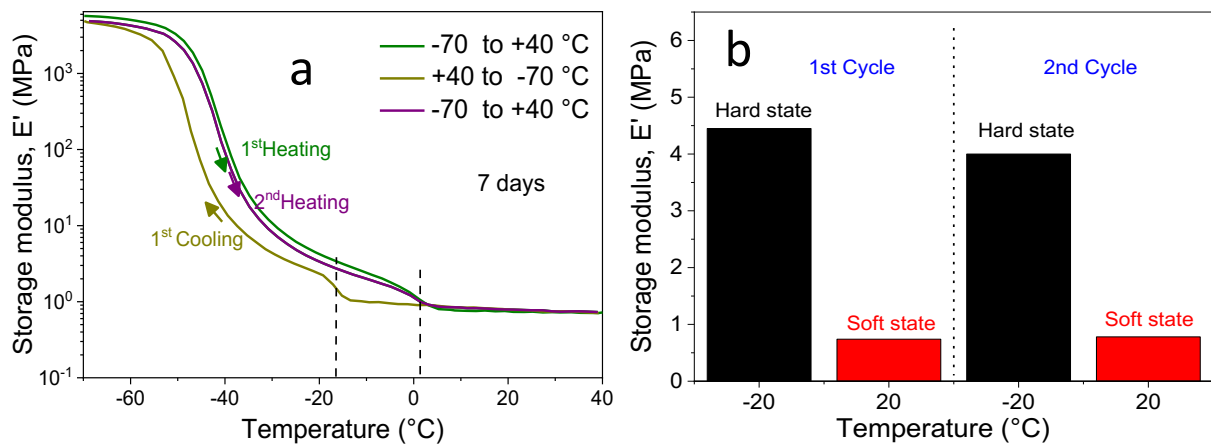


Figure 4.23 a) Cyclic temperature sweep experiment with 7 days water-swollen samples, b) bar chart showing the repeatable mechanical adaptability process for 7 days water-swollen sample.

To summarize, the storage modulus of the water filled composites clearly showed two different trends (around 0 °C) when compared to unfilled dry GECCO composites. The *in situ* generated solid ice crystal behaved as reinforcing filler below 0 °C leading to enhanced storage modulus (*hard state*), and when the temperature was increased above 0 °C, the solid ice crystals melted to form water (liquid), which in turn acted as a plasticizer, leading to decreased storage modulus (*soft state*). Thus temperature induced mechanical adaptability is achieved around 0 °C by applying phase transition of solid ice crystals to liquid water inside the elastomer matrix and a plausible mechanism is schematically shown in Figure 4.24.

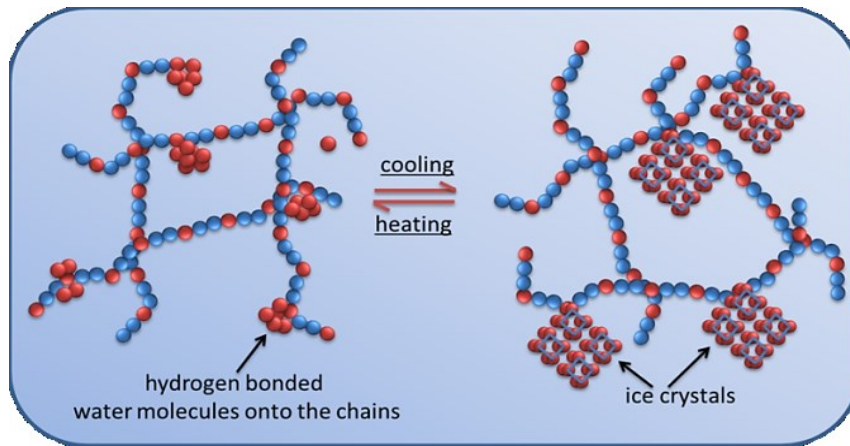


Figure 4.24 Schematic representation of rubber-filler interactions at different temperatures.

This concept of thermo-responsive mechano-adaptability can also be achieved by mixing elastomer composites with different phase change materials like paraffins and low melting alloys. Unlike melting point induced adaptable characteristics in water filled composites, the softening of the active filler could also be used in attaining adaptability. Wide variety of phase change materials can be chosen based on the desired adaptability temperatures and compatibility with the polymers and are expected to follow the same mechanism discussed in this work.

4.3 Utilization of *in situ* polymorphic alteration of the filler structure in designing mechanically adaptive elastomer composites

In the previous chapter, the temperature dependent reversible changes in mechanical properties (also called as thermo-responsive mechano-adaptability) of the elastomer composites were mainly focused. In this chapter, an attempt has been made to prepare water responsive mechano-adaptive composites that can exhibit both *hard* and *soft states* at room temperature. The phase transition behavior of calcium sulphate (anhydrite/hemihydrate to dihydrate, Figure 4.25) has been investigated over decades and is found to undergo morphology changes, leading to hardening of the material upon contact with water¹²². Calcium sulphate dihydrate, calcium sulphate hemihydrate and calcium sulphate anhydrite are considered as polymorphs of calcium sulphate occurring in presence of water/heat. This concept of polymorphism has been exploited in elastomer composites by dispersing calcium sulphate as active filler. It is expected that the polymorphism induced reversible morphological transformation inside the elastomer composite could lead to alternating mechanical properties when it comes in contact with water.

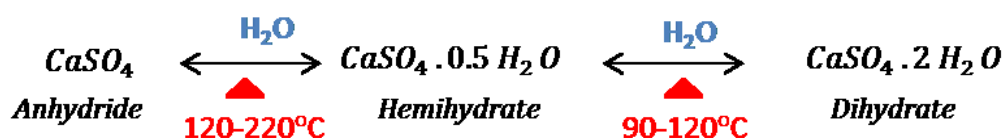


Figure 4.25 Calcium sulphate – water system (polymorphism)

The developed water swellable GECO/GEPO blend (discussed in Chapter 4.1) is utilized as the elastomer blend to fulfill the water requirement for the phase transition of calcium sulphate. More specifically, a miscible blend of 75/25 GECO/GEPO has been utilized for dispersing calcium sulphate (CaSO_4) particles using conventional rubber mixing process. The composites containing 75/25 GECO/GEPO and different amount of CaSO_4 (10, 30, 50 phr) were prepared based on the formulation shown in Table 3.3. The characteristics of calcium sulphate filled elastomer composites (as prepared) are briefly discussed before the detailed discussion about the conditions and methods for obtaining mechanical adaptability. The rheometric characteristics of the rubber composites containing different amount of calcium

Results of this chapters are published in ACS applied materials & interfaces 10 (18), 16148-16159, 2017

sulphate are shown in Figure 4.26a. Significant increase in torque values were obtained with the increase in calcium sulphate content. This could be attributed to the hydrodynamic effect of the fillers present in the composites. A decrease in cure time (t_{c90}) and scorch time (t_{s2}) (*i.e.*, enhancement in cure rate) is observed and this suggests the basic nature of the calcium sulphate particles.

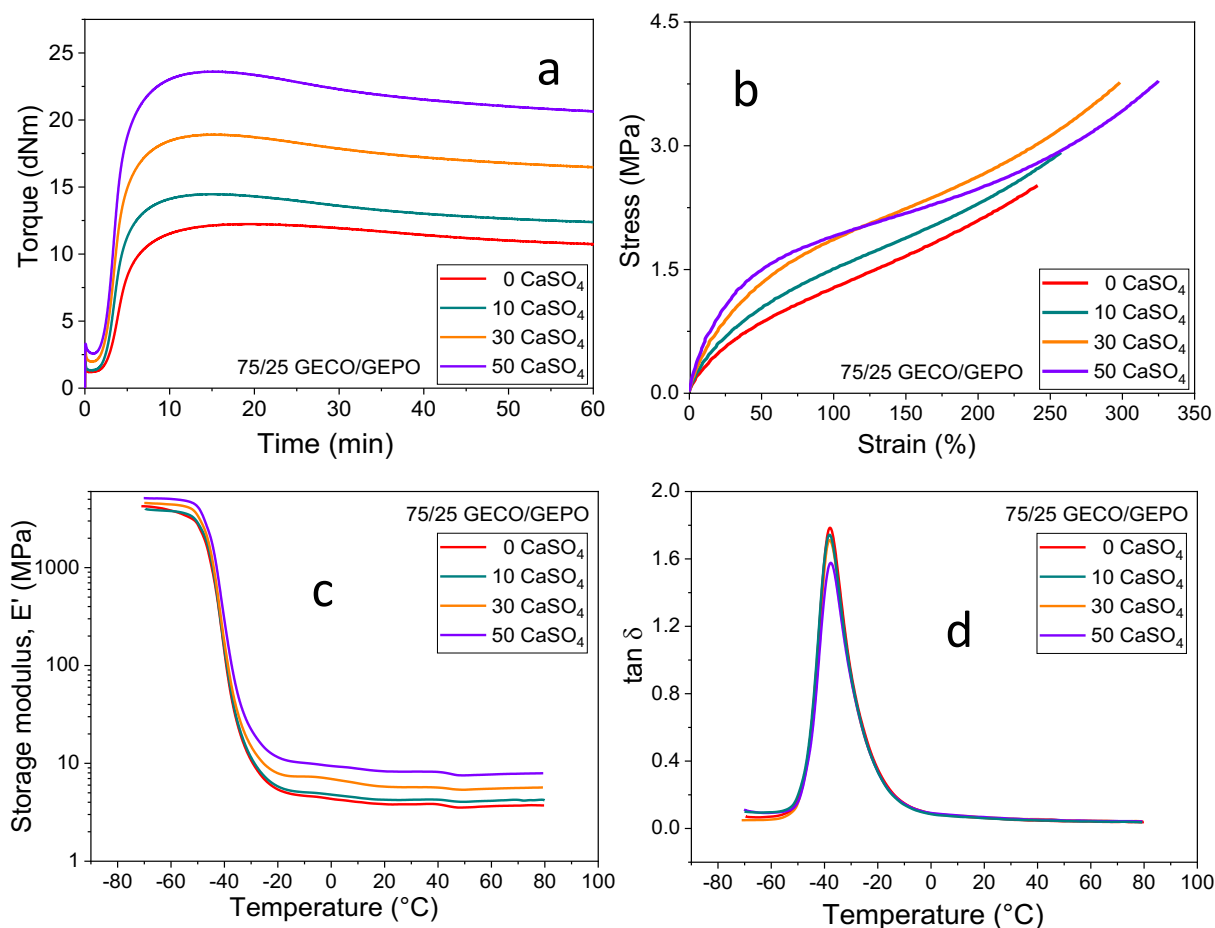


Figure 4.26 Rheological and mechanical properties of different calcium sulphate filled 75/25 GECO/GEPO composites: a) rheological characteristics, b) tensile stress–strain characteristics, and dynamic mechanical temperature sweep analysis: c) storage modulus (E'), d) $\tan \delta$.

Stress–strain characteristics of prepared samples were performed in tension mode and are shown in Figure 4.26b. TS and EB values are found to be improved by 16, 48, 50% and 7, 25, 35% for the composites containing 10, 30, 50 phr of calcium sulphate respectively. Dynamic mechanical temperature sweep analyses were performed and is shown in Figure 4.26c. Similar to stress–strain characteristics, very low improvement in storage modulus is observed with the addition of calcium sulphate. Even after addition of 50 phr of calcium sulphate, only 5 MPa enhancement in storage modulus in the rubbery region can be observed. The $\tan \delta$ peak height difference is also found to be very less with the addition of CaSO₄, indicating poor polymer–filler interaction (Figure 4.26d). From the mechanical studies, it can be

concluded that the CaSO_4 filled elastomer composites exhibited very slight improvement in mechanical properties, which is primarily due to the hydrodynamic effect and the traces of submicron sized filler particles present in the composites. Considering the higher particle size of CaSO_4 (90% $>5\ \mu\text{m}$, volume based), it is ideal to conclude that the dispersed filler is semi-reinforcing in nature.

4.3.1 Process and conditions for mechanical adaptability

Based on the above studies, the prepared sample is characterized to be in its *soft state* due to the semi-reinforcing nature of the CaSO_4 particle present in the composites. Mechanical adaptability is achieved by hydrating and dehydrating the CaSO_4 particles present in the elastomer composite (Figure 4.27). The *hard state* is achieved by hydrating the CaSO_4 particles and therefore, the prepared rubber composites were immersed in water for different times. Before characterizing, the excess water absorbed by the polymer chains has to be removed by drying the sample at room temperature for a minimum of 48–72 hours. The stable and sub-micron sized crystals of calcium sulphate dihydrate polymorphs are expected to develop during the drying process. This process of immersing the composite in water followed by drying is termed as water treatment process.

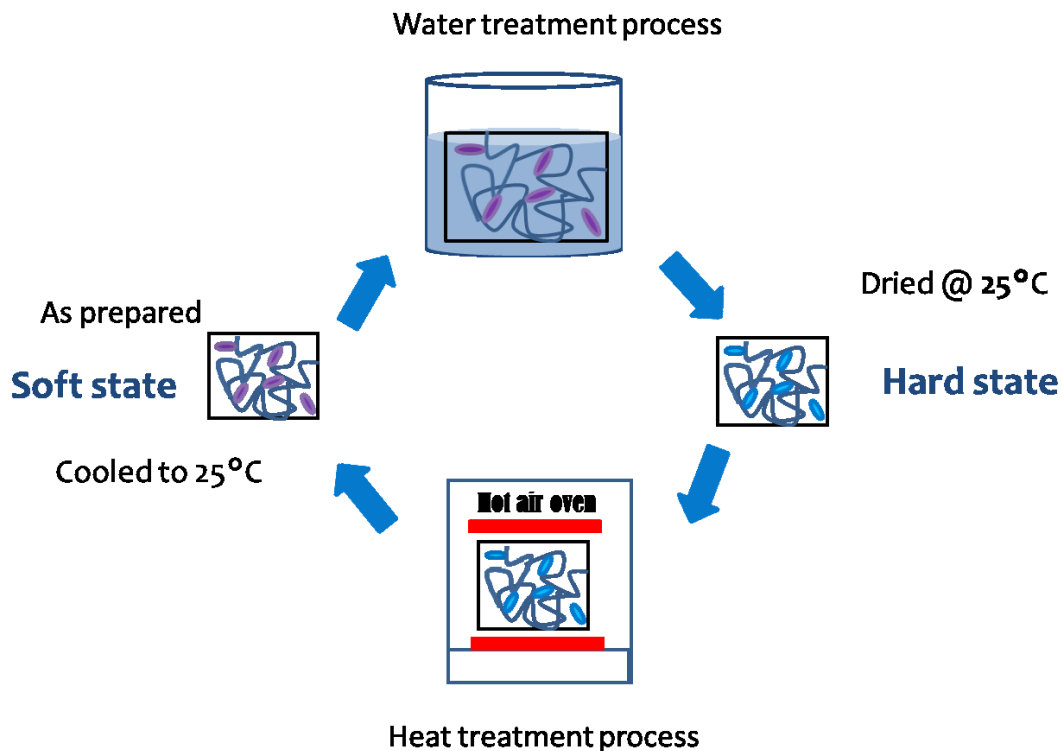


Figure 4.27 Methods and conditions of mechanical adaptability process

In order to return to the *soft state*, the water treated (*hard state*) samples were exposed to higher temperatures in a hot air oven. Then the sample was placed at room temperature for some time before the mechanical properties of composites were measured and this process is termed as heat treatment process. During the heat treatment process, it is expected that the micro-sized calcium sulphate hemihydrate/anhydride polymorph is reverted.

The conditions required for achieving superior mechanical adaptability characteristics (i.e., maximum *hard state*, reversible *soft state*) were optimized based on the storage modulus values at 60 °C (obtained from DMA) and is shown in section 4.3.1.1.

4.3.1.1 Optimization of mechanical adaptability conditions

The modulus of the *hard state* can be tuned by varying the water treatment time of the CaSO_4 filled composites (75/25/50 GECCO/GEPO/ CaSO_4) and is shown in Figure 4.28a. The modulus exhibited an increasing trend until 3 h of water treatment and then slightly decreased before levelling at around 7 h. The increasing trend could be attributed to the higher amount of particles undergoing hemihydrate to dihydrate transition with water treatment time. Further prolonged water treatment time above 3 h led to the dissolution of calcium sulphate particles in the water and thus the effective filler concentration of the composite decreased, resulting in a less reinforced state. In general, it is better to use 3–4 h of water treatment for achieving maximum *hard state* modulus.

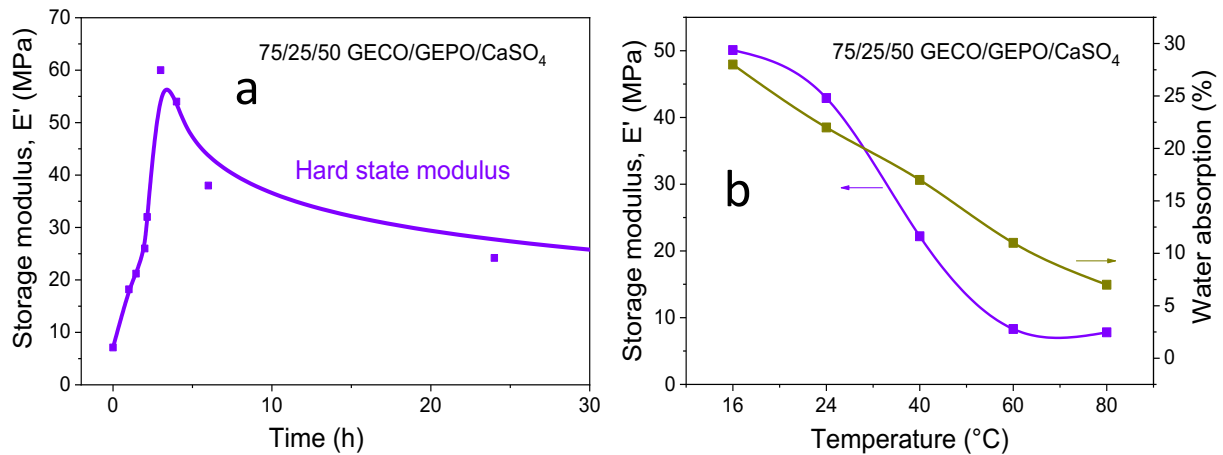


Figure 4.28 a) Effect of water immersion/treatment time on the modulus of the 75/25/50 GECCO/GEPO/ CaSO_4 composite, b) effect of temperature during water immersion/treatment process on the maximum *hard state* modulus. E' values were measured at 60 °C with a constant static and dynamic load of 1% and 0.2% respectively. Water treatment was performed till the maximum modulus is achieved at every temperature and is shown in the Figure.

The water temperature during the water treatment process is also found to play a key role in achieving the maximum *hard* state. From Figure 4.28b, the negative influence of temperature of the immersed water on the modulus of the composite can be observed. It also has to be noted here that the water absorption decreased significantly with temperature. The reduced water absorption ability is expected to restrict the CaSO_4 particles in undergoing hemihydrate–dihydrate conversion. This study concludes that the rate and amount of water absorption are crucial for achieving maximum possible adaptable state.

As the water absorption is observed to play significant role in obtaining maximum *hard state* modulus, the effect of water swelling polymer GEPO in the GECO/GEPO blend has been studied to optimize the blend ratio for achieving maximum *hard state* modulus. GECO/GEPO blend ratios were varied in the composites containing 50 phr of CaSO_4 and its effect on the maximum *hard state* modulus is shown in Figure 4.29. Further the time and water absorption required for achieving maximum modulus is also tabulated in Table 4.9.

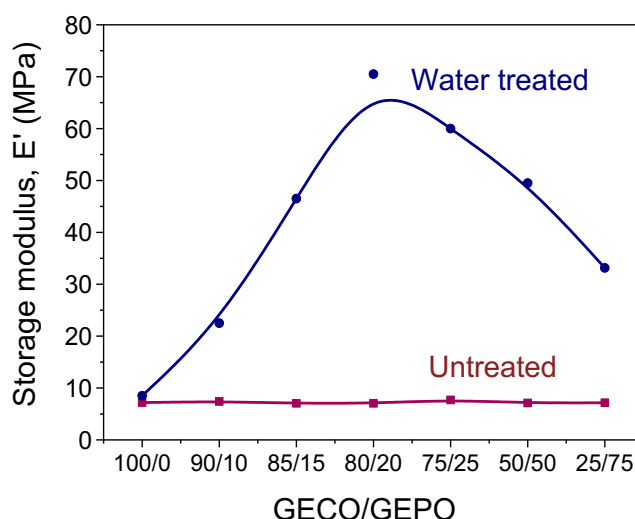


Figure 4.29 Effect of GECO/GEPO (hydrophilic polymer resin) blend ratio on the adaptability of the 50 phr CaSO_4 filled GECO/GEPO composite. E' values are measured at 60 °C with a constant static and dynamic load of 1% and 0.2% respectively. Water treatment was performed till the maximum modulus is achieved in each blend ratios and is shown in Figure.

Pure GECO composites exhibited very low enhancement in modulus due to its low water absorption characteristics. However, with the replacement of GEPO in the blend system, the modulus increased rapidly and attained a maximum value for 80/20 GECO/GEPO content. The replacement of GEPO has led to the increased water absorption and provided the amount of water essential for the hemihydrate–dihydrate transition. Contrastingly, further replacement of GEPO (>20 phr) in the blend system imparted low modulus enhancement compared to 20

phr of GEPO. This effect may be explained due to the detrimental effect of the higher amounts of water (water/powder ratio) than what is necessary for the calcium sulphate transition process. Several literature suggest the possibility of highly porous and low strength crystal morphology formation with high water content¹²³. It is interesting to note that the time required for achieving maximum modulus decreased with higher amounts of GEPO (or higher water content) (Table 4.9).

Table 4.9 Effect of blend ratio of GEPO/GEPO on the adaptability conditions.

GEPO/GEPO with 50 phr of CaSO₄	Water absorption @ maximum modulus (%)	Time @ maximum modulus (h)	Maximum hard state modulus (60 °C) (MPa)
100/0	12	72	8.5
90/10	17	5	22.5
80/20	22	4	70.5
75/25	33	3	60
50/50	57	2.5	49.5
25/75	90	2	33.12
0/100	105	1.5	28

The hemihydrate–dihydrate transition obtained during water treatment process has to be reversed to bring back the composites to its initial *soft state*. This transition is expected to occur by exposing the sample to higher temperatures (heat treatment process). The condition at which the complete recovery of modulus is achieved has to be optimized and therefore, different heat treatment conditions with varying times and temperatures were studied and are shown in Figure 4.30. Though several publications^{84, 93b, 124} state that the transition (hemihydrate – dihydrate) occurs at low temperature around 90 °C, the process is too slow as realized by the changes in the storage modulus values at 100 °C for 7 days conditioned samples (Figure 4.30a). From this figure, it can be observed that a relatively higher temperature (180–200 °C) is very effective in bringing back the modulus to its initial untreated range with very low time scales. It is assumed that the GEPO does not undergo any degradation at 200 °C in less than two hours. So, the water treated sample was exposed to 200 °C for varying times and the effect on the storage modulus recovery is shown in Figure 4.30b. A steady and exponential decrease of the storage modulus can be observed with time, which is finally approaching the modulus value of the untreated sample. At the end of 120 min, the

sample showed low modulus values, comparable with the values before water treatment. A slight trace of polymer degradation was observed at the end of 2 h and hence the water treatment time is optimized to 1 h at 200 °C.

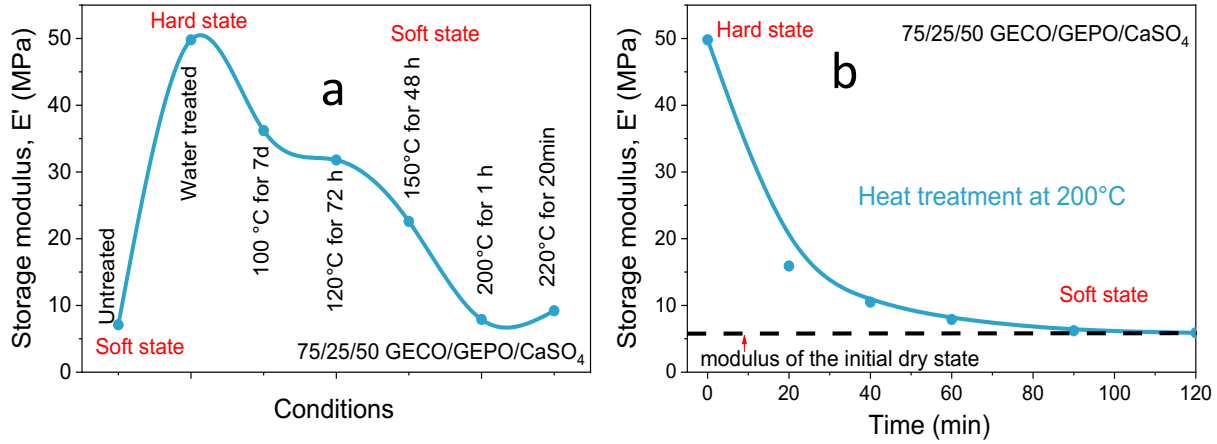


Figure 4.30 showing the effect of a) time and temperature of heat treatment on the storage modulus of water treated composites (75/25/50 GECCO/GEPO/CaSO₄) at 60°C, b) effect of heat treatment time at 200 °C on the modulus of the water treated composites at 60 °C.

Based on the above studies, it is observed that the 3–4 hours of immersion in water (at room temperature) followed by drying process provides higher *hard state* modulus. Similarly, exposing the water treated sample to higher temperature of about 200 °C for short period of time (1 h) is sufficient for achieving the *soft state*. Further studies, in this sub chapter utilized the above water and heat treatment conditions and the in-depth analysis of the mechanism of mechanical adaptability characteristics are investigated.

4.3.2 Investigation of phase transition characteristics of CaSO₄ filler

4.3.2.1 X-ray diffraction analysis (XRD)

The crystal structures of the CaSO₄ present in the elastomer composites and the phase transition (polymorphism) achieved during water and heat treatment process can be understood from XRD and Raman spectroscopy. XRD analysis of calcium sulphate powder (as supplied) (CaSO₄), water treated calcium sulphate powder (CaSO₄ Water treated), unfilled rubber (75/25 GECCO/GEPO), freshly prepared calcium sulphate rubber composite (75/25/50 GECCO/GEPO/CaSO₄, untreated), the same sample after water treatment (water treated), and at last after heat treatment of the water treated composites (heat treatment) are shown in Figure 4.31. Calcium sulphate powder (as supplied) exhibited four strong scattering peaks with 2θ values around 14.6°, 25.6°, 29.6°, and 32.1° along with two weak peaks around 31.3°

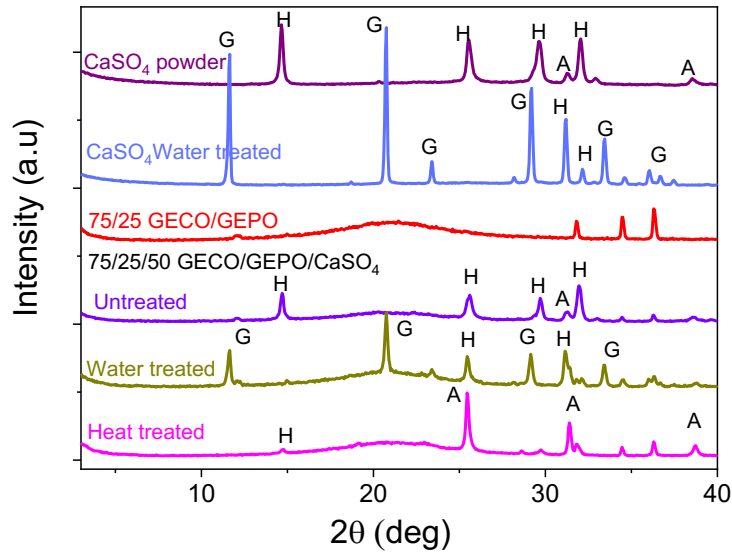


Figure 4.31 XRD analysis indicates the phase transition of CaSO₄ particles present in the composites (75/25/50 GECO/GEPO/CaSO₄), where A, H, G designates anhydride, hemihydrate, and dihydrate phase respectively.

and 38.6°. The strong peaks are attributed to the (2 0 0), (0 2 0), (4 0 0), (2 0 4) planes of hemihydrate hexagonal crystal, whereas the two weak peaks are attributed to the (0 1 2), (2 1 2) planes of anhydride orthorhombic crystal. This indicates that the majority of obtained calcium sulphate particles are present in the hemihydrate phase. Upon water treatment of the obtained calcium sulphate hemihydrate powder, several new scattering maxima are noticed around 11.63°, 20.74°, 23.41°, 29.2°, 33.4°, 34.63°, 36.68° and are attributed to the (0 2 0), (0 2 1), (1 3 0), (0 4 1), (2 2 0), (2 2 $\bar{2}$), and (2 1 $\bar{3}$) planes of monoclinic calcium sulphate dihydrate, along with some weak scattering peaks around 31.2° and 32.16°, indicating the presence of unreacted calcium sulphate hemihydrate. Unfilled GECO/GEPO rubber showed a broad amorphous peak around 20° along with few sharp peaks around 31.8°, 34.4°, and 36.3°, which could be due to the presence of other compounding ingredients like ZnO, sulphur, etc. Untreated calcium sulphate filled elastomer composites clearly showed the same scattering maxima of (as supplied) calcium sulphate powder around 14.6°, 25.5°, 29.6°, and 32.1° along with the broad amorphous peak from rubber. Therefore, it can be said that the hemihydrate phase of the CaSO₄ particles are retained even after withstanding the mixing conditions. Similarly, water treatment of the filled composites showed similar scattering maxima of water treated calcium sulphate powder samples around 11.63°, 20.74°, 23.41°, 29.2°, 31.2°, 32.16°, 33.4°, 34.63°, and 36.68° indicating the formation of monoclinic calcium sulphate dihydrate along with traces of unreacted calcium sulphate hemihydrate. Further, upon heat treating the water treated sample at 200 °C (for 1 h), strong 2θ scattering maxima values of around 25.46°,

31.41° and few weak peaks around 14.7°, 29.7° are obtained. The strong peaks are attributed to the orthorhombic calcium sulphate anhydride (soluble) and the weak peaks suggested the presence of hexagonal hemihydrate phase. It has to be noted that hemihydrate is formed upon heating the calcium sulphate dihydrate to temperatures above 80 °C, whereas anhydride (soluble) form is obtained when heated above 150 °C^{93b}.

4.3.2.2 Raman spectroscopy

Raman spectroscopy is employed due to its high sensitivity for distinguishing the chemical compounds having small structural variations (like the polymorphs). Several reports have suggested the difference in peak (wave number) for different calcium sulphate polymorphs¹²⁵. More specifically, Prieto-Taboada *et al.*¹²⁶ attributed the peak around 1025, 1015, 1008 cm⁻¹ for the identification of anhydride (soluble, III), hemihydrate and dihydrate polymorphs of calcium sulphate based on the ν_1 symmetric stretching of SO₄²⁻ tetrahedra. Hemihydrate phase of calcium sulphate powder (as supplied) and the formation of dihydrate phase on water treatment of the calcium sulphate powder are confirmed by the peak around 1015–1017 and 1008 cm⁻¹ respectively (Figure 4.32). Mixing conditions of calcium sulphate in the GECCO/GEPO composites are expected to preserve the crystal structure of the calcium sulphate and the peak around 1015 cm⁻¹ confirms the unchanged hemihydrate phase present in the untreated composites. Water treated composites confirmed the formation of dihydrate (1008 cm⁻¹) along with the presence of significant amount of unreacted hemihydrate particles (1016 cm⁻¹). Further, upon heat treatment, anhydride phase (1025cm⁻¹) is obtained along with considerable amount of hemihydrate phase (1016 cm⁻¹).

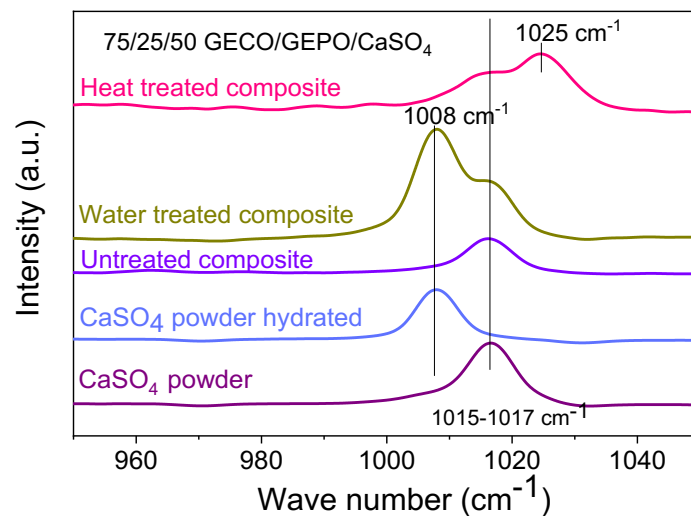


Figure 4.32 Raman spectroscopic analysis indicating the phase transition of calcium sulphate present in the composites.

From XRD and Raman spectroscopy studies, one can conclude that on water treatment, the as prepared hemihydrate phase transformed to dihydrate phase, whereas on heat treatment the dihydrate phase returned to anhydride/hemihydrate phase. In short, it can be said that the polymorphism of calcium sulphate crystals occurred *in situ* elastomer composites as a result of water and heat treatment process.

4.3.3 *In situ* morphology transformation analysis

SEM images of untreated, water treated and heat treated samples of 50 phr CaSO₄ filled 75/25 GECCO/GEPO composites are shown in Figure 4.33a-c. Figure 4.33a shows the morphology of as-prepared composite (untreated), where large and irregular shaped calcium sulphate particles are seen. Considerably higher particle size, in the order of several microns and irregular morphology of the calcium sulphate filler restricted their ability to reinforce the composite. Insignificant amount of submicron sized CaSO₄ particles are observed and is expected to be reason behind the marginal improvement in the mechanical properties (Figure 4.26). Figure 4.33b shows the image of water treated composite containing highly agglomerated CaSO₄ nanorods. The agglomeration of nanorods confirm the formation of nanoparticles from the micron sized fillers present in the untreated sample during water treatment process. In general, presence of nanorods could lead to enhanced interaction with the polymer chain and in turn expected to offer higher mechanical properties (*hard state*). Further on heat treatment, it can be observed from Figure 4.33c that all the nanoparticles assimilated to behave as a solitary micron sized particle. This process of assimilation upon heat treatment is expected to return the composite to its unreinforced *soft state* (like the untreated composite). It also has to be mentioned that the CaSO₄ morphology of the heat treated and untreated composites were totally different and might have different effects on the mechanical properties.

Transmission electron microscopy analyses were performed to clearly understand the morphology of the nanoparticles formed during the water treatment process and is shown in Figure 4.33d-f at different magnifications (200 and 100 nm). From Figure 4.33d, the agglomerated nanoparticles of varying lengths can be observed. The nanorods morphologies could be clearly distinguished in the Figure 4.33e. Formation of nanorod like morphology is an inherent material property, as described by Osterwalder¹²⁷ and several others^{87, 128}. Additionally, nanoneedles like morphology is also visualized in Figure 4.33f and is expected to be formed due to the unrestricted crystal growth of the particles, probably occurring in the

free volume present in the rubber matrix. The *in situ* formation of nanoneedles/nanorods is expected to produce highly reinforced composites forming the *hard state*.

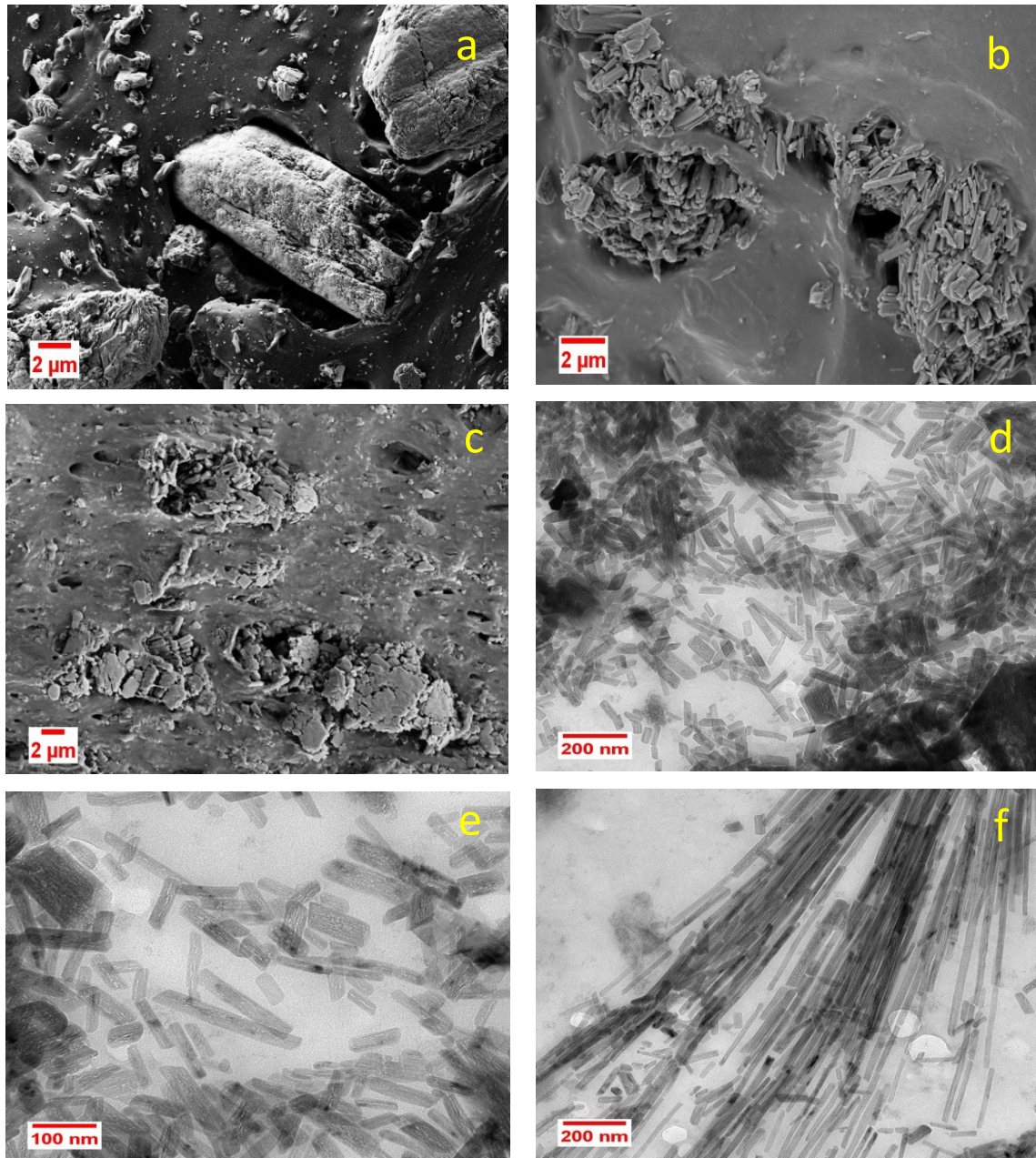


Figure 4.33 SEM images of different conditions of 75/25/50 GECCO/GEPO/CaSO₄: a) untreated, b) water treated, c) heat treated and TEM analysis of water treated samples at different magnifications: d) 500 nm, and e, f) 200 nm at different positions.

Morphology transformation of the filler and the agglomeration of nanoparticles that occurred during water/heat treatment process can be confirmed by studying the filler–filler interaction (or the so called Payne effect) using amplitude sweep analysis and is shown in Figure 4.34.

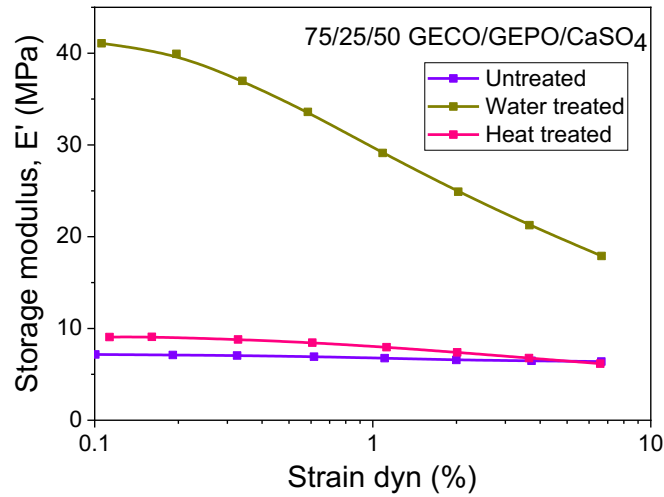


Figure 4.34 showing the amplitude sweep analysis of the untreated, water treated and heat treated samples of 75/25/50 GECCO/GEPO/CaSO₄ (mechanically adaptable composites). Non-linear strain dependence of water treated sample indicates the formation of agglomerated CaSO₄ nano-filler networks.

Table 4.10 showing the Payne effect characteristics of the mechanically adaptable composites

Filler content phr (75/25 GECCO/GEPO)	$E'_0 - E'_\infty$ (MPa)		
	Untreated	Water treated	Heat treated
10 CaSO ₄	0.4	3.4	0.5
30 CaSO ₄	0.6	16.1	1.2
50 CaSO ₄	1.8	24	2.6

Generally, it is believed that the micro fillers/semi-reinforcing fillers tend to have lower filler–filler interaction, while nanofillers exhibit very high filler–filler interaction due to their higher activity and the self-aggregating tendency. Figure 4.34 clearly indicates the higher initial modulus values (E'_0) and the strain dependent modulus values ($E'_0 - E'_\infty$) for the water treated composite, indicating the presence of nanofillers and the enhanced filler–filler interaction (as seen in Figure 4.33b) compared to the untreated sample. Similarly, very low strain dependency ($E'_0 - E'_\infty$) is observed for heat treated samples, confirming their transformation back to non-reinforcing micro-sized morphology (as seen in Figure 4.33c). When compared to untreated samples, slightly higher initial modulus and the strain dependent modulus values ($E'_0 - E'_\infty$) are observed for heat treated samples, indicating the traces of unconverted nanofillers in the composites. The amplitude of Payne effect for various

untreated, water treated and heat treated calcium sulphate (10, 30, 50 phr) filled composites are tabulated in Table 4.10. All the water treated samples of different calcium sulphate content exhibited very high strain dependent modulus values ($E'_0 - E'_\infty$) when compared to the untreated and heat treated samples, depicting the enormous filler–filler networking of the newly formed CaSO_4 nanofillers. The amplitude sweep analysis thus confirms the nanoparticle agglomeration of calcium sulphate dihydrate polymorphs seen in the TEM and SEM analysis of the water treated sample.

Together, by co-relating the phase transition analyses from XRD and the morphology transformation from SEM, it is confirmed that the phase transition induced morphology transformation occurs during water and heat treatment processes.

4.3.4 Mechanical adaptability investigations

4.3.4.1 Stress–strain behavior

Stress–strain behavior of untreated, water treated and heat treated samples of 75/25/50 GECO/GEPO/ CaSO_4 were performed at room temperature (20 °C) and is shown in Figure 4.35a. TS and EB values of untreated, water treated and heat treated samples are found to be 3.4, 5.4, 3.6 MPa and 406, 347, 432% respectively. Water treated sample exhibited enhanced stress–strain properties forming the *hard state* which is attributed to the formation of nanoneedles/nanorods. More interestingly, upon heat treating the water treated samples, the enhanced mechanical properties returned to almost its initial state (*soft state*), due to the reclamation of micro-sized particles from the agglomerated nanoparticles. It is expected that the water treated samples would exhibit considerably higher tensile strength and elongation at break values owing to the formation of the nanorods/nanoneedles during water treatment process. However, only moderate improvement in tensile strength of 59% is observed.

On the other hand, significant improvement in Young's modulus of about 300% is observed upon water treatment, which returned to its initial *soft state* after heat treatment process (Figure 4.35b). Significant improvement in Young's modulus and moderate improvement in tensile strength of the water treated samples could be attributed to the agglomeration of nanoparticles as seen in the TEM images (Figure 4.33d).

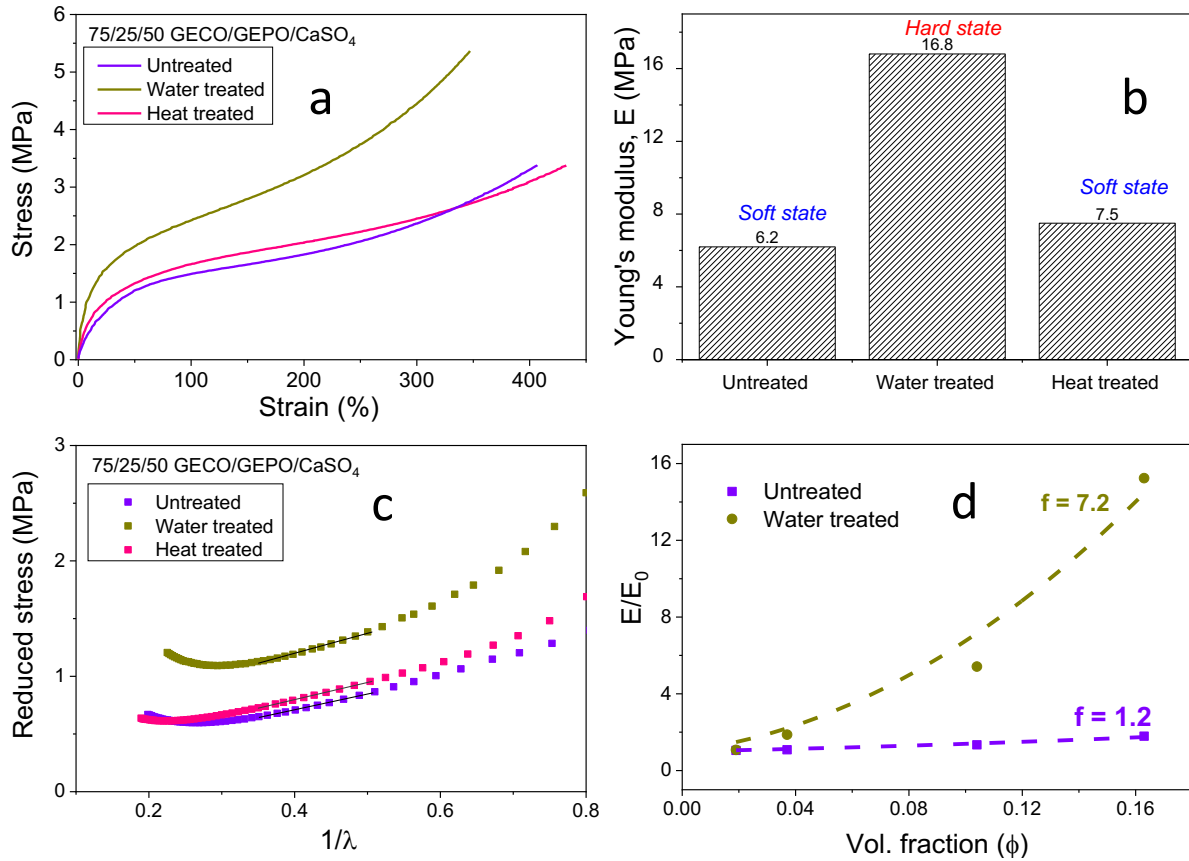


Figure 4.35 a) Stress–strain properties, b) variation of Young's modulus, c) Mooney-Rivlin plot of untreated, water treated and heat treated samples of 75/25/50 GECCO/GEPO/CaSO₄, d) modified Bachelor equation to calculate aspect ratio of the fillers present in the 75/25 GECCO/GEPO composite.

Table 4.11 Cross-link densities of 75/25/50 GECCO/GEPO/CaSO₄ samples obtained from Mooney-Rivlin equation and its constants

Sample	C_1	C_2	Cross-link density (ν) mol/cm ³
Untreated	0.17	1.36	1.37×10^{-4}
Water treated	0.51	1.73	4.12×10^{-4}
Heat treated	0.20	1.49	1.61×10^{-4}

The polymer–filler interactions can be understood from Mooney-Rivlin plot (Eq.4.13) and is shown in Figure 4.35c. Constants C_1 , C_2 and cross-link density values were obtained from the analysis of linear regime in the plot and are shown in Table 4.11. The enhanced interaction between polymer and the nanoparticles formed during water treatment process can be confirmed by the significant increase (200%) in the cross-link density values of the water treated samples. Similarly, the reclamation of micro-sized particles are expected to reduce the

polymer–filler interaction for heat treated sample and is confirmed from the reduction in the cross-link density, which is almost close to the untreated sample.

The aspect ratio of the filler structure present in the composite can be evaluated using the modified Bachelor equation by Kim and Zukoski^{119a, 129}

$$E/E_0 = 1 + 2.5f\phi + 6.0f^2\phi^2 \quad 4.15$$

Where E , E_0 are the Young's moduli of the filled and unfilled composites respectively. ϕ , f are the volume fraction and the shape factor/aspect ratio of the solid particles respectively. From Figure 4.35d, almost 500 % improvement in aspect ratio (of the filler particles present in the water treated sample ($f=7.2$)) is observed compared to the untreated sample ($f=1.2$). These results are found to be in accordance with the SEM results, where the formation of nanoparticles (higher aspect ratio) from the irregular shaped micro particles was visualized.

4.3.4.2 Dynamic mechanical analysis

Motivated by the huge difference obtained from the Young's modulus values of untreated and water treated composites, dynamic mechanical studies were performed to enhance the distinction between *hard* (water treated) and *soft* states (untreated and heat treated composites). The storage modulus curves (E') of the different composites (untreated, water treated and heat treated, 75/25/50 GECO/GEPO/ CaSO_4) against varying temperature is shown in Figure 4.36a. Glassy to rubbery transition is followed by rubbery plateau region at around -40°C . The storage modulus of the water treated sample at 60°C (rubbery regime) is found to be $\sim 700\%$ (62 MPa) higher than the untreated samples (8 MPa) and thus forming the *hard state*. This once again confirms the reinforcing ability of nanoneedles/nanorods formed during water treatment process as shown in the TEM images. Upon heat treatment, the nanorods/nanoneedles morphology collapses and forms irregular morphology and hence the enhanced modulus almost returns to its initial untreated *soft* state (~ 8 MPa) as obvious in Figure 4.36a. However, an unusual behavior was noticed in the heat treated sample at temperatures between -20°C and $+20^\circ\text{C}$. It is expected that exposure to high temperature during heat treatment process could have led to reduced interaction between GECO and GEPO phases, thus leading to the formation of crystalline GEPO domains, which melts at around 10°C .

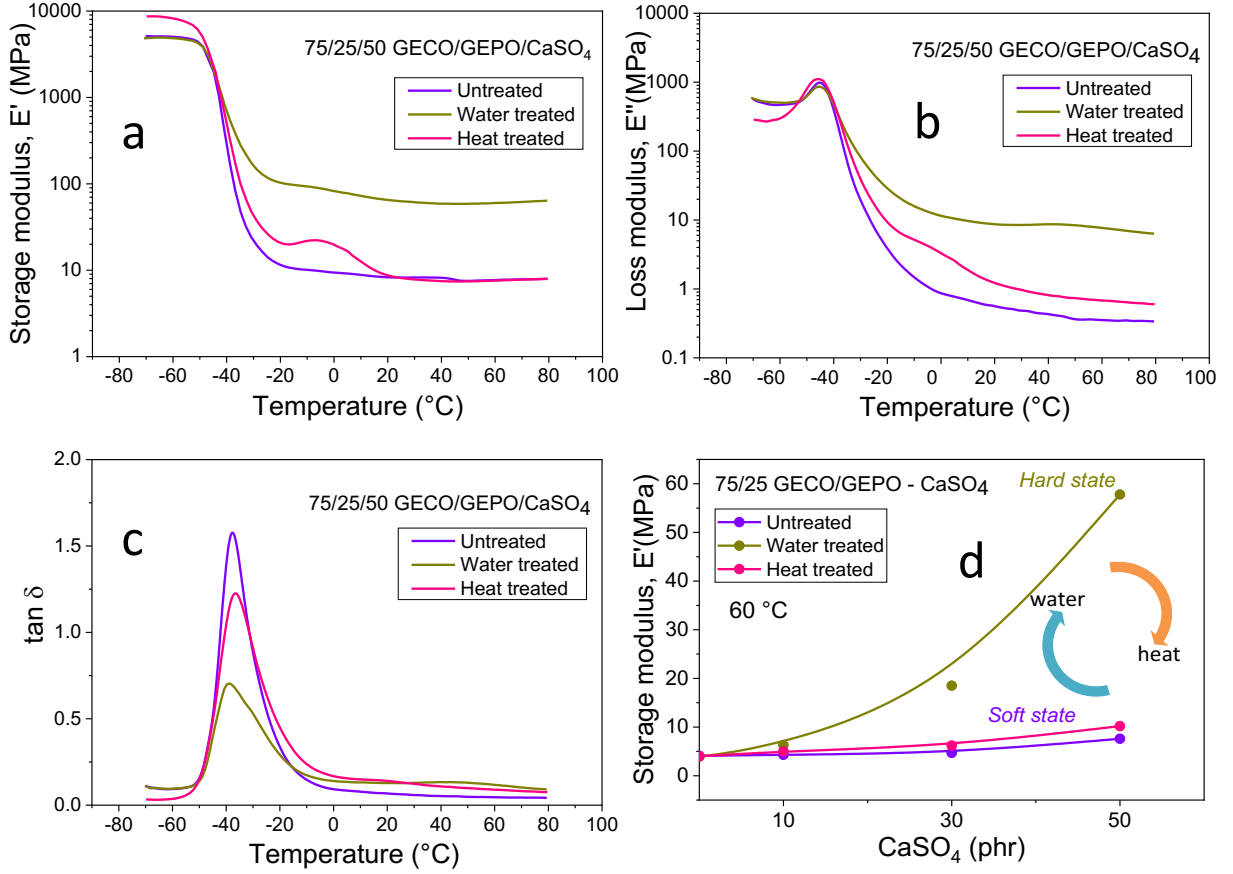


Figure 4.36 Dynamic mechanical analysis (temperature sweep) showing the mechanical adaptability: a) storage modulus (E'), b) loss modulus (E''), c) loss factor ($\tan \delta$), d) storage modulus value at 60 °C against different calcium sulphate content of 75/25 GECCO/GEPO composites.

From the above studies, it can be concluded that the *in situ* morphology changes has altered the effectiveness of filler towards reinforcing abilities. Thus effectiveness of the filler can be quantified by effectiveness coefficient factor (EC) which is¹³⁰

$$EC = \frac{\left(\frac{E'_g}{E'_r}\right)_{filled\ rubber}}{\left(\frac{E'_g}{E'_r}\right)_{gum\ rubber}} \quad 4.16$$

Where E'_g and E'_r are the storage modulus in the glassy and rubbery region respectively. It has to be noted that lower the effectiveness coefficient (EC), higher is the effectiveness of the filler towards reinforcement. As expected, lower effectiveness coefficient values are obtained for water treated samples and on the other hand, higher values are obtained for the heat treated and untreated samples for all (10, 30, 50 phr) the CaSO₄ filled composites (Figure 4.37a). So from this study, it is concluded that the change of filler structure/surface area (micro structured filler to agglomeration of nanorods/nanoneedles) during the water treatment

process has enhanced the effectiveness of the filler by 1.8, 3, 10 times for 10, 30, 50 phr CaSO_4 filled composites respectively. Similarly, effectiveness of the filler reduced when the filler structure returned to micro structured morphology on heat treatment process.

Similar trend of enhanced modulus values for the water treated samples and the low modulus values for the untreated and heat treated composites are seen in loss modulus (E'') vs temperature curves as well (Figure 4.36b). Similarly, the loss tangent behavior ($\tan \delta$) of the developed composites is shown in Figure 4.36c. Generally, the difference in $\tan \delta$ peak height could be used as a measure of extent of polymer–filler interactions in the composites. The presence of nanorods/nanoneedles shaped calcium sulphate fillers in water treated samples are expected to display higher interaction with the polymer and is confirmed by the decrease in $\tan \delta$ peak height. Further the reclamation of filler particles upon heat treatment reduced the interactions with polymer, confirmed by the higher $\tan \delta$ peak height values, compared to water treated samples. Additionally, slight shift in $\tan \delta$ peak towards lower temperature for water treated sample can be observed and this might be due to the presence of undried water molecules present in the composites. The interaction between polymer and filler can be quantitatively analyzed using the interaction parameter coefficient B obtained from the equation¹³¹:

$$\tan \delta = \frac{\tan \delta_m}{1 + 1.5B\phi} \quad 4.17$$

$\tan \delta$, $\tan \delta_m$ are the peak loss tangent value of the filled and the unfilled compound respectively. B , ϕ are the interaction parameter and the volume fraction of the filler respectively. Reduced $\tan \delta$ values indicate the reduced polymer chain mobility and this has been used to quantify the polymer–filler interaction. B value is obtained from the above equation (Eq.4.17) and is plotted against different conditions of adaptability (water/heat treatment) and filler concentration (Figure 4.37b). B values of the water treated samples are found to be higher than the untreated and heat treated samples and thus indicating the enhanced interaction of polymer chain with the newly formed nanofillers. High loading of fillers could lead to the formation of large number of nanofillers upon water treatment and thus higher polymer–filler interaction is observed. Approximately 16, 20, 23 times improvement in B values are obtained for composites containing 10, 30, 50 phr of CaSO_4 respectively, elucidating the reinforcing potentials of the newly formed calcium sulphate nanorods/nanoneedles.

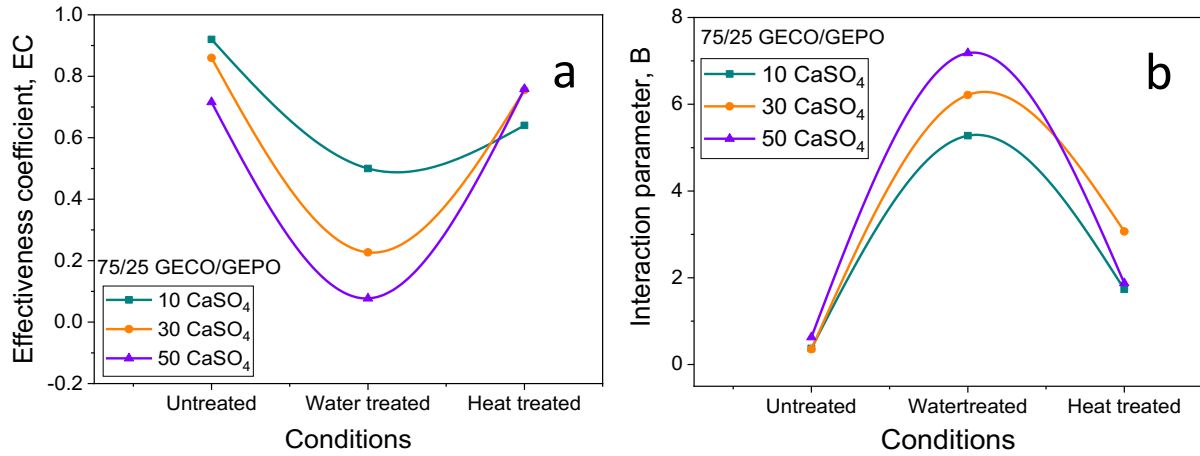


Figure 4.37 a) Effectiveness coefficient of fillers (EC), b) polymer–filler interaction parameter (B) against different conditions and varying filler contents of 75/25 GECCO/GEPO composites.

The storage modulus values at 60 °C for untreated, water treated and heat treated samples at different concentration (10, 30 and 50 phr) of calcium sulphate is shown in Figure 4.36d. The magnitude of modulus difference in the *hard/soft states* increases with the increase in the filler concentration. A maximum of adaptability ratio (modulus ratio between *hard/soft state*) of 1.5, 4, 8 are obtained for 10, 30, 50 phr CaSO₄ filled 75/25 GECCO/GEPO composites respectively.

Cyclic mechanical adaptability characteristics were studied and it is found to exhibit poor repeatable characteristics (not shown here). This is attributed to the reduced miscibility between the GECCO/GEPO blends during heat treatment process, which can be observed from the presence of crystallization peak around 0 °C in the first cycle heat treated sample (Figure 4.36a). Still several works and strategies needs to be developed in realizing the reversible/repeatable characteristics of the adaptability process.

The mechanism of mechanical adaptability obtained from the CaSO₄ filled GECCO/GEPO composites is schematically shown in Figure 4.38. The as-prepared composites exhibited very low mechanical properties due to the semi-reinforcing nature of the micron sized calcium sulphate (hemihydrate) fillers present in the composite and hence it is considered as *soft state* (Figure 4.11). The *hard state* is achieved by water treating the as-prepared soft composite. Upon water treatment, agglomerations of nanocrystals (nanorods, nanoneedles) are obtained due to the formation of dihydrate polymorph (Figure 4.31 and Figure 4.33). This *in situ* morphology change (micro to nanosized particles) resulted in enhanced polymer–filler interaction and in turn a reinforced composite is obtained (*hard state*). Further, when the

water treated sample (*hard state*) is exposed to high temperature (200 °C), the crystal water present in the nano-calcium sulphate dihydrate particles evaporated and collapsed to the micro calcium sulphate hemihydrate/anhydride particles (Figure 4.33). Reformation of micro CaSO_4 particle led to reduced polymer–filler interaction (DMA studies) and thus returning to its initial *soft state*. Thus, the *in situ* polymorphic alteration can be exploited to alter the fillers effectiveness towards reinforcement and in turn achieving the mechanical adaptability. These developed composites can be used in dynamic implants, responsive surfaces, sensors and actuators.

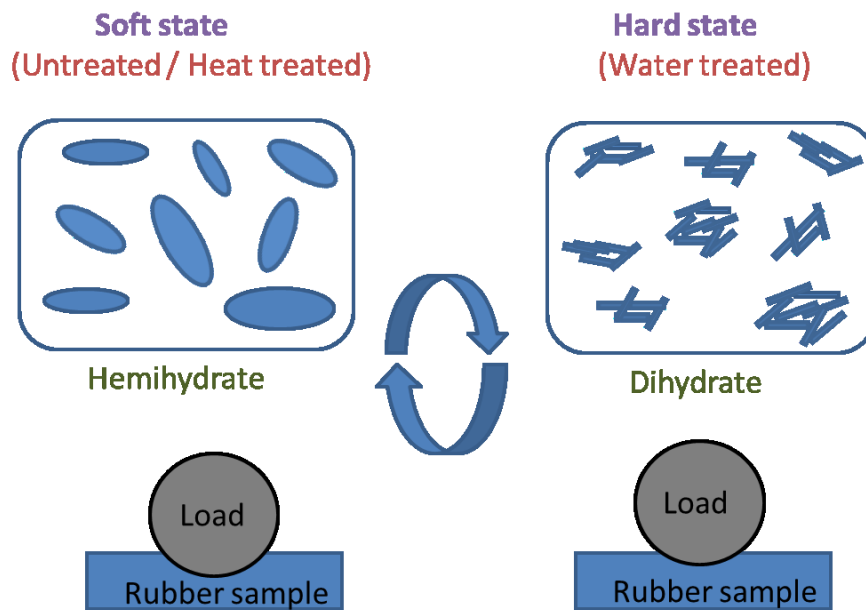


Figure 4.38 Mechanism of mechanical adaptability of calcium sulphate filled elastomer composites.

5 Conclusions and outlook

5.1 Conclusions

Mechanically adaptable polymer composites, a class of stimuli responsive polymers, have attracted material scientists in designing materials for smart and intelligent applications. In this work, easily accessible water/humidity as a stimulus was preferred for achieving adaptability; this eventually eliminates the need for extra chemicals or equipment. In such cases, elastomer composite should absorb water significantly, in order to respond quickly to the stimulus. This demanded the use of a stable water swellable elastomer composites for realizing mechanical adaptability. The water swellable elastomer composites described in the literature (mostly blends of hydrophobic rubber, hydrogel, and compatibilisers) were found to exhibit irrepeatable water swellable characteristics. Thus, an attempt has been made to develop a novel water swellable elastomer blend system with repeatable water swelling characteristics. GEEO, a special case of epichlorohydrin terpolymer was chosen as the elastomer matrix due to its highly polar and hydrophilic nature, and was blended with structurally similar hydrophilic polymer resin GEPO, which is responsible for the bulk of water absorption. Single glass transition temperature obtained for all the blends of GEEO/GEPO indicated their miscibility in all blend ratios. Additionally, the presence of melting regimes in the blends confirmed the formation of miscible amorphous–semi crystalline polymer blend system. The slight deviation in the glass transition temperature determined from experimental and the Fox equation describe the enhanced interaction between GEEO and GEPO polymer chains. The prepared GEEO/GEPO blends exhibited superior water swelling characteristics and it was found that the blend ratios can be varied to achieve 20–400% water absorption at room temperature. It was also found that the initial water absorption exhibited Fickian diffusion mechanism, while the relaxation mechanism dominated at the final stages of water absorption process (equilibrium water swelling). Retention of thermal, mechanical and water swelling characteristics over several cycles of water swelling is very important in case of developing stable water swellable composites. Except for the slight difference in the crystallinity, the water swollen-dried composites (DWD) almost retained the thermal and mechanical properties of its dry states (D). GEEO/GEPO blends exhibited excellent repeatable water swellable characteristics with very little loss in dried weight of the sample even after several swelling-drying cycles. From these studies, one can conclude that the developed GEEO/GEPO blends could be ideally used for applications requiring stable and repeatable water swellable characteristics (<400%).

Two different strategies for obtaining adaptability were explored using the developed water swellable GECO/GEPO elastomer blends. The possibility of altering the morphology or structure of the filler *in situ* the elastomer composite with the help of absorbed water as stimulus has been explored in this work. First strategy utilizes the solid–liquid phase transition of the absorbed water, while the second strategy exploits polymorphic nature of calcium sulphate.

Solid–liquid phase transition ability of the absorbed water in the elastomers and its effect on the mechanical properties were investigated to understand the potentials of the developed composite for mechanical adaptability applications. The absorbed water forms ice crystals below 0 °C and is expected to act as a reinforcing filler, enhancing the mechanical properties (*hard state*). Meanwhile, above 0 °C the ice crystals melts to form liquid water, which could act as a plasticizer and thereby reducing the mechanical properties (*soft state*). In case of developed GECO/GEPO blends, only 75/25 GECO/GEPO (DW) blend exhibited expected adaptive characteristics around 0 °C. But the presence of slight crystalline melting of GEPO around 0°C is expected to complicate the interpretation of the adaptability process. Hence, further studies were performed by modifying the cross-link density of pure amorphous GECO to increase the amount of absorbed water to attain higher adaptability characteristics. A maximum of ~40 wt-% water was absorbed by very slightly cross-linked polymer at the end of 20 days. Qualitative analysis (using DSC) indicates that the absorbed water could be present in two different states: non-freezable and freezable water. Further, it was found that >70% of absorbed water exhibited freezable characteristics to form stable ice crystals below its freezing temperature. A maximum of ~26 vol-% of ice crystals were obtained after 20 days of water immersion. The *in situ* formed ice crystals form roughly spherical to oval shaped particles with an average particle size of 400–600 nm. Hydrogen bonding was expected to be the mechanism behind the interaction between polymer and water molecules (FTIR analysis). The effect of *in situ* formation of ice crystals/liquid water on the mechanical adaptability were investigated at two different temperatures (–20 and +20 °C). Young's modulus values of the 20 days swollen samples exhibited stiffness variation from 3.14 MPa at –20 °C (*hard state*) to 0.6 MPa at +20 °C (*soft state*). Further, 100% modulus and tensile strength also exhibited similar adaptive characteristics at different temperatures (around 0 °C). This effect of solid–liquid phase transition of the absorbed water on the mechanical property was studied more effectively using temperature sweep mode in DMA. A maximum adaptability ratio (AR – ratio between *hard* and *soft state* modulus) of 20 was achieved with the 20 days water-swollen

samples between -20 and $+20$ °C. Mechanical adaptability occurs at a broad range of temperatures around 0 °C, i.e., the melting point of the ice crystals. Further, it was found that the higher the amount of absorbed water, higher the adaptability ratio (AR) and the adaptability temperature (AT). The developed composites exhibited reversible and repeatable mechanical adaptability characteristics and hence could find applications in future tires, dynamic implants, etc.

In the second approach, the polymorphic transition of calcium sulphate (CaSO_4) in presence of water and heat was exploited by dispersing it as filler into the elastomer composite. The as-obtained CaSO_4 fillers (characterized as calcium sulphate hemihydrate) offer semi-reinforcing characteristics to the elastomer composites due to its very large particle size (micro-size) and irregular particle structure. In order to obtain an adaptable modulus, the prepared elastomer composite was exposed to water treatment (immersion in water followed by drying) and heat treatment process (exposing the water treated sample to higher temperature for a short period of time). Optimum water requirement for achieving higher mechanical properties restricted the time and temperature of water treatment process to 3–4 h of water immersion at room temperature. Similarly, the time and temperature of the heat treatment process was also varied and it was found that temperatures above 180 °C are necessary for the transition to occur rapidly. After water treatment, a maximum of 300% and 700% improvement in Young's modulus and storage modulus were achieved for 50 phr filled calcium sulphate composites forming the *hard state*. A remarkable improvement in mechanical properties on water treatment were attributed to the enhanced effectiveness of the filler towards reinforcement (CaSO_4), which is due to the polymorphic transition (hemihydrate to dihydrate) induced *in situ* morphology changes (formation of nanoparticles) and its enhanced interaction with the polymer chain. More importantly, the heat treatment process was able to bring back the adapted modulus to its initial state constituting the *soft state*. This was achieved by the regeneration of micro-sized calcium sulphate anhydride/hemihydrate particles in the elastomer composites by exposing to higher temperatures. This heat treatment process led to a reduced compatibility between the polymer in the blend and the fillers, which in turn led to poor repeatable adaptability characteristics. Thus, the developed composites are best suited for application requiring one way/cycle mechanical adaptable characteristics like dynamic implants, orthoses or membranes.

5.2 Outlooks

Even though the developed strategies look promising, the choice of materials and methods should be explored widely in realizing high performance mechanically adaptive composites. In this section, the possible solutions for the shortcomings identified in this work are discussed.

Shortening the response time:

In case of mechanical adaptability driven by solid–liquid transition of the absorbed water, the response time of the developed elastomer composites depends on the rate of water absorption. The rate of water absorption of the developed composites (20 days) were found to be not appropriate for the rapid adaptability applications. So, in order to improve the response time, the rate and the degree of water absorption has to be enhanced. One of the methods to improve the degree and rate of water absorption/swelling is by blending the developed elastomer composites (GECO) with hydrophilic resins and fillers (like cellulose, chitin, and sodium chloride), etc. Choice of water swellable resin also plays a huge role in attaining mechanically adaptive composites. As observed in the case of 50/50, 25/75, 0/100 GECO/GEPO blends, the presence of crystalline region in the blend system might restrict the adaptability process and hence the selection of amorphous water swellable resin could be advantageous (Figure 4.9). Thus the selection of right water swellable resin/fillers for obtaining both stable water swellable and adaptability characteristics needs to be explored extensively.

Repeatable adaptability characteristics:

In case of polymorphism induced mechanical adaptability, poor repeatable adaptability characteristics of GECO/GEPO/CaSO₄ composites were obtained and certain attempts were made unsuccessfully to solve this issue during the course of this work. The main issue being the reduced compatibility between the polymers in the blend and the polymer–filler interactions at the elevated temperatures (200 °C). So in this regard, two different approaches could be explored:

- a) Development of phase transition techniques involving low temperature, which in turn could retain the miscibility of the polymer blends and thus improving the repeatable characteristics of mechanical adaptability.
- b) High temperature stable water swellable elastomer composites could also be developed in order to obtain repeatable adaptability characteristics.

6 References

1. (a) Kirstein, T., The future of smart-textiles development: new enabling technologies, commercialization and market trends. In *Multidisciplinary know-how for smart-textiles developers*, Elsevier: 2013; pp 1-25; (b) Liu, Y.; Du, H.; Liu, L.; Leng, J., Shape memory polymers and their composites in aerospace applications: a review. *Smart Materials and Structures* 2014, 23 (2), 023001; (c) De las Heras Alarcón, C.; Pennadam, S.; Alexander, C., Stimuli responsive polymers for biomedical applications. *Chemical Society Reviews* 2005, 34 (3), 276-285.
2. (a) Shan, W.; Diller, S.; Tutcuoglu, A.; Majidi, C., Rigidity-tuning conductive elastomer. *Smart Materials and Structures* 2015, 24 (6), 065001; (b) Schubert, B. E.; Floreano, D., Variable stiffness material based on rigid low-melting-point-alloy microstructures embedded in soft poly (dimethylsiloxane)(PDMS). *Rsc Advances* 2013, 3 (46), 24671-24679.
3. Trotter, J. A.; Lyons-Levy, G.; Chino, K.; Koob, T. J.; Keene, D. R.; Atkinson, M. A., Collagen fibril aggregation-inhibitor from sea cucumber dermis. *Matrix Biology* 1999, 18 (6), 569-578.
4. (a) Shanmuganathan, K.; Capadona, J. R.; Rowan, S. J.; Weder, C., Biomimetic mechanically adaptive nanocomposites. *Progress in Polymer Science* 2010, 35 (1), 212-222; (b) Capadona, J. R.; Shanmuganathan, K.; Tyler, D. J.; Rowan, S. J.; Weder, C., Stimuli-responsive polymer nanocomposites inspired by the sea cucumber dermis. *Science* 2008, 319 (5868), 1370-1374.
5. Montero de Espinosa, L.; Meesorn, W.; Moatsou, D.; Weder, C., Bioinspired Polymer Systems with Stimuli-Responsive Mechanical Properties. *Chemical reviews* 2017, 117 (20), 12851-12892.
6. (a) Peleg, M., A model of mechanical changes in biomaterials at and around their glass transition. *Biotechnology progress* 1994, 10 (4), 385-388; (b) Cousins, W., Young's modulus of hemicellulose as related to moisture content. *Wood science and technology* 1978, 12 (3), 161-167.
7. Tang, Z.; Kotov, N. A.; Magonov, S.; Ozturk, B., Nanostructured artificial nacre. *Nature materials* 2003, 2 (6), 413.
8. (a) Tomatsu, I.; Hashidzume, A.; Harada, A., Redox-Responsive Hydrogel System Using the Molecular Recognition of β -Cyclodextrin. *Macromolecular rapid communications* 2006, 27 (4), 238-241; (b) Auletta, J. T.; LeDonne, G. J.; Gronborg, K. C.; Ladd, C. D.; Liu, H.; Clark, W. W.; Meyer, T. Y., Stimuli-responsive iron-cross-linked hydrogels that undergo redox-driven switching between hard and soft states. *Macromolecules* 2015, 48 (6), 1736-1747.
9. (a) Mcknight, G.; Doty, R.; Keefe, A.; Herrera, G.; Henry, C., Segmented reinforcement variable stiffness materials for reconfigurable surfaces. *Journal of Intelligent Material Systems and Structures* 2010, 21 (17), 1783-1793; (b) McEvoy, M. A.; Correll, N., Thermoplastic variable stiffness composites with embedded, networked sensing, actuation, and control. *Journal of Composite Materials* 2015, 49 (15), 1799-1808.
10. (a) Ginder, J. M.; Nichols, M. E.; Elie, L. D.; Clark, S. M. In *Controllable-stiffness components based on magnetorheological elastomers*, Smart structures and materials 2000: smart structures and integrated systems, International Society for Optics and Photonics: 2000; pp 418-426; (b) Cao, C.; Zhao, X., Tunable stiffness of electrorheological elastomers by designing mesostructures. *Applied Physics Letters* 2013, 103 (4), 041901.
11. Senses, E.; Akcora, P., An interface-driven stiffening mechanism in polymer nanocomposites. *Macromolecules* 2013, 46 (5), 1868-1874.
12. (a) Musso, S.; Robisson, A.; Maheshwar, S.; Ulm, F.-J., Stimuli-Responsive Cement-Reinforced Rubber. *ACS applied materials & interfaces* 2014, 6 (9), 6962-6968; (b) Takehana, Y.; Yamada, A.; Tamori, M.; Motokawa, T., Softenin, a novel protein that softens the connective tissue of sea cucumbers through inhibiting interaction between collagen fibrils. *PloS one* 2014, 9 (1), e85644.
13. (a) Goodyear Unveils the Eagle 360 Urban, a Concept Tire Powered by Artificial Intelligence, <http://news.goodyear.eu/latest-news/goodyear-unveils-the-eagle-360-urban--a-concept-tire-powered-by-artificial-intelligence/s/9da0b0a2-1bf6-4e98-91a4-26430db82749> (accessed March 7, 2018); (b) Empire Robotics New Multitasking VERSABALL® Gripper Ushers In Fundamental Agile Manufacturing Change, BusinessWire, <http://press.hughescom.net/empire-robotics-new-multitasking-versaball-gripper-ushers-in-fundamental-agile-manufacturing-change/> (accessed Jun.15,

- 2018); (c) Artificial Muscles to Be Used on Robotic Space Explorers, <https://www.jpl.nasa.gov/news/news.php?feature=5070> (accessed July 16, 2018); (d) Renault automobiles. https://www.renault.com.gh/cars/TalismanLFDPh1/FinitionsEtEquipements-old_f6140e16-5ad3-4b9e-846f-eb2480622c88.html (accessed 6th May 2017); (e) Strickland, E., Treating Depression With Deep Brain Stimulation Works—Most of the Time In *The Human OS Blog*, *IEEE Spectrum*, 18 Apr 2017.
14. Wolf, S.; Hirzinger, G. In *A new variable stiffness design: Matching requirements of the next robot generation*, Robotics and Automation, 2008. ICRA 2008. IEEE International Conference on, IEEE: 2008; pp 1741-1746.
 15. Tonietti, G.; Schiavi, R.; Bicchi, A. In *Design and control of a variable stiffness actuator for safe and fast physical human/robot interaction*, Robotics and Automation, 2005. ICRA 2005. Proceedings of the 2005 IEEE International Conference on, IEEE: 2005; pp 526-531.
 16. (a) Kornbluh, R. D.; Prahlah, H.; Pelrine, R.; Stanford, S.; Rosenthal, M. A.; von Guggenberg, P. A. In *Rubber to rigid, clamped to undamped: toward composite materials with wide-range controllable stiffness and damping*, Smart Structures and Materials 2004: Industrial and Commercial Applications of Smart Structures Technologies, International Society for Optics and Photonics: 2004; pp 372-387; (b) Brister, M.; Brauker, J. H. Transcutaneous medical device with variable stiffness. U.S. Patent 8,812,072, Aug. 24, 2010; (c) Stalker, K. C. Variable stiffness stent. U.S. Patent 6652576B1, Nov. 25, 2003; (d) Zwolinski, J. J.; Xu, L.; Anahid, H.; Oleszko, M. A.; Dong, Y. Adaptive seating system. U.S. Patent 6,055,473, Apr. 25, 2000; (e) Asanuma, H., Intelligent Composite Materials Having Capabilities of Sensing, Health Monitoring, Actuation, Self-Repair and Multifunctionality. In *Intelligent Materials*, Royal Society of Chemistry: 2007; pp 478-490.
 17. Motokawa, T.; Tsuchi, A., Dynamic mechanical properties of body-wall dermis in various mechanical states and their implications for the behavior of sea cucumbers. *The Biological Bulletin* 2003, 205 (3), 261-275.
 18. Trotter, J. A.; Lyons-Levy, G.; Luna, D.; Koob, T. J.; Keene, D. R.; Atkinson, M. A., Stiparin: a glycoprotein from sea cucumber dermis that aggregates collagen fibrils. *Matrix biology* 1996, 15 (2), 99-110.
 19. Shan, W.; Lu, T.; Majidi, C., Soft-matter composites with electrically tunable elastic rigidity. *Smart Materials and Structures* 2013, 22 (8), 085005.
 20. Jaber, J. A.; Schlenoff, J. B., Mechanical properties of reversibly cross-linked ultrathin polyelectrolyte complexes. *Journal of the American Chemical Society* 2006, 128 (9), 2940-2947.
 21. Daigle, J.-C.; Arnold, A. A.; Piche, L.; Claverie, J. P., A functional polymer with chemically switchable crystallinity. *Polymer Chemistry* 2013, 4 (3), 449-452.
 22. (a) Biyani, M. V.; Weder, C.; Foster, E. J., Photoswitchable nanocomposites made from coumarin-functionalized cellulose nanocrystals. *Polymer Chemistry* 2014, 5 (18), 5501-5508; (b) Biyani, M. V.; Jorfi, M.; Weder, C.; Foster, E. J., Light-stimulated mechanically switchable, photopatternable cellulose nanocomposites. *Polymer Chemistry* 2014, 5 (19), 5716-5724.
 23. Shanmuganathan, K.; Capadona, J. R.; Rowan, S. J.; Weder, C., Bio-inspired mechanically-adaptive nanocomposites derived from cotton cellulose whiskers. *Journal of Materials Chemistry* 2010, 20 (1), 180-186.
 24. Annamalai, P. K.; Dagnon, K. L.; Monemian, S.; Foster, E. J.; Rowan, S. J.; Weder, C., Water-Responsive Mechanically Adaptive Nanocomposites Based on Styrene-Butadiene Rubber and Cellulose Nanocrystals • Processing Matters. *ACS applied materials & interfaces* 2014, 6 (2), 967-976.
 25. Jorfi, M.; Roberts, M. N.; Foster, E. J.; Weder, C., Physiologically responsive, mechanically adaptive bio-nanocomposites for biomedical applications. *ACS applied materials & interfaces* 2013, 5 (4), 1517-1526.
 26. Liu, M.; Peng, Q.; Luo, B.; Zhou, C., The improvement of mechanical performance and water-response of carboxylated SBR by chitin nanocrystals. *European Polymer Journal* 2015, 68, 190-206.
 27. Stone, D. A.; Wanasekara, N. D.; Jones, D. H.; Wheeler, N. R.; Wilusz, E.; Zukas, W.; Wnek, G. E.; Korley, L. T., All-organic, stimuli-responsive polymer composites with electrospun fiber fillers. *ACS Macro Letters* 2011, 1 (1), 80-83.

28. (a) Wanasekara, N. D.; Stone, D. A.; Wnek, G. E.; Korley, L. T., Stimuli-responsive and mechanically-switchable electrospun composites. *Macromolecules* 2012, 45 (22), 9092-9099; (b) Wanasekara, N. D.; Korley, L. T., Toward tunable and adaptable polymer nanocomposites. *Journal of Polymer Science Part B: Polymer Physics* 2013, 51 (7), 463-467.
29. Salmen, N.; Back, G., The influence of water on the glass transition temperature of cellulose. *Tappi* 1977, 60 (12), 137-140.
30. Plaza, G. R.; Guinea, G. V.; Pérez-Rigueiro, J.; Elices, M., Thermo-hygro-mechanical behavior of spider dragline silk: Glassy and rubbery states. *Journal of Polymer Science Part B: Polymer Physics* 2006, 44 (6), 994-999.
31. Robisson, A.; Maheshwari, S.; Musso, S.; Thomas, J. J.; Auzerais, F. M.; Han, D.; Qu, M.; Ulm, F.-J., Reactive elastomeric composites: When rubber meets cement. *Composites Science and Technology* 2013, 75, 77-83.
32. Han, D.; Qu, M.; Yue, C. Y.; Lou, Y.; Musso, S.; Robisson, A., Swellable elastomeric HNBR–MgO composite: Magnesium oxide as a novel swelling and reinforcement filler. *Composites Science and Technology* 2014, 99, 52-58.
33. Deshmukh, S. S. Field-responsive ('Smart') fluids for advanced automotive applications. Ph.D Thesis, Massachusetts Institute of Technology, September 2003.
34. Janke, L.; Czaderski, C.; Motavalli, M.; Ruth, J., Applications of shape memory alloys in civil engineering structures—overview, limits and new ideas. *Materials and Structures* 2005, 38 (5), 578-592.
35. (a) Reddy, P. V. P.; Suresh, V., A review on importance of universal gripper in industrial robot applications. *Int. J. Mech. Eng. Robot. Res* 2013, 2 (2), 255-264; (b) Manti, M.; Hassan, T.; Passetti, G.; D'Elia, N.; Laschi, C.; Cianchetti, M., A bioinspired soft robotic gripper for adaptable and effective grasping. *Soft Robotics* 2015, 2 (3), 107-116.
36. Loeve, A.; Breedveld, P.; Dankelman, J., Scopes too flexible... and too stiff. *IEEE pulse* 2010, 1 (3), 26-41.
37. Harris, J.; Hess, A. E.; Rowan, S. J.; Weder, C.; Zorman, C.; Tyler, D.; Capadona, J. R., In vivo deployment of mechanically adaptive nanocomposites for intracortical microelectrodes. *Journal of neural engineering* 2011, 8 (4), 046010.
38. Cheng, N. G.; Gopinath, A.; Wang, L.; Iagnemma, K.; Hosoi, A. E., Thermally Tunable, Self-Healing Composites for Soft Robotic Applications. *Macromolecular Materials and Engineering* 2014, 299 (11), 1279-1284.
39. Molinari, G.; Quack, M.; Arrieta, A. F.; Morari, M.; Ermanni, P., Design, realization and structural testing of a compliant adaptable wing. *Smart Materials and Structures* 2015, 24 (10), 105027.
40. Continental presents two new tire technology concepts for greater safety and comfort, <http://www.continentaltire.com/news/continental-presents-two-new-tire-technology-concepts-greater-safety-and-comfort> (accessed Feb. 10, 2018).
41. Anusonti-Inthra, P.; Gandhi, F., Helicopter vibration reduction through cyclic variations in rotor blade root stiffness. *Journal of Intelligent Material Systems and Structures* 2000, 11 (2), 153-166.
42. Walsh, P.; Lamancusa, J., A variable stiffness vibration absorber for minimization of transient vibrations. *Journal of sound and vibration* 1992, 158 (2), 195-211.
43. (a) Winkelmann, H.; Croakmann, E., Water absorption of rubber compounds. *Industrial & Engineering Chemistry* 1930, 22 (12), 1367-1370; (b) Raevskii, V.; Zhivova, É., Water absorption and its effect on rubber strength. *Mechanics of Composite Materials* 1970, 6 (1), 118-120.
44. Briggs, G.; Edwards, D.; Storey, E., Water absorption of elastomers. *Rubber Chemistry and Technology* 1963, 36 (3), 621-641.
45. (a) Rozman, H.; Yeo, Y.; Tay, G.; Abubakar, A., The mechanical and physical properties of polyurethane composites based on rice husk and polyethylene glycol. *Polymer Testing* 2003, 22 (6), 617-623; (b) Martins, M. A.; Joeques, I., Tire rubber–sisal composites: Effect of mercerization and acetylation on reinforcement. *Journal of Applied Polymer Science* 2003, 89 (9), 2507-2515; (c) Stelescu, M.-D.; Manaila, E.; Craciun, G.; Dumitrascu, M., New green polymeric composites based on

- hemp and natural rubber processed by electron beam irradiation. *The Scientific World Journal* 2014, 2014.
46. (a) Dhakal, H.; Zhang, Z.; Richardson, M., Effect of water absorption on the mechanical properties of hemp fibre reinforced unsaturated polyester composites. *Composites Science and Technology* 2007, 67 (7), 1674-1683; (b) Espert, A.; Vilaplana, F.; Karlsson, S., Comparison of water absorption in natural cellulosic fibres from wood and one-year crops in polypropylene composites and its influence on their mechanical properties. *Composites Part A: Applied science and manufacturing* 2004, 35 (11), 1267-1276.
 47. Dehbari, N.; Zhao, J.; Peng, R.; Tang, Y., Neutralisation and compatibilisation effects on novel water-swellaable rubber composites. *Journal of Materials Science* 2015, 50 (15), 5157-5164.
 48. Nakason, C.; Nakaramontri, Y.; Kaesaman, A.; Kangwansukpamonkon, W.; Kiatkamjornwong, S., Synthesis and characterization of water swellaable natural rubber vulcanizates. *European Polymer Journal* 2013, 49 (5), 1098-1110.
 49. Wang, G.; Li, M.; Chen, X., Preparation and water-absorbent properties of a water-swellaable rubber. *Journal of applied polymer science* 1998, 68 (8), 1219-1225.
 50. Wang, C.; Zhang, G.; Dong, Y.; Chen, X.; Tan, H., Study on a water-swellaable rubber compatibilized by amphiphilic block polymer based on poly (ethylene oxide) and poly (butyl acrylate). *Journal of applied polymer science* 2002, 86 (12), 3120-3125.
 51. Zhang, G.; Zhang, Z.; Xie, F.; Hu, X.; Luo, X.; Chen, X., Chlorohydrin water swellaable rubber compatibilized by an amphiphilic graft copolymer. I. Synthesis and characterization of compatibilizer PVA-g-PBA. *Journal of applied polymer science* 2000, 75 (8), 977-986.
 52. Wei, D.; He, N.; Zhao, J.; Wang, Z., Mechanical, water-swelling, and morphological properties of water-swellaable thermoplastic vulcanizates based on high density polyethylene/chlorinated polyethylene/nitrile butadiene rubber/cross-linked sodium polyacrylate blends. *Polymer-Plastics Technology and Engineering* 2015, 54 (6), 616-624.
 53. Sun, X.; Zhang, G.; Shi, Q.; Tang, B.; Wu, Z., Study on foaming water-swellaable EPDM rubber. *Journal of applied polymer science* 2002, 86 (14), 3712-3717.
 54. Saijun, D.; Nakason, C.; Kaesaman, A.; Klinpituksa, P., Water absorption and mechanical properties of water-swellaable natural rubber. *Sonklanakarin Journal of Science and Technology* 2009, 31 (5), 561.
 55. Nakamura, M.; Obayashi, S.; Takemori, S.; Tanaka, H.; Hirakawa, M. Water-swellaable elastomer composition. U.S. Patent 4590227A, May 20, 1986.
 56. (a) Ren, W.; Peng, Z.; Zhang, Y.; Zhang, Y., Water-swelling elastomer prepared by in situ formed lithium acrylate in chlorinated polyethylene. *Journal of applied polymer science* 2004, 92 (3), 1804-1812; (b) Du, A.; Peng, Z.; Zhang, Y., Water swelling rubber prepared by in situ formed sodium acrylate in EVM. *Kautschuk Gummi Kunststoffe* 2003, 56 (6), 316-316.
 57. (a) Xie, Z.; Li, M.; Chen, X.; Hu, H.; Li, S., Studies on water-swellaable elastomer. I. Synthesis and characterization of amphiphilic polymer. *Journal of applied polymer science* 1996, 61 (3), 495-499; (b) Zhang, Y.; He, P.; Zou, Q.; He, B., Preparation and properties of water-swellaable elastomer. *Journal of applied polymer science* 2004, 93 (4), 1719-1723.
 58. Riyajan, S.-A.; Chaiponban, S.; Tanbunrung, K., Investigation of the preparation and physical properties of a novel semi-interpenetrating polymer network based on epoxised NR and PVA using maleic acid as the crosslinking agent. *Chemical Engineering Journal* 2009, 153 (1), 199-205.
 59. Peng, H. T.; Martineau, L.; Shek, P. N., Hydrogel-elastomer composite biomaterials: 1. Preparation of interpenetrating polymer networks and in vitro characterization of swelling stability and mechanical properties. *Journal of Materials Science: Materials in Medicine* 2007, 18 (6), 975-986.
 60. Pouchlý, J.; Biroš, J.; Beneš, S., Heat capacities of water swollen hydrophilic polymers above and below 0 C. *Die Makromolekulare Chemie* 1979, 180 (3), 745-760.
 61. Hatakeyama, H.; Hatakeyama, T., Interaction between water and hydrophilic polymers. *Thermochimica acta* 1998, 308 (1-2), 3-22.
 62. Ping, Z.; Nguyen, Q.; Chen, S.; Zhou, J.; Ding, Y., States of water in different hydrophilic polymers—DSC and FTIR studies. *Polymer* 2001, 42 (20), 8461-8467.

63. (a) Li, W.; Xue, F.; Cheng, R., States of water in partially swollen poly (vinyl alcohol) hydrogels. *Polymer* 2005, 46 (25), 12026-12031; (b) Lue, S. J.; Shieh, S.-J., Water states in perfluorosulfonic acid membranes using differential scanning calorimetry. *Journal of Macromolecular Science* 2009, 48 (1), 114-127; (c) Guan, L.; Xu, H.; Huang, D., The investigation on states of water in different hydrophilic polymers by DSC and FTIR. *Journal of Polymer Research* 2011, 18 (4), 681-689.
64. Hodge, R.; Bastow, T.; Edward, G.; Simon, G.; Hill, A., Free volume and the mechanism of plasticization in water-swollen poly (vinyl alcohol). *Macromolecules* 1996, 29 (25), 8137-8143.
65. Blasi, P.; D'souza, S. S.; Selmin, F.; DeLuca, P. P., Plasticizing effect of water on poly (lactide-co-glycolide). *Journal of Controlled Release* 2005, 108 (1), 1-9.
66. (a) Ellis, T.; Karasz, F., Interaction of epoxy resins with water: the depression of glass transition temperature. *Polymer* 1984, 25 (5), 664-669; (b) Oksanen, C. A.; Zografi, G., Molecular mobility in mixtures of absorbed water and solid poly (vinylpyrrolidone). *Pharmaceutical research* 1993, 10 (6), 791-799; (c) Oksanen, C. A.; Zografi, G., The relationship between the glass transition temperature and water vapor absorption by poly (vinylpyrrolidone). *Pharmaceutical research* 1990, 7 (6), 654-657; (d) Sablani, S.; Kasapis, S.; Rahman, M., Evaluating water activity and glass transition concepts for food stability. *Journal of Food Engineering* 2007, 78 (1), 266-271.
67. Reimschuessel, H., Relationships on the effect of water on glass transition temperature and young's modulus of nylon 6. *Journal of Polymer Science Part A: Polymer Chemistry* 1978, 16 (6), 1229-1236.
68. Roos, Y.; Karel, M., Plasticizing effect of water on thermal behavior and crystallization of amorphous food models. *Journal of Food Science* 1991, 56 (1), 38-43.
69. Hodge, R.; Edward, G. H.; Simon, G. P., Water absorption and states of water in semicrystalline poly (vinyl alcohol) films. *Polymer* 1996, 37 (8), 1371-1376.
70. Iwamoto, R.; Miya, M.; Mima, S., Determination of crystallinity of swollen poly (vinyl alcohol) by laser Raman spectroscopy. *Journal of Polymer Science Part B: Polymer Physics* 1979, 17 (9), 1507-1515.
71. Vlasveld, D.; Groenewold, J.; Bersee, H.; Picken, S., Moisture absorption in polyamide-6 silicate nanocomposites and its influence on the mechanical properties. *Polymer* 2005, 46 (26), 12567-12576.
72. De'Nève, B.; Shanahan, M., Water absorption by an epoxy resin and its effect on the mechanical properties and infra-red spectra. *Polymer* 1993, 34 (24), 5099-5105.
73. Peresin, M. S.; Habibi, Y.; Vesterinen, A.-H.; Rojas, O. J.; Pawlak, J. J.; Seppälä, J. V., Effect of moisture on electrospun nanofiber composites of poly (vinyl alcohol) and cellulose nanocrystals. *Biomacromolecules* 2010, 11 (9), 2471-2477.
74. Alamri, H.; Low, I. M., Effect of water absorption on the mechanical properties of nano-filler reinforced epoxy nanocomposites. *Materials & Design* 2012, 42, 214-222.
75. Shirrell, C.; Halpin, J. In *Moisture absorption and desorption in epoxy composite laminates*, Composite Materials: Testing and Design (Fourth Conference), ASTM International: 1977.
76. Berens, A.; Hopfenberg, H., Diffusion and relaxation in glassy polymer powders: 2. Separation of diffusion and relaxation parameters. *Polymer* 1978, 19 (5), 489-496.
77. Kim, B.; La Flamme, K.; Peppas, N. A., Dynamic swelling behavior of pH-sensitive anionic hydrogels used for protein delivery. *Journal of Applied Polymer Science* 2003, 89 (6), 1606-1613.
78. Robert, C. C.; Buri, P. A.; Peppas, N. A., Effect of degree of crosslinking on water transport in polymer microparticles. *Journal of applied polymer science* 1985, 30 (1), 301-306.
79. Yao, K. D.; Peng, T.; Feng, H. B.; He, Y. Y., Swelling kinetics and release characteristic of crosslinked chitosan: polyether polymer network (semi-IPN) hydrogels. *Journal of Polymer Science Part A: Polymer Chemistry* 1994, 32 (7), 1213-1223.
80. (a) Chow, W.; Abu Bakar, A.; Mohd Ishak, Z., Water absorption and hygrothermal aging study on organomontmorillonite reinforced polyamide 6/polypropylene nanocomposites. *Journal of applied polymer science* 2005, 98 (2), 780-790; (b) Mishra, S.; Verma, J., Effect of compatibilizers on water absorption kinetics of polypropylene/wood flour foamed composites. *Journal of applied polymer science* 2006, 101 (4), 2530-2537; (c) Panthapulakkal, S.; Sain, M., Studies on the water absorption properties of short hemp—glass fiber hybrid polypropylene composites. *Journal of*

- Composite Materials* 2007, 41 (15), 1871-1883; (d) Tajvidi, M.; Ebrahimi, G., Water uptake and mechanical characteristics of natural filler–polypropylene composites. *Journal of Applied Polymer Science* 2003, 88 (4), 941-946.
81. Wack, H.; Bertling, J. In *Water-Swellable Materials–Application in Self-Healing Sealing Systems*, Proceedings of the First International Conference on Self Healing Materials, Springer Dordrecht, The Netherlands: 2007; pp 18-20.
 82. Akhtar, M.; Qamar, S. Z.; Pervez, T., Swelling elastomer applications in oil and gas industry. *J. Trends Dev. Mach. Assoc. Technol* 2012, 16 (1), 71-74.
 83. Nachon, M.; Clegg, S.; Mangold, N.; Schröder, S.; Kah, L.; Dromart, G.; Ollila, A.; Johnson, J.; Oehler, D.; Bridges, J., Calcium sulfate veins characterized by ChemCam/Curiosity at Gale crater, Mars. *Journal of Geophysical Research: Planets* 2014, 119 (9), 1991-2016.
 84. Ramsdell, L.; Partridge, E., The crystal forms of calcium sulphate. *American Mineralogist* 1929, 14 (2), 59-74.
 85. (a) Ling, Y.; Demopoulos, G. P., Preparation of α -calcium sulfate hemihydrate by reaction of sulfuric acid with lime. *Industrial & engineering chemistry research* 2005, 44 (4), 715-724; (b) Kong, B.; Yu, J.; Savino, K.; Zhu, Y.; Guan, B., Synthesis of α -calcium sulfate hemihydrate submicron-rods in water/n-hexanol/CTAB reverse microemulsion. *Colloids and Surfaces A: Physicochemical and Engineering Aspects* 2012, 409, 88-93.
 86. Singh, N.; Middendorf, B., Calcium sulphate hemihydrate hydration leading to gypsum crystallization. *Progress in Crystal Growth and Characterization of Materials* 2007, 53 (1), 57-77.
 87. Van Driessche, A.; Benning, L.; Rodriguez-Blanco, J.; Ossorio, M.; Bots, P.; García-Ruiz, J., The role and implications of bassanite as a stable precursor phase to gypsum precipitation. *Science* 2012, 336 (6077), 69-72.
 88. Saha, A.; Lee, J.; Pancera, S. M.; Bräeu, M. F.; Kempter, A.; Tripathi, A.; Bose, A., New Insights into the transformation of calcium sulfate hemihydrate to gypsum using time-resolved cryogenic transmission electron microscopy. *Langmuir* 2012, 28 (30), 11182-11187.
 89. Badens, E.; Veesler, S.; Boistelle, R., Crystallization of gypsum from hemihydrate in presence of additives. *Journal of Crystal Growth* 1999, 198, 704-709.
 90. Song, X.; Sun, S.; Fan, W.; Yu, H., Preparation of different morphologies of calcium sulfate in organic media. *Journal of Materials Chemistry* 2003, 13 (7), 1817-1821.
 91. Wang, P.; Lee, E. J.; Park, C. S.; Yoon, B. H.; Shin, D. S.; Kim, H. E.; Koh, Y. H.; Park, S. H., Calcium sulfate hemihydrate powders with a controlled morphology for use as bone cement. *Journal of the American Ceramic Society* 2008, 91 (6), 2039-2042.
 92. Guan, B.; Yang, L.; Fu, H.; Kong, B.; Li, T.; Yang, L., α -calcium sulfate hemihydrate preparation from FGD gypsum in recycling mixed salt solutions. *Chemical engineering journal* 2011, 174 (1), 296-303.
 93. (a) Combe, E.; Smith, D., Studies on the preparation of calcium sulphate hemihydrate by an autoclave process. *Journal of Applied Chemistry* 1968, 18 (10), 307-312; (b) Ball, M.; Norwood, L., Studies in the system calcium sulphate–water. Part I. Kinetics of dehydration of calcium sulphate dihydrate. *Journal of the Chemical Society A: Inorganic, Physical, Theoretical* 1969, 1633-1637; (c) Ostroff, A., Conversion of gypsum to anhydrite in aqueous salt solutions. *Geochimica et Cosmochimica Acta* 1964, 28 (9), 1363-1372; (d) Guan, B.; Shen, Z.; Wu, Z.; Yang, L.; Ma, X., Effect of pH on the Preparation of α -Calcium Sulfate Hemihydrate from FGD Gypsum with the Hydrothermal Method. *Journal of the American Ceramic Society* 2008, 91 (12), 3835-3840.
 94. Azimi, G.; Papangelakis, V. G., Mechanism and kinetics of gypsum–anhydrite transformation in aqueous electrolyte solutions. *Hydrometallurgy* 2011, 108 (1), 122-129.
 95. (a) Murariu, M.; Ferreira, A. D. S.; Degée, P.; Alexandre, M.; Dubois, P., Polylactide compositions. Part 1: Effect of filler content and size on mechanical properties of PLA/calcium sulfate composites. *Polymer* 2007, 48 (9), 2613-2618; (b) Sobkowicz, M. J.; Feaver, J. L.; Dorgan, J. R., Clean and green bioplastic composites: comparison of calcium sulfate and carbon nanospheres in polylactide composites. *CLEAN–Soil, Air, Water* 2008, 36 (8), 706-713; (c) Gorrasi, G.; Vittoria, V.; Murariu, M.; Ferreira, A. D. S.; Alexandre, M.; Dubois, P., Effect of filler content and size on transport

- properties of water vapor in PLA/calcium sulfate composites. *Biomacromolecules* 2008, 9 (3), 984-990.
96. Koenig, J. L., *Spectroscopy of polymers*. Elsevier, Amsterdam: 1999.
 97. (a) Park, J. H.; Kim, D., Preparation and characterization of water-swellaable natural rubbers. *Journal of applied polymer science* 2001, 80 (1), 115-121; (b) Liu, C.; Ding, J.; Zhou, L.; Chen, S., Mechanical properties, water-swelling behavior, and morphology of water-swellaable rubber prepared using crosslinked sodium polyacrylate. *Journal of applied polymer science* 2006, 102 (2), 1489-1496.
 98. (a) Schneider, H. A., Glass transition behaviour of compatible polymer blends. *Polymer* 1989, 30 (5), 771-779; (b) Liberman, S. A.; Gomes, A. D. S.; Macchi, E. M., Compatibility in poly (ethylene oxide)-poly (methyl methacrylate) blends. *Journal of Polymer Science Part A: Polymer Chemistry* 1984, 22 (11), 2809-2815; (c) Utracki, L. A., *Commercial polymer blends*. Springer Science & Business Media: Berlin, 2013.
 99. (a) Ibrahim, S.; Johan, M. R., Thermolysis and conductivity studies of poly (ethylene oxide)(PEO) based polymer electrolytes doped with carbon nanotube. *Int J Electrochem Sci* 2012, 7, 2596-2615; (b) Qian, X.; Gu, N.; Cheng, Z.; Yang, X.; Wang, E.; Dong, S., Impedance study of (PEO) 10LiClO₄-Al₂O₃ composite polymer electrolyte with blocking electrodes. *Electrochimica acta* 2001, 46 (12), 1829-1836.
 100. (a) Nishi, T.; Wang, T., Melting point depression and kinetic effects of cooling on crystallization in poly (vinylidene fluoride)-poly (methyl methacrylate) mixtures. *Macromolecules* 1975, 8 (6), 909-915; (b) Kwei, T.; Patterson, G.; Wang, T., Compatibility in Mixtures of Poly (vinylidene fluoride) and Poly (ethyl methacrylate). *Macromolecules* 1976, 9 (5), 780-784.
 101. (a) Fox, T. G., Influence of Diluent and of Copolymer Composition on the Glass Temperature of a Poly-mer System. *Bull. Am. Phys. Soc.* 1956, 1, 123; (b) Fried, J., Applications of thermal analysis to the study of polymer blends. In *Developments in Polymer Characterisation—4*, Springer, Dordrecht: 1983; pp 39-90.
 102. Penzel, E.; Rieger, J.; Schneider, H., The glass transition temperature of random copolymers: 1. Experimental data and the Gordon-Taylor equation. *Polymer* 1997, 38 (2), 325-337.
 103. Kwei, T., The effect of hydrogen bonding on the glass transition temperatures of polymer mixtures. *Journal of Polymer Science Part C: Polymer Letters* 1984, 22 (6), 307-313.
 104. Kalogeras, I. M.; Brostow, W., Glass transition temperatures in binary polymer blends. *Journal of Polymer Science Part B: Polymer Physics* 2009, 47 (1), 80-95.
 105. He, Y.; Zhu, B.; Inoue, Y., Hydrogen bonds in polymer blends. *Progress in Polymer Science* 2004, 29 (10), 1021-1051.
 106. Wetton, R.; Corish, P., DMTA studies of polymer blends and compatibility. *Polymer testing* 1988, 8 (5), 303-312.
 107. Unemori, M.; Matsuya, Y.; Matsuya, S.; Akashi, A.; Akamine, A., Water absorption of poly (methyl methacrylate) containing 4-methacryloxyethyl trimellitic anhydride. *Biomaterials* 2003, 24 (8), 1381-1387.
 108. Ritger, P. L.; Peppas, N. A., A simple equation for description of solute release II. Fickian and anomalous release from swellable devices. *Journal of controlled release* 1987, 5 (1), 37-42.
 109. (a) Ren, W.; Zhang, Y.; Peng, Z.; Zhang, Y., Investigation on the water-swelling properties of chlorinated polyethylene modified by in situ formed sodium acrylate. *Polymer Testing* 2004, 23 (7), 809-816; (b) Bartil, T.; Bounekhel, M.; Cedric, C.; Jeerome, R., Swelling behavior and release properties of pH-sensitive hydrogels based on methacrylic derivatives. *Acta Pharmaceutica* 2007, 57 (3), 301-314.
 110. Yoon, J. S.; Jung, H. W.; Kim, M. N.; Park, E. S., Diffusion coefficient and equilibrium solubility of water molecules in biodegradable polymers. *Journal of applied polymer science* 2000, 77 (8), 1716-1722.
 111. Ostrowska-Czubenko, J.; Gierszewska-Drużyńska, M., Effect of ionic crosslinking on the water state in hydrogel chitosan membranes. *Carbohydrate Polymers* 2009, 77 (3), 590-598.
 112. Hancock, B. C.; Zografi, G., The relationship between the glass transition temperature and the water content of amorphous pharmaceutical solids. *Pharmaceutical research* 1994, 11 (4), 471-477.

113. Kumai, M., Hexagonal and cubic ice at low temperatures. *J. Glaciol* 1968, 7, 95-108.
114. Payne, A.; Whittaker, R., Low strain dynamic properties of filled rubbers. *Rubber chemistry and technology* 1971, 44 (2), 440-478.
115. Kraus, G., Swelling of filler-reinforced vulcanizates. *Journal of Applied Polymer Science* 1963, 7 (3), 861-871.
116. Heinrich, G.; Klüppel, M., Recent Advances in the Theory of Filler Networking in Elastomers. In *Filled Elastomers Drug Delivery Systems*, Springer: Berlin, Heidelberg, 2002; pp 1-44.
117. Socrates, G., *Infrared and Raman characteristic group frequencies: tables and charts*. John Wiley & Sons: New York, 2004.
118. (a) Mark, J., Experimental determinations of crosslink densities. *Rubber Chemistry and Technology* 1982, 55 (3), 762-768; (b) Pradhan, S.; Costa, F.; Wagenknecht, U.; Jehnichen, D.; Bhowmick, A.; Heinrich, G., Elastomer/LDH nanocomposites: Synthesis and studies on nanoparticle dispersion, mechanical properties and interfacial adhesion. *European Polymer Journal* 2008, 44 (10), 3122-3132; (c) Morris, M., Network characterization from stress-strain behavior at large extensions. *Journal of applied polymer science* 1964, 8 (2), 545-553.
119. (a) Domurath, J.; Saphiannikova, M.; Ausias, G.; Heinrich, G., Modelling of stress and strain amplification effects in filled polymer melts. *Journal of Non-Newtonian Fluid Mechanics* 2012, 171, 8-16; (b) Hsiao-Sheng, C.; Acrivos, A., The effective elastic moduli of composite materials containing spherical inclusions at non-dilute concentrations. *International Journal of Solids and Structures* 1978, 14 (5), 349-364.
120. (a) Robertson, C. G.; Lin, C.; Rackaitis, M.; Roland, C., Influence of particle size and polymer-filler coupling on viscoelastic glass transition of particle-reinforced polymers. *Macromolecules* 2008, 41 (7), 2727-2731; (b) Akay, M., Aspects of dynamic mechanical analysis in polymeric composites. *Composites science and technology* 1993, 47 (4), 419-423.
121. (a) Ahmad, M. B.; Huglin, M. B., DSC studies on states of water in crosslinked poly (methyl methacrylate-co-n-vinyl-2-pyrrolidone) hydrogels. *Polymer international* 1994, 33 (3), 273-277; (b) Kumarasamy, K.; An, J.; Yang, J.; Yang, E.-H., Numerical techniques to model conduction dominant phase change systems: A CFD approach and validation with DSC curve. *Energy and Buildings* 2016, 118, 240-248.
122. (a) Kontrec, J.; Kralj, D.; Brečević, L., Transformation of anhydrous calcium sulphate into calcium sulphate dihydrate in aqueous solutions. *Journal of crystal growth* 2002, 240 (1-2), 203-211; (b) Powell, D., Transformation of the α - and β -forms of calcium sulphate hemihydrate to insoluble anhydrite. *Nature* 1958, 182 (4638), 792.
123. (a) Baroud, G.; Cayer, E.; Bohner, M., Rheological characterization of concentrated aqueous β -tricalcium phosphate suspensions: The effect of liquid-to-powder ratio, milling time, and additives. *Acta Biomaterialia* 2005, 1 (3), 357-363; (b) Pina, S.; Olhero, S.; Gheduzzi, S.; Miles, A. W.; Ferreira, J., Influence of setting liquid composition and liquid-to-powder ratio on properties of a Mg-substituted calcium phosphate cement. *Acta biomaterialia* 2009, 5 (4), 1233-1240.
124. Ball, M.; Urie, R., Studies in the system calcium sulphate-water. Part II. The kinetics of dehydration of β -CaSO₄ · ½H₂O. *Journal of the Chemical Society A: Inorganic, Physical, Theoretical* 1970, 528-530.
125. (a) Sarma, L.; Prasad, P.; Ravikumar, N., Raman spectroscopic study of phase transitions in natural gypsum. *Journal of Raman spectroscopy* 1998, 29 (9), 851-856; (b) Chang, H.; Huang, P. J.; Hou, S., Application of thermo-Raman spectroscopy to study dehydration of CaSO₄ · 2H₂O and CaSO₄ · 0.5 H₂O. *Materials Chemistry and Physics* 1999, 58 (1), 12-19.
126. Prieto-Taboada, N.; Gómez-Laserna, O.; Martínez-Arkarazo, I.; Olazabal, M. Á.; Madariaga, J. M., Raman Spectra of the Different Phases in the CaSO₄-H₂O System. *Analytical chemistry* 2014, 86 (20), 10131-10137.
127. Osterwalder, N.; Loher, S.; Grass, R. N.; Brunner, T. J.; Limbach, L. K.; Halim, S. C.; Stark, W. J., Preparation of nano-gypsum from anhydrite nanoparticles: strongly increased Vickers hardness and formation of calcium sulfate nano-needles. *Journal of Nanoparticle Research* 2007, 9 (2), 275-281.
128. (a) Wang, Y.-W.; Kim, Y.-Y.; Christenson, H. K.; Meldrum, F. C., A new precipitation pathway for calcium sulfate dihydrate (gypsum) via amorphous and hemihydrate intermediates. *Chemical*

- Communications* 2012, 48 (4), 504-506; (b) Wang, Y.-W.; Meldrum, F. C., Additives stabilize calcium sulfate hemihydrate (bassanite) in solution. *Journal of Materials Chemistry* 2012, 22 (41), 22055-22062.
129. (a) Batchelor, G.; Green, J.-T., The hydrodynamic interaction of two small freely-moving spheres in a linear flow field. *Journal of Fluid Mechanics* 1972, 56 (2), 375-400; (b) Song, Y.; Zheng, Q., A guide for hydrodynamic reinforcement effect in nanoparticle-filled polymers. *Crit Rev Solid State Mater Sci* 2016, 41 (4), 318-346.
130. Pothan, L. A.; Oommen, Z.; Thomas, S., Dynamic mechanical analysis of banana fiber reinforced polyester composites. *Composites Science and Technology* 2003, 63 (2), 283-293.
131. (a) Ziegel, K.; Romanov, A., Modulus reinforcement in elastomer composites. I. Inorganic fillers. *Journal of Applied Polymer Science* 1973, 17 (4), 1119-1131; (b) Rooj, S.; Das, A.; Stöckelhuber, K. W.; Reuter, U.; Heinrich, G., Highly Exfoliated Natural Rubber/Clay Composites by "Propping-Open Procedure": The Influence of Fatty-Acid Chain Length on Exfoliation. *Macromolecular Materials and Engineering* 2012, 297 (4), 369-383.

7 Appendix

Mechanism of water absorption

The mechanism behind the water absorption behavior of GECCO/GEPO blends is investigated in section 4.1.2.1. The experimental data's of the water swelling characteristics of GECCO/GEPO blends are fitted with the Fickian diffusion equation (Eq.2.1) and is shown in Figure 7.1. From Figure 7.1, it can be seen that the experimental data exhibited perfect fit till $\frac{M_t}{M_\infty}$ values of 0.8. This indicates that the Fickian mechanism occurring below $\frac{M_t}{M_\infty} = 0.8$.

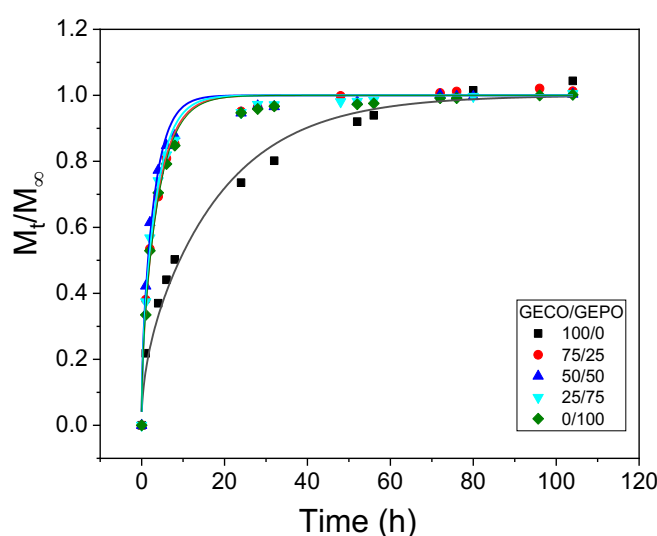


Figure 7.1 Water swelling process fitted by Fickian diffusion mechanism equation. The symbol, lines represent the experimental data and the fitted curves.

Rheology of the GECCO compounds with varying cross-link density

In order to enhance the water absorption characteristics of GECCO compounds, GECCO compounds with varying curative contents (SC1 – 2.5/1/1, SC2 – 0.5/0.5/0.5, SC3 – 0.25/0.25/0.25 TMTD/MBTS/S, Table 3.3) were prepared and investigated in section 4.2. Figure 7.2 shows the rheological properties of the different GECCO compounds. It can be observed that the reduction in curative content led to reduced torque values, which confirms the reduced cross-link density. SC3 compound exhibited very high water absorption capabilities of ~40% (Figure 4.11) and is attributed to the low cross-link density values.

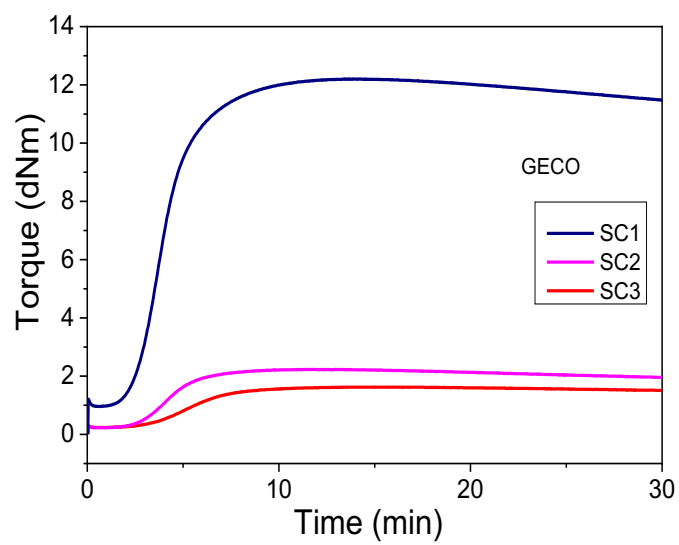


Figure 7.2 Rheometric characteristics of GECO compounds with varying curatives content operated at 160 °C.

8 Abbreviations

AGE	Allyl glycidyl ether
AR	Adaptability ratio
AT	Adaptability temperature
ATR	Attenuated total reflectance
Bp-CNCs	Benzophenone derivatized cellulose nanocrystals
BR	Poly(butadiene) rubber
cEPM	Conductive poly (propylene-co-ethylene) rubber
CNC	Cellulose nanocrystals
CNC-c	Cellulose nanocrystals obtained from cotton
CNC-t	Cellulose nanocrystals obtained from tunicates
CO	Epichlorohydrin
Cou-CNCs	Coumarin derivatized cellulose nanocrystals
CPE	Chlorinated poly(ethylene)
CPE-g-PEG	Chlorinated poly(ethylene)-graft-poly(ethylene glycol)
cryo-TEM	Cryo-transmission electron microscopy
D	Dry sample
DMA	Dynamic mechanical analysis
DSC	Differential scanning calorimetry
DW	Water swollen sample (Dry-Wet)
DWD	Water swollen and dried sample (Dry-Wet-Dry)
ECO	Poly(ethylene oxide-co-epichlorohydrin)
EFTEM	Energy filtered transmission electron microscopy
EGDMA	Ethylene glycol dimethacrylate
ENR	Epoxidised poly(cis-1,4 isoprene) or Epoxidised natural rubber
EO	Ethylene oxide
EPDM	Poly(ethylene-co-propylene-co-ethylidene norbornene) rubber
FTIR	Fourier-transform infrared
GECO	Poly(ethylene oxide-co-epichlorohydrin-co-allyl glycidyl ether)
GEPO	Poly(ethylene oxide-co-propylene oxide-co-allyl glycidyl ether)
GO	Graphene oxide

HEMA	2-hydroxyethyl methacrylate
HNBR	Hydrogenated poly (nitrile-co-butadiene) rubber
IPN	Interpenetrating polymer networks
LiAA	Lithium acrylate
LMPA	Low melting point alloy
MBTS	Mercapto benzothiazole disulfide
Mg(OH) ₂	Magnesium hydroxide
MgO	Magnesium oxide
NaAA	Sodium acrylate
NMR	Nuclear magnetic resonance
NR	Poly(cis-1,4 isoprene) rubber
P(AA-AM)	Poly(acrylic acid-co-acrylic amide)
PAA	Poly(acrylic acid)
PALS	Positron annihilation lifetime spectroscopy
PDADMA	Poly(diallyldimethylammonium)
PDMS	Poly(dimethyl siloxane)
PEG	Poly(ethylene glycol)
PEO	Poly(ethylene oxide)
phr	Parts per hundred rubber
PMMA	Poly(methyl methacrylate)
PO	Propylene oxide
PSS	Poly(styrene sulfonate)
PVA	Poly(vinyl alcohol)
PVAc	Poly(vinyl acetate)
S	Sulphur
SAED	Selected area electron diffraction
SANS	Small-angle neutron scattering
SBR	Poly(styrene-co-butadiene) rubber
SEM	Scanning electron microscopy
TEM	Transmission electron microscope
TGA	Thermogravimetric analysis

TMTD	Tetramethyl thiuram disulphide
UV	Ultraviolet
XRD	X-ray diffraction
XSBR	Carboxylated poly(styrene-co-butadiene) rubber
ZnO	Zinc Oxide

9 Symbols

ϕ	Volume fraction of the dispersed filler (Ice crystals/CaSO ₄)
θ	Angle between the incident beam and planes (°)
Ψ_F	Volume fraction of absorbed water due to Fickian mechanism
Ψ_R	Volume fraction of absorbed water due to relaxation mechanism
φ'_{GEPO}	Weight fraction of the amorphous GEPO phase
φ_{GEPO}	Weight fraction of GEPO in the GECO/GEPO Blend
φ_i	Weight fraction of the polymer
ΔC_{pi}	Difference in specific heat during glass transition of the polymer (J/K)
ΔH^0_{PEO}	Melting enthalpy of 100% crystalline PEO (J/g)
ΔH_{bw}	Melting enthalpy of the bulk water (J/g)
$\Delta H_{m, blend}$	Melting enthalpy of GECO/GEPO blend (J/g)
ΔH_{ws}	Melting enthalpy of the water swollen elastomer (J/g)
γ	Particular strain (Payne effect)
γ_c	Critical strain (Payne effect)
γ_o	Very low strain (Payne effect)
λ	Extension ratio
λ_i	Wavelength of the incident wave (nm)
ν	Cross-linking density (mol/cm ³)
σ	Applied stress (MPa)
A	Calcium sulphate anhydride
B	Interaction parameter (polymer-filler)
C	Concentration of the diffused liquid at time t and position x (g)
C_1, C_2	Mooney-Rivlin (MR) constants
CaSO ₄	Calcium sulphate
CaSO ₄ . 0.5 H ₂ O	Calcium sulphate hemihydrate
CaSO ₄ . 2 H ₂ O	Calcium sulphate dihydrate
d	Distance between the crystal lattices (nm)
D_c	Diffusion Coefficient (mm ² /s)
DS	Degree of water swelling (%)
E	Young's modulus of filled composites (MPa)

E'	Storage modulus (MPa)
$E'(\gamma)$	Storage modulus at strain γ (MPa)
E''	Loss modulus (MPa)
E'_0	Storage modulus at low strain γ_0 (MPa)
E'_∞	Storage modulus at very large strain (MPa)
E'_g	Storage modulus in the glassy region (MPa)
E'_r	Storage modulus in the rubbery region (MPa)
E_0	Young's modulus of unfilled composites (MPa)
EB	Elongation at break (%)
EC	Filler effectiveness coefficient
f	Shape factor (filler)
G	Calcium sulphate dihydrate
h	Thickness (mm)
H	Calcium sulphate hemihydrate
H_2O	Water/Moisture
k	Characteristic constant (power law)
k_B	Boltzmann constant
k_{GT}	Gordon Taylor volume additivity constant
k_{KW}	Kwei volume additivity constant
k_r	Relaxation rate constant
m	Strain sensitivity constant
M_∞	Equilibrium water absorption (g)
M_t	Water absorption at time t (g)
$M_{i,F}$	Fickian contribution to water absorption at time t
$M_{i,R}$	Relaxation mechanism contribution to water absorption at time t
n	integer
q	Kwei interaction parameter
Q	Swelling ratio
r	Swelling exponent (Power law)
RH	Relative humidity (%)
RT	Room temperature (°C)
T	Temperature (°C)

t	Time (s), (min), (h), (d)
$\tan \delta$	Dissipation factor or loss tangent of the filled compound
$\tan \delta_m$	Dissipation factor or loss tangent of the unfilled/gum compound
t_{c90}	Cure time (min)
T_g	Glass transition temperature (°C)
T_{gw}	Glass transition temperature of water absorbed sample (°C)
T_m	Melting temperature (°C)
T_s	Softening temperature (°C)
TS	Tensile strength (MPa)
t_{s2}	Scorch time (min)
$vol\%$	Volume percent of the filler (%)
W_d	Weight of the dry sample (g)
W_{dw}	Weight of sample containing water (g)
W_{dwd}	Weight of the dried sample after water swelling (g)
W_f	Freezable water content (g)
W_{nf}	Non-freezable water content (g)
W_t	Total absorbed water (g)
$wt\%$	Weight percent of the filler (%)
W_w	Weight of the water swollen sample (g)
X_c	Degree of crystallinity (%)

10 Figures

Figure 1.1 Future applications of mechanically switchable materials (images adapted from ¹³).	3
Figure 2.1 a) Cyclic studies of Fe crosslinked hydrogel when the electric potential is applied/removed. The enhanced rate and degree of switchability of graphene oxide dispersed hydrogels can also be observed here, b) Fe^{3+} crosslinked composite exhibited higher mechanical properties and the load carrying capabilities than the Fe^{2+} crosslinked hydrogel (adapted and redrawn with permission from ^{8b}).	9
Figure 2.2 a) Schematic diagram of sample preparation and the mechanism behind the switchability (cross-linking between the polymer), b) temperature sweep analysis (DMA) of 10 wt-% Bp-CNC and Cou-CNC nanocomposites before and after UV irradiation. Enhanced modulus values after UV irradiation can be clearly seen (adapted and redrawn with permission from ²²).	10
Figure 2.3 a) Mechanically adaptable behavior of sea cucumber dermis, b) material design for mimicking the sea cucumber dermis, c) results (mechanical switchability) obtained from the developed materials mimicking sea cucumber dermis (adapted and redrawn with permission from ^{4a}).	11
Figure 2.4 Development of strong and hard material from soft and flexible material using water as stimuli in HNBR/Cement composites. Comparison of FTIR analysis of dry and water swollen sample indicating the formation of carboxylate anion in the water-swollen sample. Also the morphology of the composite and the mechanism of mechanical adaptable process is also shown below (adapted with permission from ³¹).	13
Figure 2.5 SEM images of NR/sodium polyacrylate vulcanisates (with PEO as compatibilisers): a) before and (b) after water immersion. The loss of water absorbent resin from the elastomer composites leading to holes/pores is shown in the image (adapted with permission from ⁴⁸).	18
Figure 2.6 a) Water absorption characteristics and b) mechanical properties of CPE-LiAA containing composites before and after water swelling process (adapted and redrawn with permission from ^{56a}).	19
Figure 2.7 a) Effect of amphiphilic compatibilisers (CPE-g-PEG) on the water swelling ratio, b) Water swelling abilities after three consecutive cycles of CPE/P(AA-AM) composites (adapted and redrawn with permission from ^{57b}).	20

Figure 2.8 a) Schematic drawing showing the position of different types of water present in the swollen polymer, b) DSC curves of the polymer composites containing different water content, explaining the different states of water (adapted with permission from ⁶²).	21
Figure 2.9 Effect of water absorption on the variation of glass transition temperature T_g for different hydrophilic polymer showing the plateau T_{gw} after the critical water content (T_g , T_{gw} – glass transition temperature of initial sample and water absorbed sample respectively) (adapted and redrawn with permission from ⁶⁷).	23
Figure 2.10 XRD analyses of poly(vinyl alcohol) containing different amounts of water. The image indicates the reduction of crystallinity with water absorption (adapted and redrawn with permission from ⁶⁹).	24
Figure 2.11 a) Self-healing seals (fundamental principle of the sealing system), b) Zonal isolation by elastomer swell packers (adapted with permission from ⁸¹⁻⁸²).	26
Figure 2.12 Calcium sulphate and its polymorphs (adapted with permission from ⁸⁶).	27
Figure 2.13 SEM images of nano CaSO_4 crystals synthesized using various concentrations of calcium chloride: a) 35.5 wt-%, b) 31.5 wt-%, c) 27.5 wt-%, d) 23.5 wt-% (adapted with permission from ⁹¹).	28
Figure 3.1 Chemical structure of GECO (Hydrin T3108).	30
Figure 3.2 Chemical structure of GEPO (Zeospan 8030)	31
Figure 3.3 a) Internal mixer (Haake Rheomix), b) Banbury rotors.	33
Figure 3.4 a) Two roll mill and b) top view of the front and back rolls.	34
Figure 3.5 a) Moving die rheometer (Scarabeus SIS-V50), b) upper and lower dies, c) die design	34
Figure 3.6 a) Compression molding machine, b) mold (2 mm)	35
Figure 3.7 a) Differential scanning calorimeter (DSC Q2000), b) thermogravimetric analysis (TGA Q500)	36
Figure 3.8 a) Dynamic mechanical analyzer (Eplexor 2000N) with tensile clamp, (b) view of the clamps inside the test chamber (highlighted by red dotted box)	37
Figure 3.9 a) Zwick 1456 Universal testing machine, b) typical optical extensometer	38
Figure 3.10 Vertex 80v FTIR spectrometer (Bruker, Germany) equipped with an Mercury cadmium telluride detector and a Golden Gate Diamond ATR unit.	38
Figure 3.11 a) Zeiss Ultra Plus SEM machine, b) Libra 120 TEM machine	39
Figure 3.12 X-ray diffraction instrument (Seifert XRD 3003 θ/θ)	40
Figure 3.13 Raman spectrometer with microscope (Alpha 300 R+)	41

Figure 4.1 Cure characteristics of different GECO/GEPO blends using moving die rheometer operated at 160 °C.	43
Figure 4.2 DSC curves: a) heating curve, b) cooling curve (recrystallization studies). A single glass transition temperature and the semi-crystalline nature of the GECO/GEPO blends were evident from the Figure.	44
Figure 4.3 Model fitting of glass transition prediction equations of the different GECO/GEPO blends against the weight fraction of GEPO phase in the GECO/GEPO blends corrected based on blend crystallinity (ϕ_{GEPO}') (black symbols denote the actual experimental data, plotted as a function of the overall weight fraction of GEPO in the blend and the arrow marks indicate the shift in the weight fraction).	46
Figure 4.4 Dynamic mechanical analysis of GECO/GEPO blends: temperature dependence of a) Loss factor ($\tan \delta$), b) loss modulus (E''), c) storage modulus (E'), and d) effect of GEPO content (ϕ_{GEPO}) on T_g and $\tan \delta$ peak height values.	48
Figure 4.5 a) Stress–strain curves of GECO, GEPO and their blends, b) comparison of all the mechanical properties with varying GECO/GEPO blend ratios.	49
Figure 4.6 Water absorption characteristics of different GECO/GEPO blends against a) time (at 23 °C), b) blend ratio (GECO/GEPO), c) temperature and (d) images of water- swollen samples compared with dry sample (from left, Dry, 100/0, 75/25, 50/50, 25/75, 0/100 GECO/GEPO).	50
Figure 4.7 Water swelling (experimental data) fitted by Hopfenberg-Berens model. The symbol, lines represent the experimental data and the fitted curves respectively.	52
Figure 4.8 DSC analyses of dry (D) and water swollen–dried (DWD) samples of GECO/GEPO blends: a) heating curve, b) cooling curve. Very slight alteration in the recrystallization behavior of the GECO/GEPO blends with water absorption is illustrated. ..	54
Figure 4.9 Dynamic mechanical analysis of GECO/GEPO blends when the sample is dry as prepared (D), Water-swollen (DW) and the water swollen-dried (DWD): a)100 GECO, b) 75/25 GECO/GEPO, c) 50/50 GECO/GEPO, d) 25/75 GECO/GEPO, e) 100 GEPO.	56
Figure 4.10 a) Weight loss analysis of the GECO/GEPO blend samples after few cycles of water swelling, b) TGA of GECO/GEPO blends before (D) and after water swelling-dried (DWD) samples, c) repeatable water swelling characteristics of the GECO/GEPO blends. ...	59
Figure 4.11 Water absorption characteristics of GECO with varying curative content. The composite (SC3) containing slight amount of S/TMTD exhibited higher water absorption characteristics.	61

Figure 4.12 DSC analyses of Dry, 2, 7, and 20 days water-swollen samples. Melting of ice crystals formed in water-swollen samples can be visualized in the temperature around 0 °C.	62
Figure 4.13 Thermogravimetric analysis of dry and 20 days water-swollen sample. Derivative weight of the GECO -water composites as a function of temperature (inset).....	64
Figure 4.14 a) <i>In situ</i> formation of ice crystals are observed in cryo-TEM image of water-swollen GECO sample, b) freeze drying process leading to the formation of holes in the composites indicating the presence of ice crystals, c) EFTEM, Elemental mapping of carbon and oxygen over a), d) selected area electron diffraction (SAED) image of GECO-ice crystals composite. The indexed rings correspond to hexagonal crystal structure of ice.....	65
Figure 4.15 Particle size distribution of ice crystals from cryo-TEM images	66
Figure 4.16 Storage modulus (E') as a function of dynamic strain at –20 °C. The data for high strains are extrapolated for hydrodynamic reinforcement from the dry GECO. Solid dots and lines represent experimental values and fitted (Kraus equation) curves respectively.....	67
Figure 4.17 Time sweep analysis of dry and 20 days water-swollen GECO samples. Phase transition of water to ice crystals and their reinforcing efficiency can be observed from this study.	68
Figure 4.18 ATR-FTIR spectra of GECO composites: a) Dry and 20 days water-swollen GECO sample, b) FTIR spectra at room and elevated temperatures: Dry sample at RT, after 1h treatment at 120 °C, after cooling back to RT and in 21 hours at RT.....	69
Figure 4.19 Schematic representation of intermolecular hydrogen bonding between water molecules and polymer chains in the GECO composite.	70
Figure 4.20 Molecular dynamics simulation of the polymer and water system (red - oxygen, gray – carbon, white – hydrogen atom, dashed lines: blue – intramolecular bonding in water, white – intermolecular hydrogen bonding between polymer and water).....	70
Figure 4.21 a) Stress–strain properties establishing the adaptability of 20 days water-swollen samples at –20 °C and +20 °C compared to dry samples, b) Mooney-Rivlin plot of the dry and 20 days water-swollen GECO composites at different temperatures.	71
Figure 4.22 Dynamic mechanical analyses of water-swollen GECO composites: a) storage modulus (E'), b) loss factor ($\tan \delta$), c) loss modulus (E'') as a function of temperature with different days water-swollen GECO samples, d) adaptability ratio and temperature as a function of water swollen time (water content).	74
Figure 4.23 a) Cyclic temperature sweep experiment with 7 days water-swollen samples, b) bar chart showing the repeatable mechanical adaptability process for 7 days water-swollen sample.....	75

Figure 4.24 Schematic representation of rubber-filler interactions at different temperatures.	76
Figure 4.25 Calcium sulphate – water system (polymorphism).....	77
Figure 4.26 Rheological and mechanical properties of different calcium sulphate filled 75/25 GECO/GEPO composites: a) rheological characteristics, b) tensile stress–strain characteristics, and dynamic mechanical temperature sweep analysis: c) storage modulus (E'), d) $\tan \delta$	78
Figure 4.27 Methods and conditions of mechanical adaptability process.....	79
Figure 4.28 a) Effect of water immersion/treatment time on the modulus of the 75/25/50 GECO/GEPO/CaSO ₄ composite, b) effect of temperature during water immersion /treatment process on the maximum <i>hard state</i> modulus. E' values were measured at 60 °C with a constant static and dynamic load of 1% and 0.2% respectively. Water treatment was performed till the maximum modulus is achieved at every temperature and is shown in the Figure.	80
Figure 4.29 Effect of GECO/GEPO (hydrophilic polymer resin) blend ratio on the adaptability of the 50 phr CaSO ₄ filled GECO/GEPO composite. E' values are measured at 60 °C with a constant static and dynamic load of 1% and 0.2% respectively. Water treatment was performed till the maximum modulus is achieved in each blend ratios and is shown in Figure.	81
Figure 4.30 showing the effect of a) time and temperature of heat treatment on the storage modulus of water treated composites (75/25/50 GECO/GEPO/CaSO ₄) at 60°C, b) effect of heat treatment time at 200 °C on the modulus of the water treated composites at 60 °C.	83
Figure 4.31 XRD analysis indicates the phase transition of CaSO ₄ particles present in the composites (75/25/50 GECO/GEPO/CaSO ₄), where A, H, G designates anhydride, hemihydrate, and dihydrate phase respectively.....	84
Figure 4.32 Raman spectroscopic analysis indicating the phase transition of calcium sulphate present in the composites.	85
Figure 4.33 SEM images of different conditions of 75/25/50 GECO/GEPO/CaSO ₄ : a) untreated, b) water treated, c) heat treated and TEM analysis of water treated samples at different magnifications: d) 500 nm, and e, f) 200 nm at different positions.	87
Figure 4.34 showing the amplitude sweep analysis of the untreated, water treated and heat treated samples of 75/25/50 GECO/GEPO/CaSO ₄ (mechanically adaptable composites). Non-linear strain dependence of water treated sample indicates the formation of agglomerated CaSO ₄ nano-filler networks.....	88

Figure 4.35 a) Stress–strain properties, b) variation of Young’s modulus, c) Mooney-Rivlin plot of untreated, water treated and heat treated samples of 75/25/50 GECO/GEPO/CaSO ₄ , d) modified Bachelor equation to calculate aspect ratio of the fillers present in the 75/25 GECO/GEPO composite.	90
Figure 4.36 Dynamic mechanical analysis (temperature sweep) showing the mechanical adaptability: a) storage modulus (E'), b) loss modulus (E''), c) loss factor ($\tan \delta$), d) storage modulus value at 60 °C against different calcium sulphate content of 75/25 GECO/GEPO composites.	92
Figure 4.37 a) Effectiveness coefficient of fillers (EC), b) polymer–filler interaction parameter (B) against different conditions and varying filler contents of 75/25 GECO/GEPO composites.	94
Figure 4.38 Mechanism of mechanical adaptability of calcium sulphate filled elastomer composites.	95
Figure 7.1 Water swelling process fitted by Fickian diffusion mechanism equation. The symbol, lines represent the experimental data and the fitted curves.	109
Figure 7.2 Rheometric characteristics of GECO compounds with varying curatives content operated at 160 °C.	110

11 Tables

Table 2.1 Materials, stimuli and strategies used in achieving mechanical adaptability throughout the literature survey: (AR-adaptability ratio)	15
Table 2.2 Combination of rubbers, water absorbent resins, and compatibilisers used for preparing water swellable elastomer composites	17
Table 3.1 Specifications of GECCO (Hydrin T3108).....	30
Table 3.2 Specifications of GEPO (Zeospan 8030)	31
Table 3.3 Compounding formulation	32
Table 4.1 DSC profile of the GECCO/GEPO blends	44
Table 4.2 Power law exponents of water absorption process	51
Table 4.3 Fickian and relaxation constants derived from Hopfenberg-Berens equation.	53
Table 4.4 DSC analyses of GECCO/GEPO blends before (D) and after water swelling process (DWD).....	55
Table 4.5 Retention of mechanical properties in water swollen and dried (DWD) composites	58
Table 4.6 DSC melting profile and volume percentage of the filler (ice crystals) formed in GECCO composites	63
Table 4.7 Amplitude sweep analysis of the water-swollen samples at $-20\text{ }^{\circ}\text{C}$: values derived from Kraus model.....	68
Table 4.8 Cross-link density values obtained from Mooney-Rivlin equations.....	72
Table 4.9 Effect of blend ratio of GECCO/GEPO on the adaptability conditions.	82
Table 4.10 showing the Payne effect characteristics of the mechanically adaptable composites	88
Table 4.11 Cross-link densities of 75/25/50 GECCO/GEPO/ CaSO_4 samples obtained from Mooney-Rivlin equation and its constants	90

12 Publications

Journal articles

1. Temperature-Dependent Reinforcement of Hydrophilic Rubber Using Ice Crystals
Natarajan, T.S., Stöckelhuber, K.W., Malanin, M., Eichhorn, K.J., Formanek, P., Reuter, U., Wießner, S., Heinrich, G., and Das, A.,
ACS Omega, 2017, 2(2), 363-371.
2. In-situ Polymorphic Alteration of Filler Structures for Biomimetic Mechanically Adaptive Elastomer Nanocomposites
Natarajan, T.S., Okamoto, S, Stöckelhuber, K.W., Reuter, U., Wießner, S., Fischer, D., Ghosh, A. K., Heinrich, G., and Das, A.,
ACS Applied Materials & Interfaces 2018, 10(18), 16148-16159.
3. Piezoresistive natural rubber-multiwall carbon nanotube nanocomposite for sensor applications
Natarajan, T.S., Eshwaran, S.B., Das, A., Stöckelhuber, K.W., Wießner, S., Pötschke, P., Nando, G.B., Chervanyov, A.I., and Heinrich, G.
Sensors and Actuators A: Physical, 239, 2016, 102-113.
4. Strong Strain Sensing Performance of Natural Rubber Nanocomposites
Natarajan, T.S., Eshwaran, S.B., Stöckelhuber, K.W., Wießner, S., Pötschke, P., Heinrich, G. and Das, A.,
ACS Applied Materials & Interfaces, 9(5), 2017, 4860-4872.

Patents

1. Rubber or elastomer compositions and processes for their manufacturing
Natarajan, T. S., Das, A., Stöckelhuber, K. W., Jurk, R., Hong, H. L., Wießner, S., and Heinrich, G.
U.S. Patent Application US20170342240A1,
Deutsche Patentanmeldung DE102016209098A1.

2. Elastomeric composition and process for its preparation

Natarajan, T. S., Das, A., Stöckelhuber, K. W., Hong, H. L., Jurk, R., Wießner, S., and Heinrich, G.

U.S. Patent Application US20170342265,

Deutsche Patentanmeldung DE102016109620A1,

Europäische Patentanmeldung EP3249014A2.

Conferences:

1. Reinforcement effect of ice crystals in hydrophilic rubber matrix

Natarajan, T. S., Stöckelhuber, K.W., Wießner, S., Das, A and Heinrich, G.
Rubbercon, May 23-25, 2017, Prague, Czech Republic.

2. Mechano-adaptive rubbers by active filler morphology

Natarajan, T. S., Wießner, S., Das, A and Heinrich, G.,
Elastomers 2017, Nov 21-23, 2017, Warsaw, Poland.

3. New strategy for utilizing non-reinforcing calcium sulphate as reinforcing filler for hydric elastomers

Natarajan, T. S., Stöckelhuber, K.W., Wießner, S., Das, A and Heinrich, G.
DKG Nord meeting, May 11-12, 2017, Hannover, Germany.

4. Exploiting structural phase transitions when designing adaptive rubbers

Natarajan, T. S., Stöckelhuber, K.W., Wießner, S., Das, A and Heinrich, G.
Frontiers of Rubber Science and Technology, May 3-4, 2017, Dresden, Germany.

5. Exploiting phase transition of fillers when designing mechanically adaptive elastomer composites

Natarajan, T. S., Wießner, S., Das, A and Heinrich, G.
Deutsche Kautschuk Tagung, July 2-5, 2018, Nürnberg, Germany.

6. Water responsive mechano-adaptive elastomer composites based on active filler morphology

Natarajan, T. S., Wießner, S., Das, A and Heinrich, G.
International elastomer conference, Oct. 9-11, 2018, Louisville, Kentucky, US.